

ANKARA YILDIRIM BEYAZIT UNIVERSITY

GRADUATE SCHOOL OF NATURAL AND APPLIED SCIENCES



COMPUTER BASED GRADING OF BLADDER CARCINOMA

M.Sc. Thesis by

Ali DEĞİRMENÇİ

Department of Electrical and Electronics Engineering

January, 2017

ANKARA

COMPUTER BASED GRADING OF BLADDER CARCINOMA

A Thesis Submitted to

the Graduate School of Natural and Applied Sciences of

Ankara Yıldırım Beyazıt University

**In Partial Fulfillment of the Requirements for the Degree of Master of Science
in Electrical and Electronics Engineering, Department of Electrical and
Electronics Engineering**

by

Ali DEĞİRMENCİ

January, 2017

ANKARA

M.Sc. THESIS EXAMINATION RESULT FORM

We have read the thesis entitled “**COMPUTER BASED GRADING OF BLADDER CARCINOMA**” completed by **ALİ DEĞİRMENCİ** under the supervision of **ASSIST. PROF. DR. ÖMER KARAL** and co-supervision of **ASSOC. PROF. DR. İLYAS ÇANKAYA** and we certify that in our opinion it is fully adequate, in scope and in quality, as a thesis for the degree of Master of Science.

Assist. Prof. Dr. Ömer KARAL

Assoc. Prof. Dr. İlyas ÇANKAYA

Supervisor

Co-Supervisor

Prof. Dr. Recep DEMİRCİ

Assist. Prof. Dr. Enver ÇAVUŞ

Jury Member

Jury Member

Assoc. Prof. Dr. Berrak GÜMÜŞKAYA ÖCAL

Jury Member

Prof. Dr. Fatih V. ÇELEBİ

Director

Graduate School of Natural and Applied Sciences

ETHICAL DECLARATION

I hereby declare that, in this thesis which has been prepared in accordance with the Thesis Writing Manual of Graduate School of Natural and Applied Sciences,

- All data, information and documents are obtained in the framework of academic and ethical rules,
- All information, documents and assessments are presented in accordance with scientific ethics and morals,
- All the materials that have been utilized are fully cited and referenced,
- No change has been made on the utilized materials,
- All the works presented are original,

and in any contrary case of above statements, I accept to renounce all my legal rights.

2017, 24 January

Ali DEĞİRMENÇİ

ACKNOWLEDGMENTS

I would like to express my sincere gratitude to my supervisors Assist. Prof. Dr. Ömer KARAL and Assoc. Prof. Dr. İlyas ÇANKAYA for their support and guidance.

I would also like to express my gratitude to Assoc. Prof. Dr. Berrak GÜMÜŞKAYA ÖCAL for her support and guidance.

Finally, I would like to thank my family, Mather, Father, Brother for being and supporting me all the way.

2017, 24 January

Ali DEĞİRMENÇİ

COMPUTER BASED GRADING OF BLADDER CARCINOMA

ABSTRACT

Cancer is one of the most important diseases that ends up with losing lives, despite many new improvements in medicine. Cancer, which has more than a hundred species, causes uncontrolled division and multiplication of cells and abnormalities in cell shape due to the damage in DNA. The early diagnosis and prognosis of cancer has great importance and will help to reduce loss of lives from this disease. Although many methods are used in the diagnosis and prognosis of cancer, the most effective method is to examine the obtained tissue sample under the microscope by the pathologist after various procedures have been applied. At this stage, pathologists diagnose the cancer by examining the structural properties of the cells.

Recently, image processing techniques have been applied to obtained pathological images as well as in other fields of medicine. By using these techniques, the cell locations in pathological images can be determined and the cell characteristics can be extracted from the determined cell locations. In this thesis, visualization of the pathological bladder data is performed and the area can be cropped from these images. An algorithm is designed to determine whether the case is at high grade bladder cancer or low grade bladder cancer using the structural features of the cell nucleus in the region specified by these images. Computer Assisted Diagnosis (CAD) is a system, which is developed to help doctors to diagnose the disease and to decide on the treatment method to be applied. For this purpose, a graphical user interface (GUI) was designed by using the MATLAB software. With the help of the extracted features, it can be decided that loaded sample of the bladder is at high grade or low grade. As a result, developed software allows easy and accurate detection of bladder cancer. As a future work, another study may be performed to identify types of the bladder cancer.

Keywords: Medical Image Analysis, Contour Detection, Feature Extraction, Classification, Segmentation, The Cancer Genome Atlas, MATLAB GUI.

MESANE KARSİNOMUNUN BİLGİSAYAR TEMELLİ DERECELENDİRİLMESİ

ÖZ

Tıptaki gelişmelere rağmen, kanser hastalığı ölümlerine sonuçlanan hastalıkların en önemlilerinden bir tanesidir. Yüzden fazla türü olan kanser hastalığı, DNA da meydana gelen hasarlardan dolayı, hücrelerin kontrolsüz olarak bölünüp çoğalmasına ve hücre şekillerinde anormalliklere sebep olmaktadır. Kanser hastalığının erken tanısı ve teşhisi büyük önem taşımaktadır ve bu hastalıktan kaynaklanan ölümlerin azalmasına yardımcı olacaktır. Kanser hastalığının tanı ve teşhisinde birçok yöntem kullanılsa da en etkili yöntem hastadan alınan doku örneğinin çeşitli işlemlerden geçtikten sonra patoloğ tarafından mikroskop altında incelenmesiyle olmaktadır. Bu aşamada patoloğlar hücrelerin yapısal özelliklerini inceleyerek teşhis koymaktadır.

Son zamanlarda, görüntü işleme teknikleri tıbbın diğer alanlarında olduğu gibi patolojik görüntülerde de uygulanması yaygınlaşmaktadır. Bu teknikler kullanılarak patolojik görüntülerdeki hücre konumları belirlenebilmekte ve hücre konumlarından hücrelere ait özellikler çıkartılabilmektedir. Bu tez çalışmasında, mesaneye ait patolojik görüntülerin görselleştirilmesi ve seçilen bölgedeki çekirdeğinin yapısal özelliklerinden yararlanılarak, vakanın yüksek dereceli veya düşük dereceli kanser olduğuna karar veren bir algoritma geliştirilmiştir. Bilgisayar Destekli Tanı (BDT), hastalığın teşhisini koymada ve uygulanacak tedavi metoduna karar vermede doktorlara yardımcı olması için geliştirilen sistemlerdir. Bu amaca yönelik olarak MATLAB kullanılarak bir Grafik Kullanıcı Ara yüzü (GKA) tasarlanmıştır. Seçilen hücre çekirdeklerine ait sınırların belirlenmesi ve elde edilen sınır bilgilerinden hücre çekirdeklerine ait özellikler çıkartılmaktadır. Bu özellikler yardımıyla yüklenen mesane örneğinin yüksek dereceli veya düşük dereceli olduğuna karar verilebilmektedir. Sonuç olarak bu program vasıtasıyla mesane kanserinin kolay ve doğru bir şekilde tespiti sağlanabilmektedir. Buna ek olarak, Mesane kanseri türlerinin tespitine yönelik bir çalışma da yapılabilir.

Anahtar sözcükler: Tıbbi Görüntü Analizi, Kontur Bulma, Özellik Çıkarımı, Sınıflandırma, Bölütleme, The Cancer Genome Atlas, MATLAB GUI

CONTENTS

M.Sc. THESIS EXAMINATION RESULT FORM.....	ii
ETHICAL DECLARATION	iii
ACKNOWLEDGMENTS	iv
ABSTRACT.....	v
ÖZ	vi
NOMENCLATURE.....	ix
LIST OF TABLES	x
LIST OF FIGURES	xi
CHAPTER 1 – INTRODUCTION	1
1.1 Objective of Thesis.....	3
1.2 Outline of Thesis	5
CHAPTER 2 – DIGITAL PATHOLOGY	6
2.1 Preparation of Tissue Sample.....	9
2.2 Whole Slide Imaging (WSI).....	13
2.2.1 Storage and Visualization of WSI.....	16
2.3 The Cancer Genome Atlas (TCGA).....	19
CHAPTER 3 – BACKGROUND FOR IMAGE PROCESSING	20
3.1 Concept of Image Processing	20
3.2 Types of Images	23
3.3 Color Space	25
3.4 Geometric Configurations of Objects	29
3.5 Distance Transformation	32
3.6 Connected Component Labelling.....	34
3.7 Image Filtering	37
3.7.1 Spatial Domain Smoothing Filters	39
3.7.2 Spatial Domain Sharpening Filters.....	44
CHAPTER 4 – IMAGE SEGMENTATION AND CONTOUR DETECTION. 48	
4.1 Thresholding.....	50
4.1.1 Basic Global Thresholding.....	54
4.1.2 Otsu’s Thresholding Method.....	56

4.2 Edge Detection	58
4.2.1 Canny Edge Detection.....	64
4.3 Contour Detection.....	67
CHAPTER 5 – APPLICATION OF CELL DETECTION AND CLASSIFICATION IN PATHOLOGICAL IMAGES	70
5.1 Application of Cell Detection and Classification in Urinary Bladder	
Carcinoma	71
5.1.1 Procedure of the Cell Detection.....	72
5.1.1.1 Tracing Potential Contours.....	74
5.1.1.2 Color Decomposition on Stained Tissue Images	77
5.1.1.3 Calculation of Contour Value	80
5.1.1.4 Removing Overlapping Contours and Non-compact Pixels	82
5.1.1.5 Classification.....	83
5.1.2 Graphical User Interface of the Application for Bladder Carcinoma Diagnosis.....	85
CHAPTER 6 – CONCLUSIONS AND FUTURE WORKS	94
REFERENCES.....	96
CURRICULUM VITAE.....	105

NOMENCLATURE

BT	:	Benign Tumor
MT	:	Malignant Tumor
TCC	:	Transitional Cell Carcinoma
BC	:	Bladder Cancer
BW	:	Bladder Wall
H&E	:	Hematoxylin and Eosin
WSI	:	Whole Slide Image
TCGA	:	The Cancer Genome Atlas
GUI	:	Graphical User Interface
TIFF	:	Tagged Image File Format
NIH	:	National Cancer Institute
NHGRI	:	National Human Genome Research Institute
DIP	:	Digital Image Processing
2D	:	2 Dimensional
CIE	:	International Commission Illumination
RGB	:	Red, Green and Blue
CMY(K)	:	Cyan Magenta Yellow Black
HSI	:	Hue Saturation Intensity
DT	:	Distance Transform
ED	:	Euclidian Distance
CCL	:	Connected Component labelling
ET	:	Equivalence Table
CAD	:	Computer Aided Diagnosis
OD	:	Optical Density
UBC	:	Urothelial Bladder Carcinoma

LIST OF TABLES

Table 3.1 Possible digit-replacement couples and inverse-digits.....	30
Table 3.2 Area calculation.....	32



LIST OF FIGURES

Figure 2.1 Microscope and its parts	7
Figure 2.2 Process of telepathology in whole slide images	9
Figure 2.3 Cystoscope and its parts.....	10
Figure 2.4 (a) Plastic cassette, (b) Taking a small section from the sample to fit it in a cassette	11
Figure 2.5 Stained glass sample	13
Figure 2.6 Methods to obtain digital slide, (a) Tile scanning method, (b) Line scanning method.....	15
Figure 2.7 Pyramid structure of the whole slide Image	18
Figure 3.1 Coming lights from the source (a), reflected lights by the object (b) captured by the imaging system (c), the continuous image shown after process of sampling and quantization the output of the digitalized image obtained (e)	21
Figure 3.2 Changing gray levels and spatial resolution. (a) 8-bit, 1600x1600 original image; (b) 6-bit original image; (c) 3-bit original image; (d)1-bit (binary) original image; (e) 1/8 times reduction of spatial resolution; (f) 1/16 times reduction of spatial resolution.....	22
Figure 3.3 After sampling and quantization applied to cameraman image storage into the memory. Top-left corner accessed with (1,1) and right bottom is equal to the image size (M,N). Intensity values of that location can be accessed by entering the rows and columns of the desired pixel.	23
Figure 3.4 Cameraman image and small section of it both in numerical and the image form. In numerical form, lower values represent darker pixels. Intensity values closer to 255 maps for white areas in the image.....	24
Figure 3.5 Lena image and three intensity values of the determined area. Each color intensity value storage requires 8-bit and totally 24-bit.....	25
Figure 3.6 RGB color cube	26
Figure 3.7 HSI color model.....	28
Figure 3.8 Eight neighborhood.....	29
Figure 3.9 Set of encoded points	31
Figure 3.10 Application of distance transform (a) binary image as an input (b) distance transform of the image	33
Figure 3.11 Implementation of the connected components algorithm of 3 ‘u’ shaped letters, (a) 4 connected, (b) 8 connected	35
Figure 3.12 Eight connected neighborhood, (a) central pixel E and the eight neighborhoods, (b) forward scan mask, (c) backward scan mask.....	36
Figure 3.13 Padding part of an image with, (a) symmetric padding method, (b) wrap padding method.....	39

Figure 3.14 (a) Autumn image as an input RGB image and increasing filter size of the averaging mask applied images with, (b) 3x3, (c) 5x5, (d) 7x7	40
Figure 3.15 Process of the median filter with 3x3 kernel and output	41
Figure 3.16 (a) Salt and pepper noise added lifting body image, (b) 3x3 median filter applied image, (c) 7x7 median filter applied image.....	42
Figure 3.17 3D representation of the Gaussian kernel with 5x5 mask size and 1σ and 3σ (a), (b) respectively, (c) Gaussian filter with parameters in (a) applied image, (d) Gaussian filter with parameters in (b) applied image.	43
Figure 3.18 (a) High pass filter applied cameraman image, (b) sharpened cameraman image with $k = 1$	45
Figure 3.19 Laplacian kernels for implementing the equation 3.14 in image processing	46
Figure 3.20 Representation of the Laplacian sharpening procedure of an image, (a) circuit gray scale image as an input, (b) Laplacian filtered image, (c) sharpened image	47
Figure 4.1 Over segmentation and under segmentation image (a) Lena is segmented into 3, (b) Lena image is segmented into 15.	49
Figure 4.2 (a) Image with 3 letters with different intensity values, (b) histogram of the image (a), (c) Cameraman image, (d) histogram of the cameraman image (c).	52
Figure 4.3 Flowchart of the basic global thresholding method.....	55
Figure 4.4 Flowchart of the Otsu's thresholding method.....	58
Figure 4.5 Source of edges.....	59
Figure 4.6 (a) X directional derivative of Cameraman image, (b) y directional derivative of cameraman image	61
Figure 4.7 Derivative operators (a) Roberts cross x direction, (b) Roberts cross y direction, (c) Sobel x direction, (d) Sobel y direction, (e) Prewitt x direction, (f) Prewitt y direction.....	62
Figure 4.8 Different edge detector operators applied to an input Lenna image, (a) Lenna image, (b) Roberts operator applied image, (c) Sobel operator applied image, (d) Prewitt operator applied image.....	63
Figure 4.9 Result of the Canny edge detection image of Lenna	67
Figure 4.10 Flowchart of contour tracing algorithm	69
Figure 5.1 Antonie van Leeuwenhoek's microscope	71
Figure 5.2 Flowchart of the bladder cancer grading application.....	73
Figure 5.3 Seed points shown as black dots to input image.....	75
Figure 5.4 All possible valid edges drawing to the input image with different colors	77
Figure 5.5 Color deconvolution applied image.....	79

Figure 5.6 Non-overlapping segmentation and non-compact pixels removed contours	83
Figure 5.7 MATLAB GUI main window	86
Figure 5.8 File menu	86
Figure 5.9 Open Image pop-up window	87
Figure 5.10 Pathological image zooming and scrolling	88
Figure 5.11 Area selection from pathological images.....	89
Figure 5.12 Tools menu	90
Figure 5.13 Example of sending e-mail	90
Figure 5.14 (a) Macro photograph of the pathology sample, (b) a barcode.....	91
Figure 5.15 Demonstration of nuclei boundaries and calculations	92
Figure 5.16 Result of cancer grading, (a) low grade (b) high grade	93

CHAPTER 1

INTRODUCTION

Human body consists of more than trillion of cells. In normal conditions, these cells grow, divide, multiply, and die to fulfill the normal functions of the body. The capabilities of the cells are limited. Sometimes the routine does not work as expected and as a result, the cells begin to grow abnormally and begin to divide more than the specified rate. This causes the lump, called as a tumor. In medical science, there are two subtypes of tumors, which are benign and malignant. In general, benign tumors (BT) are not cancerous and do not lead to the loss of life. When compared to malignant tumor (MT) cells, BT cells do not spread to other parts of the body, and the growth rate of BT cells is smaller than MT cells. When the cancer at a certain part of the body spreads to other parts of the body, it grows a tumor, which is called as metastasis.

The name of the cancer is determined by the location where the cancer first started. For example, if the starting location of the cancer is bladder, it is called as a bladder cancer. Cancer types can be classified into four main categories according to the type of cells they are originated from [1,2]. Main subtypes of cancer are:

- Carcinoma – cells originated from epithelial cells
- Sarcoma – cells originated from bone or soft tissue
- Lymphoma – lymphatic system
- Leukemia – white blood cells and bone marrow

The treatment of a cancer depends on the type of cancer, the part of the body which is exposed to cancer, and the cancer stage. Current treatment methods of the cancer in medical science are surgery, radiation therapy, chemotherapy, immune therapy, targeted therapy, hormone therapy, stem cell transplant and precision medicine [3]. Despite all these treatment procedures, the best thing is obviously not getting cancer.

Cancer is not caused by only one reason, so it is not easy for human beings to reduce the risk of getting cancer. Since tobacco contains carcinogenic substances, the use of tobacco increases the risk of getting different types of cancer. Lung cancer is mainly caused from smoking. Usage of alcohol increases the risk of getting mouth, throat, liver, breast and many other cancer types. On the other hand, regular exercise, maintaining a good physical condition and healthy diet help to reduce the risk of cancer [1,3,4].

Organs are the parts of the body which have a specific functioning. Bladder is an organ in the body which holds the urine coming from the kidney. When the abnormal cell growth starts at the epithelial lining of the bladder, it is called bladder cancer. Urothelial carcinoma (transitional cell carcinoma (TCC)), squamous cell carcinoma, adenocarcinoma, small cell carcinoma and sarcoma are common types of bladder cancer. TCC is the most common type of bladder cancer. Approximately, 1-2% of bladder cancers are squamous cell carcinoma. Almost 1% of bladder cancers are adenocarcinoma and less than 1% are small-cell carcinoma. The occurrence of sarcoma is very rare, but there are other types of bladder cancer which are less common than sarcoma. The rate of getting bladder cancer is 4 times higher in men compared to women. It is estimated that over 16,000 people will die of bladder cancer within this year according to the Cancer Facts and Figures. In addition, more than 75,000 new cases of bladder carcinoma are expected in the US in 2016. Approximately 90% of bladder cancer patients are over 55 years old and the average age at diagnosis is 73 [4,5]. Early diagnosis has a crucial role in treatment of cancer.

The parts of body can be visualized with different techniques to assist to healthcare professionals during the period of diagnosis. By using these images, the diagnosis of the disease can be made earlier. Thus, the duration of healing is reduced, and disease gives less damage to the body. Therefore, the analysis of the captured medical image plays a crucial role in diagnosis and treatment. The analysis of the image helps to deduce from available information. The information in these images can be extracted by using one or a combination of several image processing methods. Image processing takes an input image, and some mathematical operations are applied to the input image.

As an output, it gives a processed image, or extracts information from the input image. One of the important application areas of image processing is in medical field [6].

1.1 Objective of Thesis

There are many methods to diagnose bladder cancer (BC). In diagnostic process, the technology can assist doctors. In the literature, many studies have been performed with different imaging techniques for BC detection. For example, Jaume et al. made identification of tumor with measuring abnormalities of the bladder wall (BW) from computed tomography images [7]. In this study, the segmentation of the BW was made manually and the detection of the tumor in BW was performed automatically, then the BW thickness was calculated. To recognize the differences between testing BW and normal BW, thickness map was created. Comparison of them was made with z-score. If the calculated z-score of the region is higher than the threshold value, it is called as a tumor, and the value is lower than the threshold value, it is considered normal. In another study, Shi et al. performed discrimination of normal and cancerous BW tissue in three steps by tissue analysis from magnetic resonance images [8]. Firstly, region of interest was determined manually. Then, textures were extracted from the region. Finally, t-test was used for analysis of the textures. As a result, there are some differences between normal and cancerous BW tissues in terms of entropy, uniformity, smoothness, relation and contrast.

Another method to diagnose bladder cancer is the examination of the biopsy specimen. For this purpose, if a suspected area is found during the cystoscopy, biopsy sample is taken from the area and sent to the laboratory to be examined. The examination process requires expertise in the area, so it is done by the pathologist. The tissue sample contains millions of cells and is analyzed manually using the microscope. Therefore, it is very slow and subjective. During the diagnostic period, the pathologist uses the structural properties of the nucleus to determine if the patient is cancerous. In addition, these features help to determine the degree of cancer. Spyridonos et al. performed grading of urinary bladder carcinomas from the selected part of tissue samples which were taken from hematoxylin and eosin (H&E) stained bladder samples of human [9]. In total, 92 patients were used. 63 of them were at low grade and 29 of them were at

high grade bladder carcinoma according to the four different pathologists based on World Health Organization grading system. In the study, foreground and background segmentation of the image processing was made by using 5x5 mask. Foreground pixels were referred as cell nucleus. After that, the textural and morphological properties were calculated. The quadratic non-linear Bayesian classification method was used for classification.

High-quality images obtained from the tissue sample allow the diagnosis of disease without having to examine the prepared slide under the microscope from the pathologist. Since whole slide images (WSI) can be stored and transferred via memory devices; pathologists can examine WSI whenever and wherever they want. Although the memory consumption of WSI data is high, it can be managed with the current technology. Accessing the medical data is not easy, especially when researcher is not working in the medical field. Furthermore, if it can be accessed, usage of the medical data requires research ethics committee approval.

To improve diagnosis and treatment of cancer, The Cancer Genome Atlas (TCGA) project was started in 2005. The aim of this project was to provide medical information about the cancer. One of these medical data is WSI. In this thesis, Urothelial Bladder Carcinoma WSI generated by the TCGA research network is used: <http://cancergenome.nih.gov/> [10].

Bladder cancer grading is carried out by image classification methods using the acquired nucleus properties. So, BC contour detection of the nucleus from a loaded image and calculation of features from detected cell is computed by MATLAB which is a programming language used by engineers in different areas. To make it easier to use, Graphical User Interface (GUI) was designed for pathologists. By using GUI, the user can load a WSI, visualize the data, and perform simple operations such as zooming, scrolling, and removing a specific area from the loaded image. Moreover, the user can select the desired area from the uploaded image and perform nucleus detection on the selected area.

1.2 Outline of Thesis

The following sections of the presented thesis are organized as follows:

In chapter 2, processed medical data is explained. Obtaining procedure of biopsy samples and histochemical staining process is briefly presented. Then, sufficient information about TCGA is expressed. In addition, TCGA's contributions to the researchers are indicated.

In chapter 3, brief information about the principles of image and the types of images are given. Different colored space models, conversion of one color model to another model and properties of each model are shown. Geometric properties of outline of an object are exhibited in depth. Enhancing the image quality with different filtering operations on the image is explained and in addition, filtered output images are illustrated.

In chapter 4, image segmentation methods are discussed. The primary differences in image segmentation methods are mentioned. Thresholding, edge detection and contour tracing methods of the segmentation are stated, and usage of them are presented. For each subsection of the segmentation methods, the mathematical background and process are described in detail.

In chapter 5, performed algorithms are explained in a detailed way. Flowcharts of the algorithms are drawn. The results of the algorithm are shown with a small part of the pathological image. Instructions about the designed GUI are presented in detail.

Chapter 6 is the final chapter, conclusion of the thesis and comparison of the results of designed algorithm success is demonstrated. Finally, increase in percentage of cell detection, accuracy increase in the grading of the BC, and lowering the process time is stated as a future work.

CHAPTER 2

DIGITAL PATHOLOGY

Pathology, one of the branches in medicine, examines diseases by scientific methods. To determine causes of the disease, organs, tissues and cells can be analyzed in the pathology. However, pathology does not only examine the human, it also investigates animals and plants. The person who is a specialist in this area is called pathologist.

Tissue samples, which will be analyzed, can be obtained by biopsy method or from the part of the suspected area taken from human body. Once the obtained specimens have been subjected to specific procedures, they are ready to be examined under the microscope by the pathologist. Then, the report is prepared according to the results of the examination. The diagnosis of the disease and the methods to be applied for the treatment of the disease are determined with the help of the pathology report. Therefore, success rate of the treatment and diagnose of the disease is highly dependent on the prepared report by pathologist.

In histology, the analysis of the cell structure is fulfilled under the microscope whether it is affected by the disease or not. Histopathology is one of the subsection of the pathology. Histopathology analyzes diseased tissues to diagnose the disease which is carried out under the microscope by a specialist doctor. Commonly, cancer cases are analyzed in the histopathology. After the analysis of the tissue sample is performed by the pathologist, the final decision for the presence of cancer, cancer staging and cancer grading are determined. At this stage, sight of the pathologist has a great importance on diagnosing the disease. Therefore, it is obvious that being a pathologist requires special training and some skills. The person completing the medical faculty must successfully complete a four-year training program in order to become a pathologist in Turkey. Generally, pathologists develop pattern recognition and writing skills. Pathologist may analyze the sample perfectly but if the pathologist cannot express it in writing, diagnosis of the disease may not be made sufficiently. The communication between the doctor who determines the treatment method and the pathologist who analyzes the sample is accomplished by the pathology report organized by the

pathologist. For this reason, a good pathologist should adequately express what is seen on the analyzed sample for a better diagnosis.

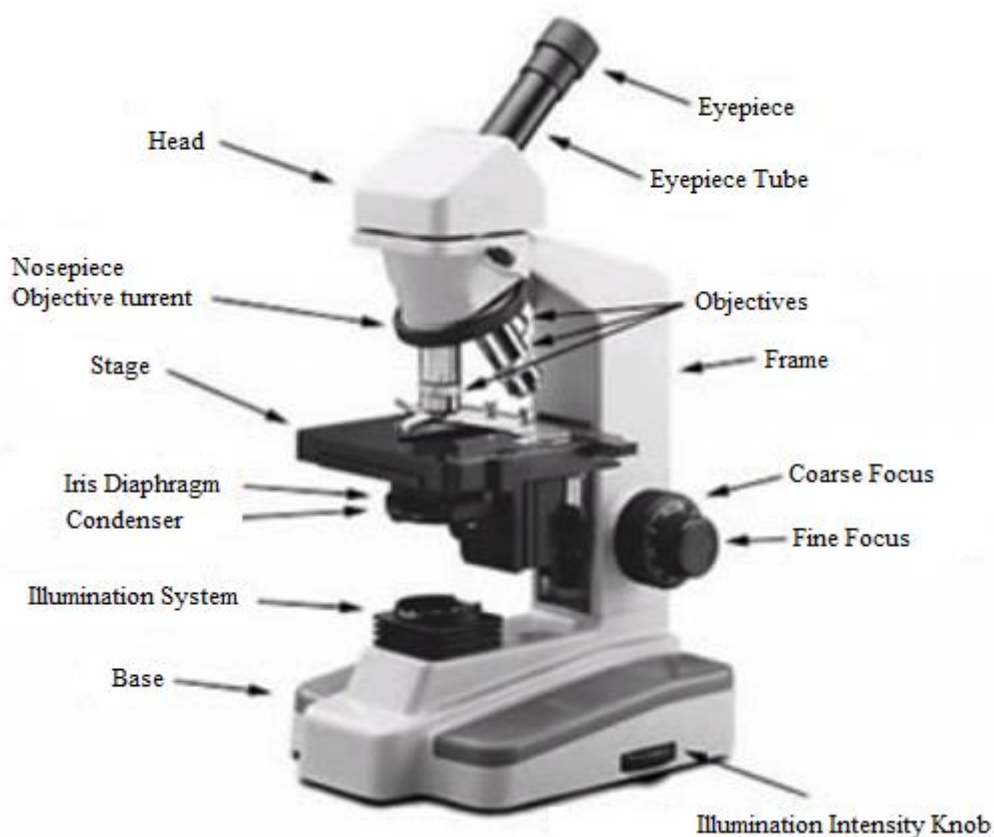


Figure 2.1 Microscope and its parts [11]

There exist many kinds of microscopes which are used in the pathology to diagnose the disease such as electron, fluorescence, stereo and so on. In the traditional pathology, glass slides are analyzed under the light microscope. In Figure 2.1, a light microscope and its functional parts are demonstrated.

Pathologists need a light microscope to observe the prepared glass slides. Additionally, the prepared glass slides requires an area to be stored and special handling to prevent any damages. Different from traditional pathology, digital pathology analyzes the image of the slides which are taken via virtual microscopy. Virtual microscopy allows the prepared glass slide to be stored in the form of a digital slide. After digital slides are obtained, analysis, visualization and storing of digital slides become possible at

any moment and anywhere free of existence of a light microscope. To analyze the disease with digital slides, pathologists would just need an access to a computer.

Since the size of digital slides is big, the memory capacity required to store digital slides is large. However, storage capacities of the memories have increased rapidly and also cloud storage which enables to store the data through internet makes possible to store and access to digital slides. This allows some jobs to be carried out easily. In some cases, it may be necessary to get a second opinion from another specialist. At that time, either the glass slide should be sent to another pathologist, or that pathologist should go to the center where the glass slides are located. Sending glass slides to a pathologist contains risks of damage during the delivery. Obviously, it also takes some time depending on the distance. In the digital pathology, accessing the slide sample is very easy because it can be accessed via the internet. However, access time to data may be low depending on internet data rate. Although digital slides consume data in gigabytes in memory, access time to data is still much faster compared to traditional method. Digital pathology also reduces the cost of storing slides and transferring to other pathologists. The analysis of digital slides can be performed all the time by means of computer programs which enable to view digital slides. Furthermore, digital pathology contributes to the field of education by visualizing the same tissue sample to all the students in the laboratory. Examination of the tissue sample in the same image quality can be performed, moreover, quality of the image is not affected by ambient conditions. Examination of the digital slides by more than one pathologist increases the truthfulness of diagnosis of the disease. As a result, digital pathology has many advantages over traditional pathology [12]. The process of obtaining and analyzing digital slides by multiple users is shown in Figure 2.2.

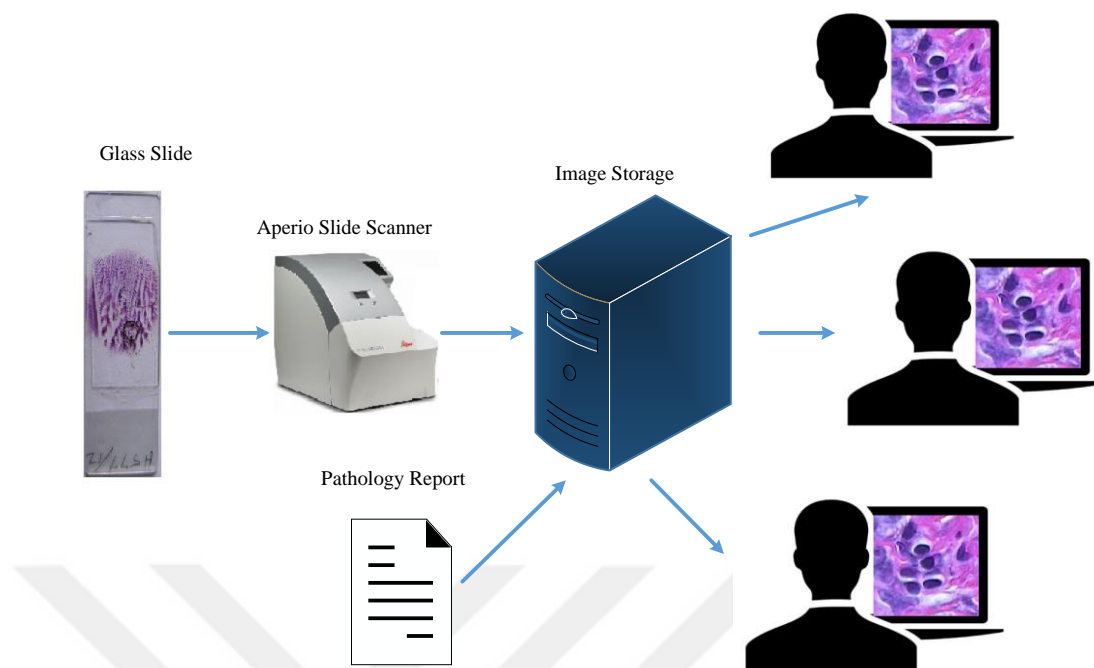


Figure 2.2 Process of telepathology in whole slide images

2.1 Preparation of Tissue Sample

Bladder cancer can be diagnosed by a variety of methods including urine analysis, CT, MRI, cystoscopy, and biopsy. In the urine cytology, the sample, which is taken from urine, is analyzed by using a microscope by the pathologist. In this process, the presence of cancerous cells is tried to be found out by the pathologist. Although it is a cheap and frequently used method for detecting bladder cancer, it may not be possible to detect the early stage of bladder cancer. Since there is a probability of the urine cytology to be non-diagnostic, urine analysis and the other methods, cystoscopy methods are used for determination of the presence of a cancer especially at the early stage. In this approach, a specially designed device with a built-in camera is used to display the interior surface of the bladder. This device is named as cystoscope and shown in Figure 2.3. This allows the visualization of the bladder for examination performed by the urologist. During this procedure, tissue specimen may be taken from suspicious areas in the bladder or the entire suspected area may be resected. Obtained tissue samples are sent to pathology for examination. After that, diagnosis of the bladder cancer, determination of type and stage of the bladder cancer can be done [12,13].

When the tissue sample is cut out from the human body, it is prone to be harmed and decay. In order to make an accurate diagnosis, obtained tissue sample has to be carefully preserved. Therefore, specific procedures are applied to the specimen to keep in the same condition as it is taken from the human body.

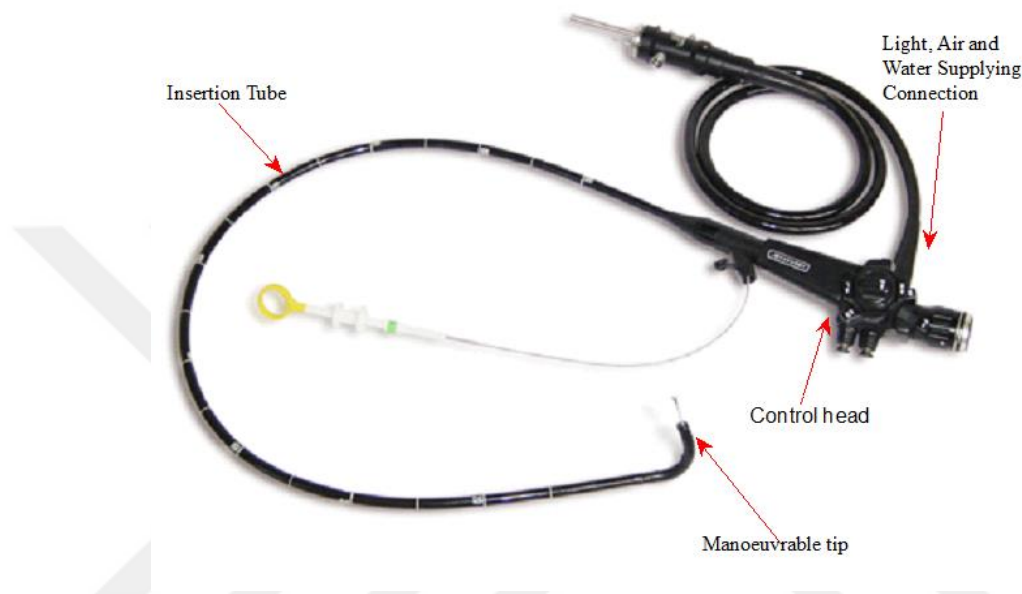


Figure 2.3 Cystoscope and its parts

These procedures contain:

- Fixation
- Grossing
- Processing
- Embedding
- Sectioning
- Staining

Fixation:

Fixation is an initial procedure of glass slide preparation, it affects the results of other procedures. If the quality of the fixation is not sufficient, it is difficult to get a small

section from the sample and the quality of staining becomes low. Even, it may end up with taking a new sample again from the patient and start the whole process from scratch. This leads to wasting money and slowing down the job to be carried out.

Autolysis which is the digestion of the cell by itself, starts after tissue is separated from the living organism and it is done by enzymes. Besides, the bacteria found in the tissue can damage the cells. Therefore, specimens are put into a fixative that preserves the structure of cells in the tissue and prevents it from shrinking during the application of other process. Time period of the sample in the fixative is determined by the thickness of the specimen, solution and so on. Formalin, which is a 10% formaldehyde solution, is used in the process of fixation.

Grossing:

In grossing process, obtained specimens are placed into a cassette which is shown in Figure 2.4 (a). If the taken sample is too big to fit in a cassette, it will be sectioned into smaller pieces. The maximum size of the specimen is 3-4mm thick.



(a)



(b)

Figure 2.4 (a) Plastic cassette, (b) Taking a small section from the sample to fit it in a cassette [14]

Processing:

As an initial step of the process, existing water in the cells are removed. It is called dehydration. Generally, dehydration is made by using alcohols. Ethyl alcohol is usually used in the dehydration but there are other alcohol types which can be used in this process. Then clearing process is started to separate dehydration substance (alcohol) from the tissue. This can be achieved by xylene, chloroform and so on.

Embedding:

After processing operations are finished, processed tissues are not hard enough to cut ultrathin sections from the tissue sample. Paraffin which is a kind of wax, is used for hardening the tissue. Generally, molten wax is used in this process because of the fact that it is easy to use and it does not give much harm to the tissue.

Sectioning:

Microtome is a special device which is used for cutting ultrathin sections from prepared samples. This device has very sharp blades to cut the specimen at the desired thickness level. Although there are several types of microtome devices, mostly rotary microtome device is used. In that device blade is fixed, and prepared tissue sample is positioned in the sample holder which is moved up and down to cut the sample. In the downward movement of the sample holder, cutting process occurs. Generally, thickness of the specimen varies between 3-5 μ . After that, sliced parts are put into the warm water and placed onto the glass slides.

Staining:

Sections of tissues on slides are colorless. Therefore, staining is applied to visualize the tissues for analysis. Since the stains used are water or alcohol based, cells must be filled with water again. For this purpose, all operations applied up to this point are performed in reverse order. The sample needs to be separated from paraffin which is called deparaffinization. Firstly, xylol is applied to remove paraffin. After that, alcohol is implemented to separate xylene, and tissue sections are steeped into the water for filling the cells with water, which is called rehydration. When these processes are

completed, the sample is ready for staining. Mostly used stains are H&E. In this case, hematoxylin stains the nuclei of the cells with color of blue, and eosin stains the cytoplasm with pink. After samples are treated with xylol for clearing, slides are mounted with balsam and cover slipped. Finally, the tissue samples are ready for analysis under the microscope. Prepared glass sample is demonstrated in Figure 2.5.

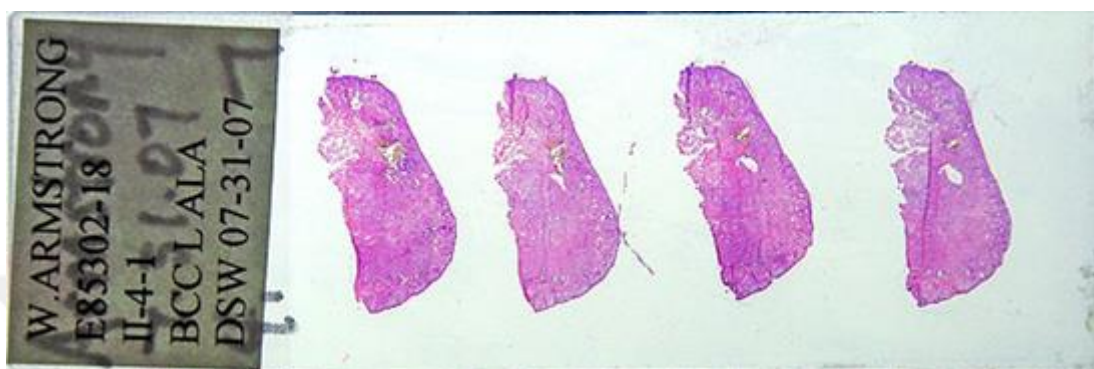


Figure 2.5 Stained glass samples [15]

2.2 Whole Slide Imaging (WSI)

Digital imaging in pathology has been started with capturing of the region of interest from prepared glass slide by mounting a camera onto the microscope. These images have been used in telepathology. Telepathology analyzes the glass slide at different locations by different specialist doctors. This reduces the consultation time with another specialist for the second opinion. This also enables to make diagnosis of the disease, when there is no specialist doctor. Obtained images may not be sufficient to diagnose the disease because the images show only a part of the glass slide. To solve this problem, robotic microscopy, which is used for a better diagnosis, provides the analysis of the glass slide from different locations. Consequently, storing whole glass slide into the memory becomes possible by using robotic microscopy.

WSI facilitates to share, analyze, research and teach by using digital slides. Since WSI is capable of the storing an entire image of glass slide, it enables to analyze the entire slide under the same conditions all the time. WSI images are obtained by using both hardware and software. Hardware part consists of slide handling, slide scanning, optics and detection while software part consists of acquisition software [13]. Slide handling

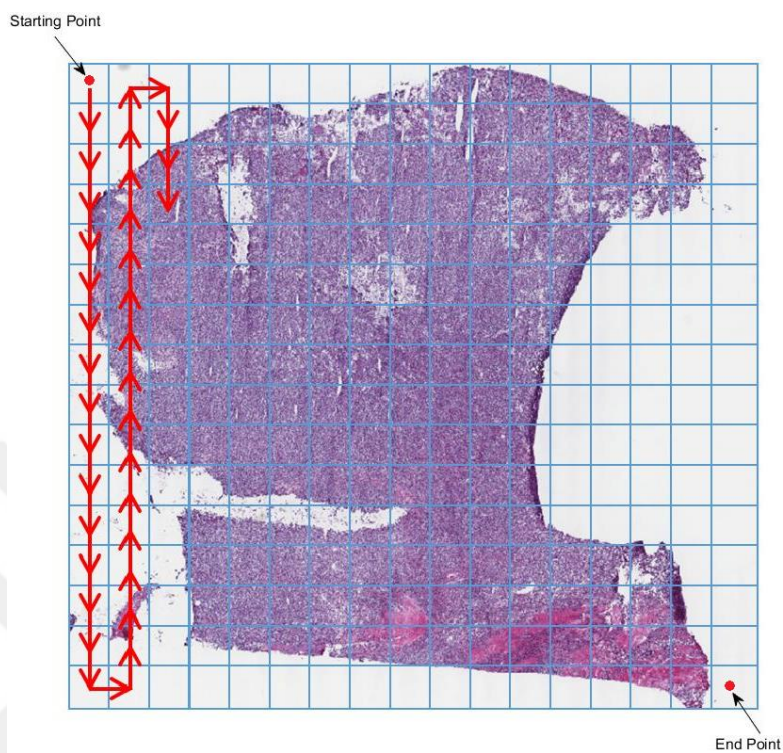
mechanism varies from model to model. When slide handling capacity increases, price of the WSI scanner goes up as well. Capability of scanning different sizes of the glass slides varies based on the model and the manufacturer. Glass slides are held in the slide magazines, besides bigger scanners have a holder to hold more slides. Robotics are used for both loading a new glass slide for scanning and moving the scanned glass slide. This is very important in batch processing because the glass slides should not be damaged when they are replaced.

After glass slides are prepared and loaded to the slide scanner, scanning process starts. It can be carried out by several ways. One of these methods is “tile scanning” which has been patented by Bacus [16], and shown in Figure 2.6 (a). In this method, the slide is divided into small grids and the image of each grid is captured. To produce WSI, taken images are aligned to each other which can be done either simultaneously or after scanning of the entire tile is finished in the glass slide. Another technique to obtain WSI is “line scanning” which has been patented by Aperio [17], and demonstrated in Figure 2.6 (b). Strips of the entire axis are captured and connected to each other similar to the previous method.

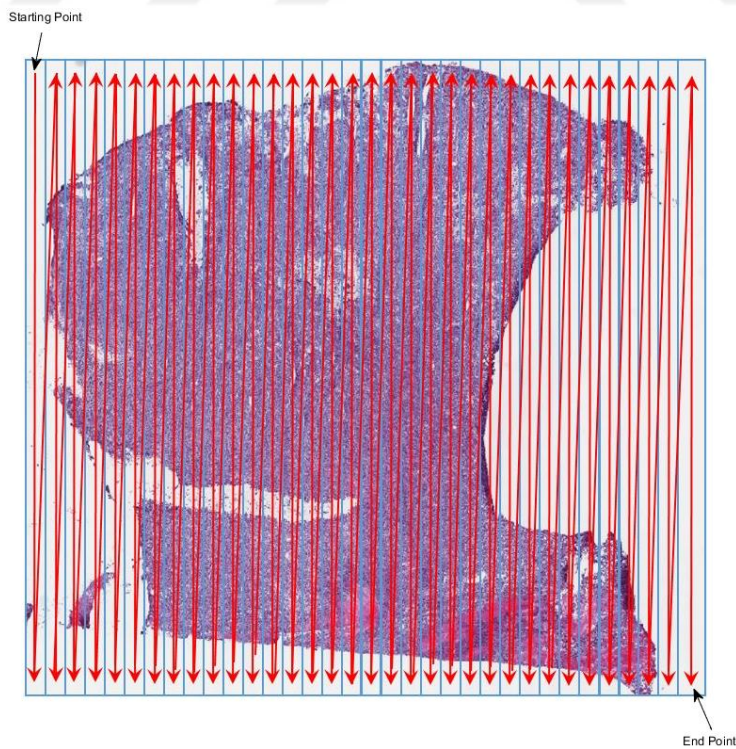
Quality of the digital slide is determined by the objective of the microscope, the camera sensor and the utilized software. There is a trade off between quality of the image and required storage space in the memory. If the quality of the image is increased, the fine details on the scanned glass slide image can be detected. To accomplish this, resolution of the scanned slide image must be increased. However, the required memory for storage of the digital slide should be escalated.

Focusing determines sharpness of the scanned digital slide. In traditional pathology, focusing is adjusted by the specialist by looking at the glass type of prepared tissue sample, thickness of the obtained sample and so on. Focusing is automatically implemented at the WSI. One of the methods is adjustment of focus after every certain number of fields is captured. It is a very simple method. The other method is called focus map. The focal points, where the focus calibration is made, are scattered all over the glass slide. The number of focus points can be increased or decreased based on the choice of the user. As the number of focus points increases, the time required to obtain the WSI escalates, since focus calculation is done more frequently, hence the

computation time of focusing expands. On the other hand, quality of the scanned tissue image improves.



(a)



(b)

Figure 2.6 Methods to obtain digital slide, (a) Tile scanning method, (b) Line scanning method

2.2.1 Storage and Visualization of WSI

Images obtained from scanning glass slide should be stored into the memory to visualize, analyze and access at any time. Digital slides are stored in the memory with different magnification levels, which determine the details on the image. Generally, glass slides are scanned up to 20X and 40X magnification levels. Some scanners can scan up to 100X magnification. In the 20X magnification, 0.5 microns per pixels (mpp) are captured and in the 40X magnification, 0.25 mpp represented by 1 pixel. Calculation of the digital slide size and memory space required for 20mm X 15mm glass slide at 40X magnification is

$$\begin{aligned} \frac{20mm}{0.25 \times 10^{-3}} \times \frac{15mm}{0.25 \times 10^{-3}} &= 80000 \times 60000 \text{ pixel} \\ &= 240000000 \text{ pixel} \end{aligned} \quad (2.1)$$

Since each pixel is combination of three colors in RGB image and each color requires eight-bit. So, required memory for storing that size of slide is

$$\begin{aligned} 240000000 \text{ pixel} \times 3 \text{ channel} \times 8 \text{ -bit} &= 5.76 \times 10^{10} \text{ bit} \\ &= 7.2 \times 10^9 \text{ byte} \\ &= 6.7 \text{ Gigabyte} \end{aligned} \quad (2.2)$$

That amount of memory is required in the raw format to store a single digital slide. Such a big image data of the digital slide can be stored by in less memory by using either lossless image compressing or lossy image compression methods. Tagged Image File Format(TIFF) is one of the lossless image compression methods. It provides storage and transferring of the same data with less memory than the original data without any image quality degradation. However, reduction in the file size is relatively small and all platforms do not work with this file type [18]. JPEG 2000 was done by a committee of Joint Photographic Experts Group in the year of 2000, which is a lossy image compression method [19]. Reduction in the file size is large compared to the lossless image compression methods. However, details on the image cannot be preserved because some of the data is lost during compression. Therefore, blurs on the

image occur after lossy compression methods. It is not an appropriate method if the sharp transition on the image must be preserved for the processing.

Each stored WSI data which contains multiple images with different magnification levels is denominated as a pyramid format. The structure of the data stored in the file, which contains different resolution levels of the same image, is similar to the shape of the pyramid as displayed in the Figure 2.7. The cross-sectional area gets smaller while approaching the top of the pyramid. So, the lowest resolution image of the glass slide which is called as a “Thumbnail Image” is represented near the top of the pyramid. In this zoom level, the entire area of the scanned glass slide is seen but details of the image cannot be observed. The bottom of the pyramid has the highest cross section area which is represented by the highest resolution image. This is called as “Baseline Image”. In the baseline image, details of the prepared tissue sample can be seen, but only a smaller part of the digital slide can be analyzed between the thumbnail image and baseline image, several images are captured at different magnification levels. They constitute “Intermediate Zoom Image”. Transitions between different zoom levels are done by using software which also contains the panning function. During the analysis, this allows to slide any direction of the higher resolution levels of the image, since viewing the entire digital slide image is not possible at higher resolution levels.

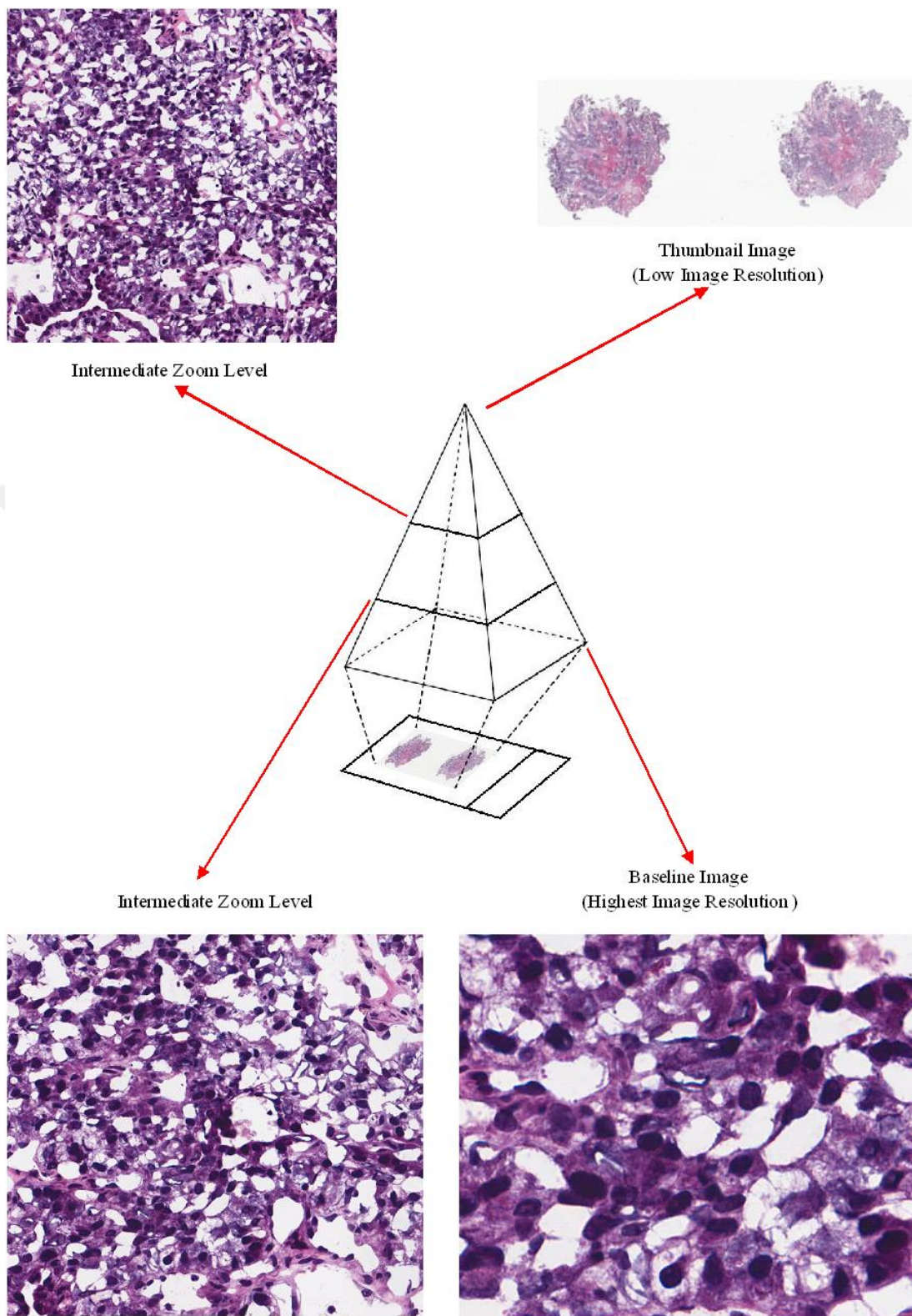


Figure 2.7 Pyramid structure of the whole slide Image

2.3 The Cancer Genome Atlas (TCGA)

Detecting the cancer disease at an early stage increases the survival rate. Determining the stage of cancer correctly has also a vital importance. It affects the treatment method, and it also determines which medication can be used for the treatment. One of the most accurate methods for diagnosing the cancer is histopathological examination of the obtained tissue sample from the patient under microscope. Analysis of the prepared glass slide can be made after digitalization of the prepared sample, which is possible by using slide scanner, and this was available more than a decade ago. Purchasing one of the slide scanners is expensive and therefore, possessing one of the slide scanners is not available at every hospital or medical faculty. Analysis of the same slide under equal conditions is significantly important for teaching as well.

In 2005, the project of the TCGA started to supply WSI and other data to assist researchers. TCGA enables to access many different samples of the major cancer types. Effects of the same cancer type to different people can be analyzed. This enables to make better diagnosis and prognosis. In 2006, policies, production pipeline, collaborative research network database and tools for analysis was under the guidance of National Cancer Institute (NIH) and National Human Genome Research Institute (NHGRI). American Recovery and Reinvestment Act invested \$175 million to generate genomics map of the cancer types in the following five years, which started in September 2009. TCGA provides more than 30 different cancer types and 10 of them are rare cancer types. Totally, obtained cancer data in the TCGA exceeds petabytes of data which are collected from more than 10000 cases. More than \$300 million has been invested to collect, maintain and provide that amount of information. TCGA offers cancer data to researchers freely. More than 2700 papers have been published using TCGA data since then [20-25].

CHAPTER 3

BACKGROUND FOR IMAGE PROCESSING

Digital image processing (DIP) methods are used to analyze images which are obtained from digital camera, and to improve image quality. These methods are applied to the images via computers. DIP is rapidly grown in the last four decades. Developments are derived from improvements of the computer technology in consequence of memory storage and data processing speed. Another factor is that attention of the researchers has increased to DIP. Today, the usage of DIP is widespread and widely used in everyday life. In particular, DIP has been applied in various areas such as image enhancement, medical image analysis, remote sensing, transmission and encoding, machine vision, pattern recognition, law enforcement and forensics, document processing, space image analysis and so on.

3.1 Concept of Image processing

Simply, the image can be thought of as the optical reflection of the specific area recorded in memory, and can also be viewed through the monitor at the same time. The procedure of obtaining the image via camera can be defined by gathering the reflective lights from the desired area or object by using camera lenses. These reflective lights produce analog signals that represent the image. These analog signals should be converted to digital signals since computers cannot interpret analog signals. To generate a digital signal from the analog signal, the samples are taken from the analog signal at equal distances, which is called sampling. In each sample point holds the amplitude of the analog signal which is called intensity or brightness value of that location from the analog signal. To visualize, these sample values are stored on the equally spaced grid form. Here the intensity values are still continuous. To discretize these values, quantization is applied. Quantization is the transformation of the continuous set of values into the discrete values. After that, the values stored on the computer at a certain range and consumed less memory. In Figure 3.1, image capturing process is presented.

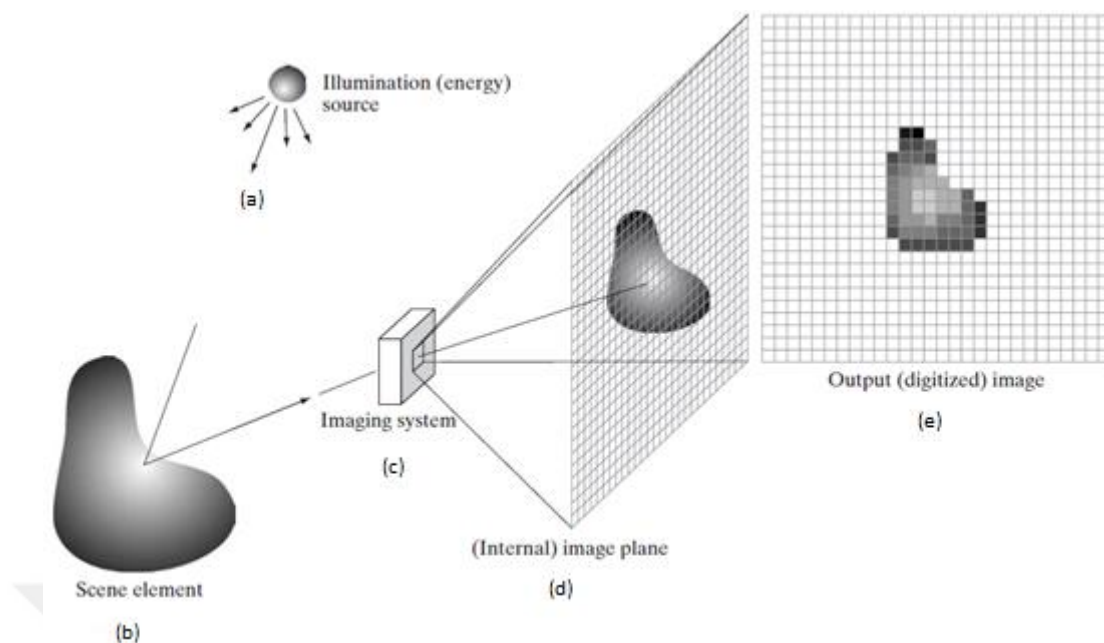


Figure 3.1 Coming lights from the source (a), reflected lights by the object (b) captured by the imaging system (c), the continuous image shown after process of sampling and quantization the output of the digitalized image obtained (e) [26].

Maximum value to store the sample values was calculated with the equation in (3.1). “n” corresponds the number of bits that can be used to store in each sample. The values were stored with varies in $\{0,1, 2, \dots, 2^n - 1\}$ [26,27].

$$L = 2^n \quad (3.1)$$

The quality and the storage of the image are determined by both the sampling interval and the quantization level. In each value of the pixels was stored as a two-dimensional (2D) array in the memory. The resolution of the image will be determined by how many samples were taken from that image and the memory space was required to store. Image can be calculated as multiplication of the sample size by number of bits used to store each pixel. As can be seen in Figure 3.2, original image is an 8-bit image, when used quantization levels are reduced, transition between the gray levels of the image increases and false contouring effect can be observed. Reducing the spatial resolution of the image, details of the image may be lost and checkerboard effects might occur. In both cases, the quality of the image is reduced. When only a single bit is used, binary image is obtained.

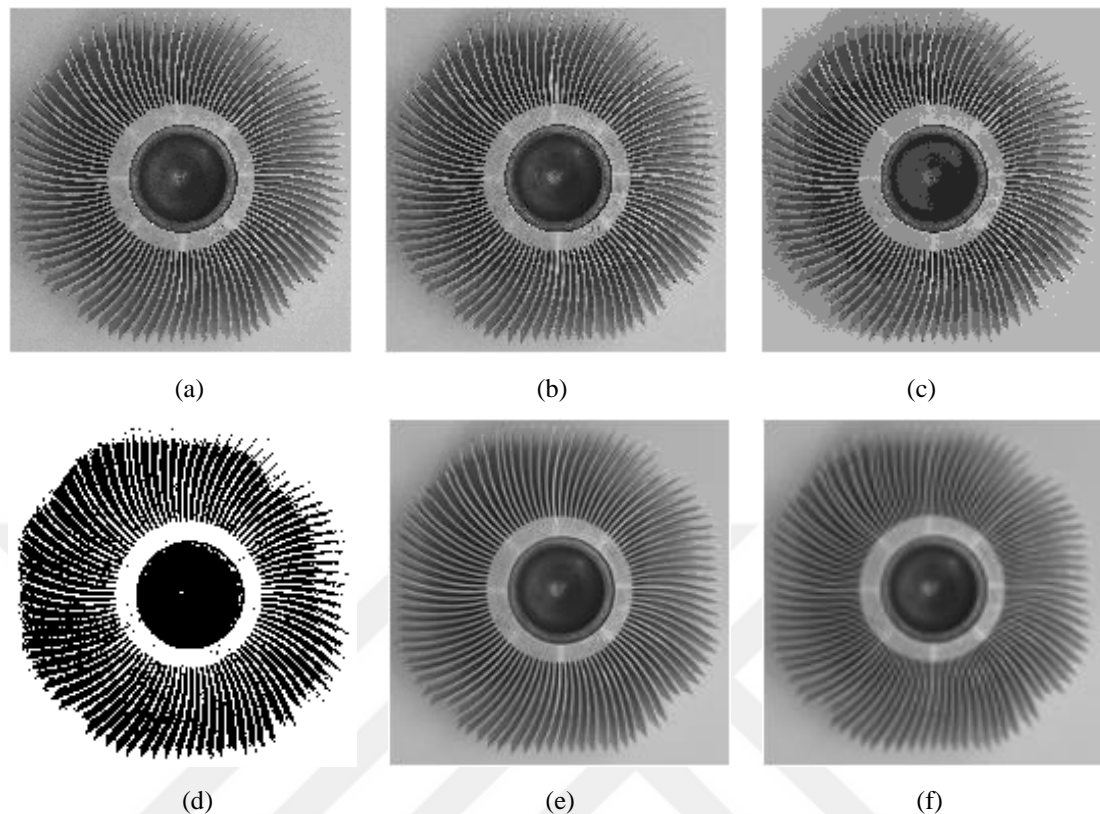


Figure 3.2 Changing gray levels and spatial resolution. (a) 8-bit, 1600x1600 original image; (b) 6-bit original image; (c) 3-bit original image; (d) 1-bit (binary) original image; (e) 1/8 times reduction of spatial resolution; (f) 1/16 times reduction of spatial resolution

Each element of an 2D image array is considered as a pixel and holds the intensity values of specified location after sampling and quantization. The dimension of the array generally represented by M -rows and N -columns denoted by $M \times N$. Multiplication of these values gives the resolution of the image. To access the elements of the array, the index numbers are used as in matrix operations in algebra. The top-left corner defines the first pixel of the image and is accessed by the image (1,1), the bottom-right value is accessed by the image (M,N) as seen in the Figure 3.3. To access the other elements in the image (i,j), range of i starts from 1 to number of rows and j starts from 1 to number of columns [26,27].

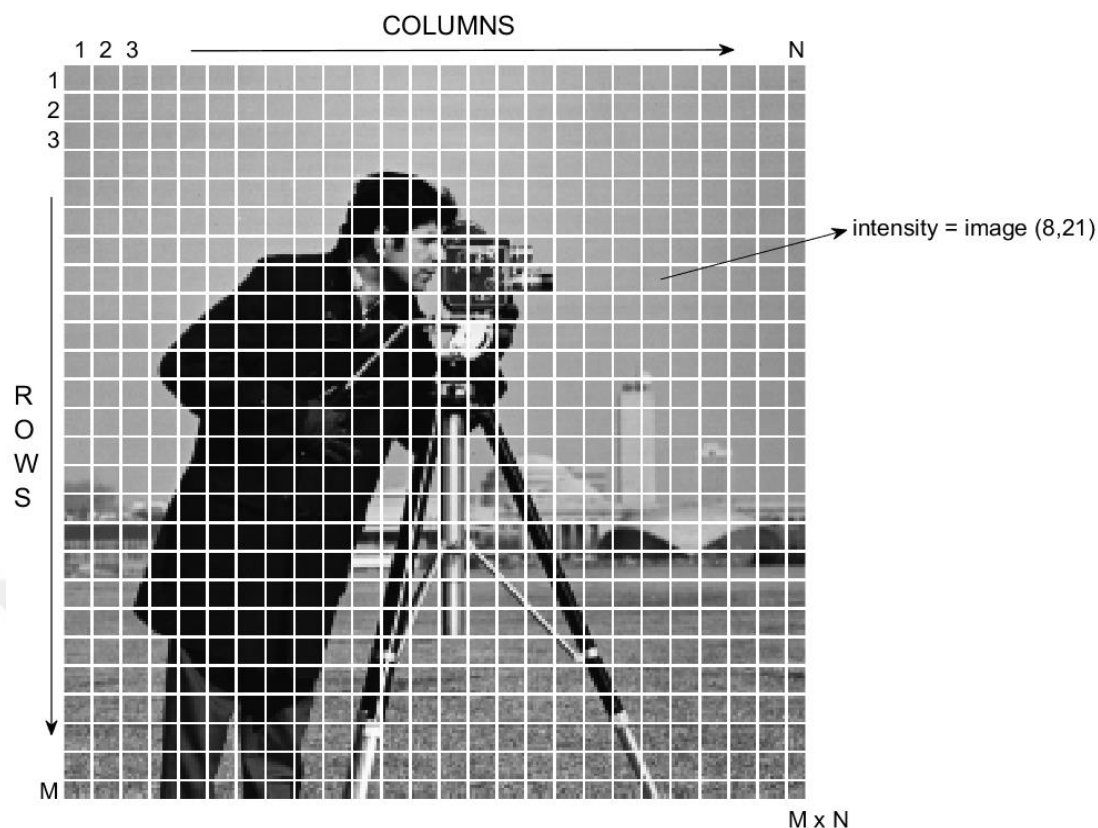


Figure 3.3 After sampling and quantization applied to cameraman image storage into the memory. Top-left corner accessed with (1,1) and right bottom is equal to the image size (M,N). Intensity values of that location can be accessed by entering the rows and columns of the desired pixel.

3.2 Types of Images

When an image is formed only at black and white pixel values, it is called a binary image. It consists of two values which are zero and one. Zero represents the background pixels and one represents the foreground pixels. To clarify, zeros equal to the black pixels and ones equal to the white pixels which are the parts of the object pixels. The number of bits required in each pixel in binary image is one, so their size is small. For these reasons, it is generally used in fax machines and laser printers [27].

Since binary images contain only black and white values, it's not possible to detect details of the object or understand what is in that picture. The number of bits used per pixel must be increased to produce meaningful images. For this reason, samples taken from the image can be mapped into shades of gray called as gray scale image. In this

case, pictures can contain the shades of gray values or gray levels. The number of gray levels can be determined by equation (3.1). For example, when n chosen three, it will only be capable of storing the numbers in $\{0,1,\dots,7\}$, zero represents the black and seven represents the white. The gray colors between black and white separated into 6 levels and closer to zero values represents the dark gray values. Lighter gray colors are represented by higher values. Usually eight bits per pixel are used to create adequate details in the picture. Therefore, gray level range varies from 0 to $2^8 - 1$ which is 255 [26,27,28]. Grayscale image and small section of the grayscale image and intensity values as a matrix form are shown in Figure 3.4.

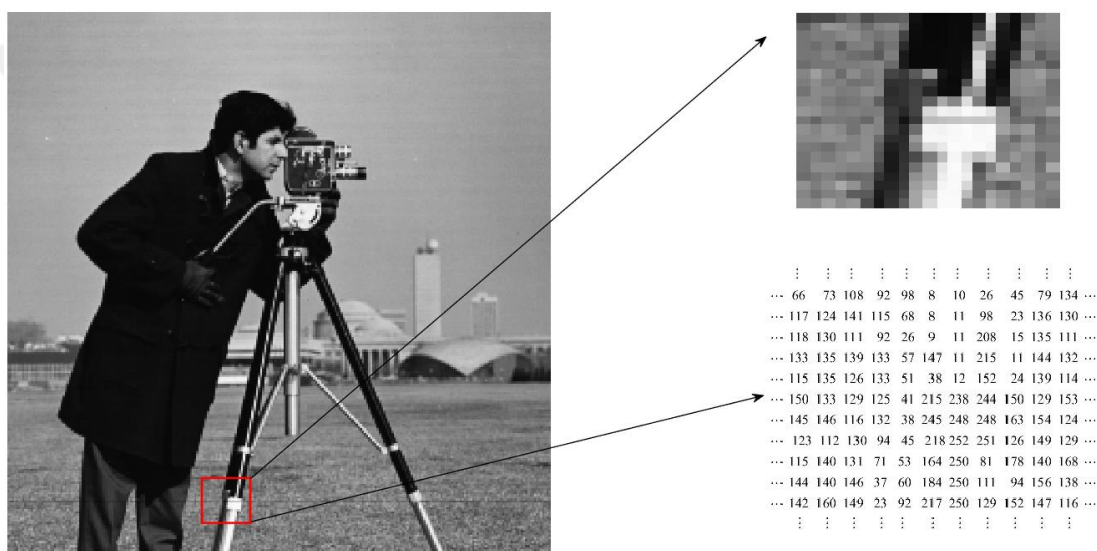


Figure 3.4 Cameraman image and small section of it both in numerical and the image form. In numerical form, lower values represent darker pixels. Intensity values closer to 255 maps for white areas in the image.

The human visual system views objects as a color image rather than a gray scale or binary image. To represent a color image, basically three main colors are used: red, green and blue. Different colors can be derived by using these three main colors in different ratios. In the process of image obtainment, stimulated photons are collected in the small light cavities. To generate colorful images, color filter is applied to each small cavity. Using this color filter, it is possible to measure how much of each of three main colors is contained. The filter only passes certain colors and rejects other colors. Generally, Bayes Array filter is used as a color filter [29]. Since a colorful

picture contains three different density values for each pixel, the storage of a colorful image requires three 2D arrays for each main color and each one is stored as eight-bit intensity levels so that each pixel's representation is 24 bits. Three components and combinations of the colorful image are shown in Figure 3.5.



Figure 3.5 Lena image and three intensity values of the determined area. Each color intensity value storage requires 8-bit and totally 24-bit

3.3 Color Space

Color modeling is required to describe and to analyze images in details. The color space helps to understand the pixel's properties. The International Lighting Commission on Color Illumination (CIE) XYZ [30] created the first color model using the human color detection system. Other color models are derived from this color model.

The color model commonly used in computer graphics is the red green and blue (RGB) color model. In this model, the diversity of colors is obtained by adding these primitive colors in different combinations. Computers store each primary color in three different matrices, and range values vary from 0 to 255. When the pixel value of one of the primary colors is equal to zero, that component is not added. When it equals to the

255, which states full intensity, one of RGB colors are fully added to the combination of the pixel. For example, to get a white color, all three primary color values must be equal to 255. Since there is no color component for the black color, all the primary color values are equal to zero. When a color is represented by three different color components and each color is 8 bits, $(2^8)^3$ different colors can be obtained. As can be seen in the Figure 3.6, origin (0,0,0) represents the black, the farthest point from the origin i.e., (255,255,255) is white, gray scale values are in the diagonal line between black and white colors. Primary color represented in the corners of each axis and remaining corners represents cyan, magenta and yellow [26].

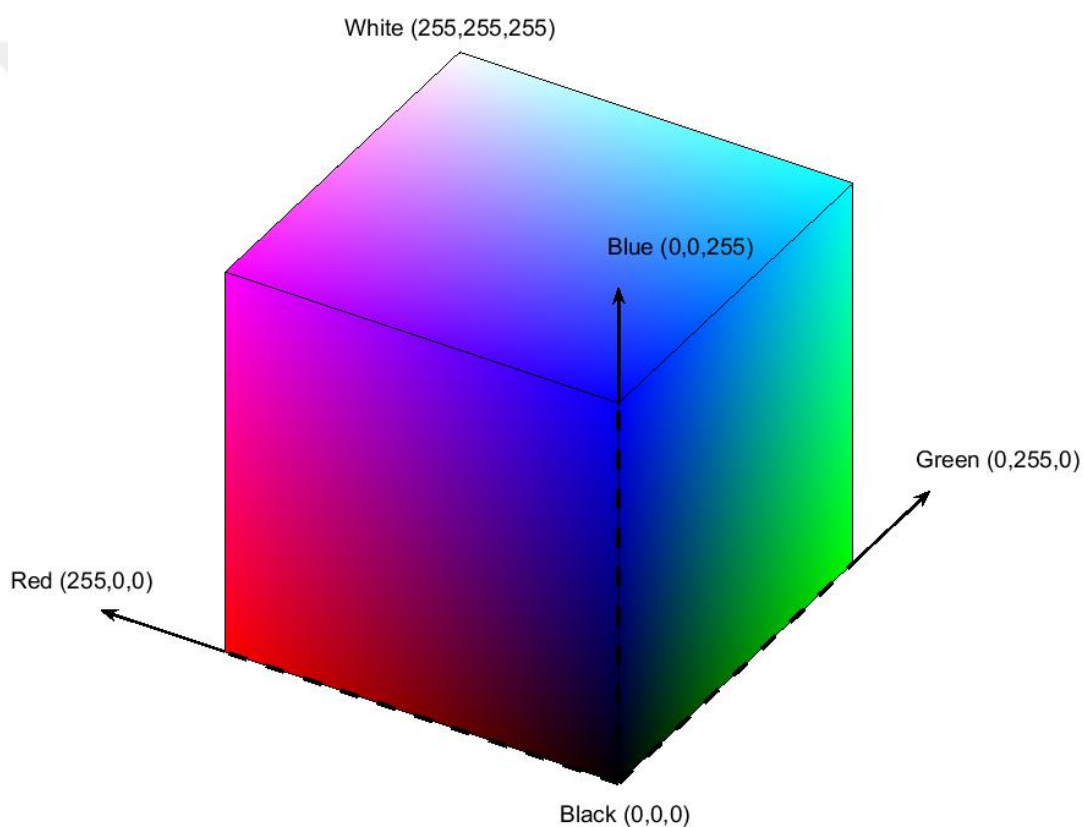


Figure 3.6 RGB color cube

The Cyan Magenta Yellow Black (CMY(K)) color model is a color model that differs from the RGB model, and is often used in printing. Yellow is one of the primary colors of subtractive colors. On the other hand, it is obtained by combining red and green colors in RGB model. Because the CYM model is subtractive, yellow light can be

obtained when the blue light is subtracted from the reflected white light. If the quality of dark tones is to be increased, black color is added to that color space. When these main colors are removed, the resulting color is white. A white paper is shown as white when ink is not sprayed. If the paper is sprayed ink in any color, the intensity of the sprayed color is subtracted from that of white color and it gives a different color. Theoretically, blue, magenta and yellow should give a black color when combined, but it actually gives a dark brown color, so black is added to this area to achieve an adequate black color and improve the quality of dark tones [26,31,32]. Color conversion between RGB and CMY, and from CMY to CMYK are obtained by the following equations [33].

$$\begin{bmatrix} \text{Cyan} \\ \text{Magenta} \\ \text{Yellow} \end{bmatrix} = \begin{bmatrix} 1 \\ 1 \\ 1 \end{bmatrix} - \begin{bmatrix} \text{Red} \\ \text{Green} \\ \text{Blue} \end{bmatrix} \quad (3.2a)$$

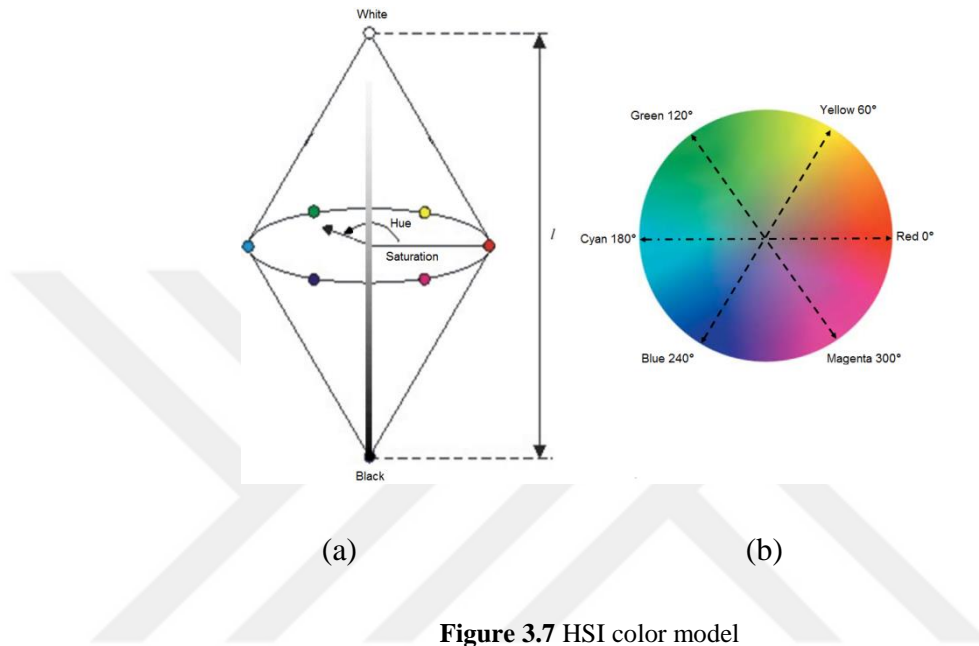
$$\text{Black} = \text{minimum} (\text{Cyan}, \text{Magenta}, \text{Yellow})$$

$$\begin{aligned} \text{Cyan} &= \frac{\text{Cyan} - \text{Black}}{1 - \text{Black}} \\ \text{Magenta} &= \frac{\text{Magenta} - \text{Black}}{1 - \text{Black}} \\ \text{Yellow} &= \frac{\text{Yellow} - \text{Black}}{1 - \text{Black}} \end{aligned} \quad (3.2b)$$

Where, all parameters of the color name represent the level of color intensity between 0-1. The color intensity value in the range of 0-1 can be obtained by dividing each intensity value by 255 for the eight bit representation.

One of the models describing a color is Hue Saturation and Intensity (HSI), and at the same time, similar to the human description system of colors. Hue represents the color of the pixel on the color wheel ranging from 0-360. The red color corresponds to 0 degrees, the green 120 degrees, the blue 240 degrees. The saturation determines the color purity. If the color is pure, it is saturated and not diluted with white light. When it is not saturated, the hue component passes through the center of the circle and obtained color is becoming duller. When the saturation is equal to 0, all colors become

the gray center of the circle. Simply, saturation defines how much gray paint has been added to that color. Intensity range is between [0,1], 0 denotes black and 1 denotes white. At the middle, it is equal to gray and original color is obtained at 0.5 intensity. HSI color model, and hue and saturation representations at intensity level of 0.5 are illustrated in Figure 3.7.



Conversion from RGB to HSI is given below:

$$I = \frac{1}{3} (R + G + B) \quad (3.3a)$$

$$S = 1 - \frac{3}{(R + G + B)} [\min(R, G, B)] \quad (3.3b)$$

$$\theta = \cos^{-1} \left\{ \frac{\frac{1}{2} [(R - G) + (R + B)]}{\left[(R - G)^2 + (R - B)(G - B) \right]^{1/2}} \right\} \quad (3.3c)$$

$$H = \begin{cases} \theta & \text{if } B \leq G \\ 360 - \theta & \text{if } B > G \end{cases} \quad (3.3d)$$

Equation (3.3a) gives the calculation of the intensity at which R, G, and B represent the intensity values of the pixel. The equation (3.3b) gives the calculation of the saturation. To calculate θ , the equations (3.3c) and (3.3d) are used.

3.4 Geometric Configurations of Objects

Object properties can be calculated from an outline of an object which is referred as contour. The contour of the object stored by the pixel location in the computer is similar to the Cartesian coordinate system. The difference between them is that y axis increases downward, x axis rightward [26]. Since the contour pixels are connected to each other, they are located at one of the adjacent pixels. For this reason, storing the next pixel in true x and y coordinates is a waste of memory. Then, after the contour has started a pixel from the pixel location, other locations can be determined by one of eight directions from that point and are encoded on a computer. In this way, only three bits, which are sufficient to represent each point of the contour, will reduce memory usage.

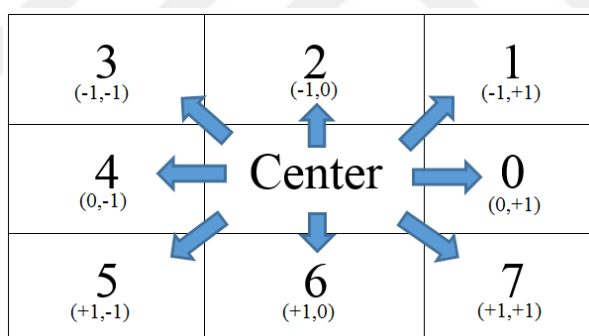


Figure 3.8 Eight neighborhood

Inverse digits are used to calculate both path reduction and determination of whether an arbitrary geometric curve is open or closed. Inverse digits can be estimated by finding symmetrical directions of the candidate points into the origin. Another way of finding the inverse digit is making vector summation. When vector summation of two digits' direction is equal to zero, it states that they are inverse digits. For example, vector summation of 3 (-1,-1) and 7 (1,1) gives (0,0) and also 3 is symmetrical to the origin by 7.

Table 3.1 Possible digit-replacement couples and inverse-digits [34].

	0	1	2	3	4	5	6	7
0			2	3	*	6	7	
1				22	2	*	0	0
2	1				3	4	*	0
3	2	22				44	4	*
4	*	2	3				5	6
5	6	*	4	44				66
6	7	0	*	4	5			
7		00	0	*	6	66		

Path reduction helps to calculate the minimum distance between the starting and ending points of the arbitrary geometric curve. Encoded digits contain inverse digits so that they cancel each other in the process of path reduction because the position of the ending point is not affected by the deletion of inverse points. In short, the goal of path reduction is to find the close distance between the starting and ending points. Two digits can be replaced with one digit to reduce memory usage and also two digits can be represented by two digits to simplify the calculation. During this process, the refunctioned digits do not have to be one of the eight neighboring pixels of the reduced pixel. Eight neighborhoods of the pixel are shown in Figure 3.8. Two digits' replacement and inverse digits are represented in Table 3.1. For example, when 1 and 4 are seen on the path, they can be reduced to 2. When 5 and 3 are seen on the path, they can be represented as 44, which is equal to the distance, as well as easier to calculate. The inverse digits are indicated by the symbol * in the Table 3.1. To find the inverse digits in the table, the inverse digit to be found in a row is followed up to * symbol, after that, it should be referred to the first column of the * symbol. The digit in the top column of the * symbol is called the inverse digit. When the inverse of 2 is required, the * symbol can be found on the seventh element in the table, the first element of this column is 6, so the inverse of 2 is 6.

When the adjacent pixel is horizontal, the distance between each adjacent pixel is assumed to be 1 unit, and if the adjacent pixels are diagonal, the distance between each adjacent pixel is equal to the square root 2. For the calculation of any contour length, even digits are counted and summed with the number of odd digits by $\sqrt[2]{2}$ times.

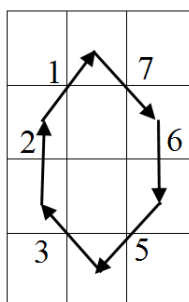


Figure 3.9 Set of encoded points

Open curve does not end with a starting point position but the closed curve defines a continuous curve whose starting and ending points are at the same location. Thus, if there are no digits after the path reduction, it defines a closed curve. On the other hand, if it does not provide this property it is called an open curve. For instance, consider the set of points 1-7-6-5-3-2, where 1 and 5, 2 and 6, 3 and 7 points are inverse digits since there are no digits after the path reduction. Therefore, it defines a closed curve. If the path does not contain any of the digits from the set, one of the digits will not be deleted and it will be an open curve. The coverage area of a closed curve calculation can be carried out in several ways. One of the easy methods is the summation of the number of pixels in that region. The other area measurement method is based on Freeman's algorithm. In this method, only two variables are needed: modifier B and a variable for the holding summation of area that will be activated continuously for all of the encoded digits in the path. The previous modifier variable B is used for the calculation because the current value of B is the modifier value of the leading edge. To simplify the calculation, starting point of the contour is overlapped the origin and initial value of the starting point B is assumed to be zero. Table 3.2 gives the calculation of the area of a contour.

Having the set of equations in Figure 3.9, the first encoded digit is 1, so the area is equal to $\frac{1}{2}$ and B equals to 1, then the next digit is 7, the area is equal to $\frac{1}{2} + 1 - \frac{1}{2} = 1$ and so on. Finally, the area is equal to 4 and B is equal to 0. Precision of the calculation gives better results when compared to the first method.

Table 3.2 Area calculation [34]

Slope	Change in Area	Change in Modifier
0	+B	0
1	$+B + \frac{1}{2}$	+1
2	0	+1
3	$-B - \frac{1}{2}$	+1
4	-B	0
5	$-B + \frac{1}{2}$	-1
6	0	-1
7	$+B - \frac{1}{2}$	-1

3.5 Distance Transformation

Distance transform (DT) is one of the fundamental operations in image processing and computer vision. DT is applied to binary images consisting of object pixels and background pixels. DT calculates the minimum distance from the object pixel to the background pixel according to the selected distance metric.

Most commonly used distance metrics are city block distance, Euclidean distance (ED), and chessboard distance [35-37]. The mathematical definitions of these distance measurements are given below.

$$\text{City-block distance: } D = |x_1 - x_2| + |y_1 - y_2| \quad (3.4a)$$

$$\text{Chessboard distance: } D = \max(|x_1 - x_2|, |y_1 - y_2|) \quad (3.4b)$$

$$\text{Euclidian distance: } D = \sqrt{(x_1 - x_2)^2 + (y_1 - y_2)^2} \quad (3.4c)$$

Where x_1, y_1, x_2, y_2 are the locations of the points k and l respectively, D is the distance which is calculated on the basis of the method used. The chessboard distance is the maximum value of the differences in both coordinates so that it is equal to 1 in the eight neighbors of the middle pixel. City-Block is also known by different names such as Manhattan distance, L_1 norm or taxi cab metric. In this method, the distance measurement is computed as the sum of the absolute differences between the coordinate points. As its name implies, a cab cannot pass through a building, it must go around the building to arrive its destination. ED or L_2 norm is the shortest distance between two points, which is calculated with equation (3.4c). All three distance measurements have the same value in 4-neighbors and also the diagonal neighbors of the center pixel have the same value in chessboard. However diagonal neighbors are different in city block and ED. In city block distance, diagonal neighbors of the center pixel have the value of 2. In the ED, they have the value of $\sqrt{2}$. In Figure 3.10, three letter distance conversion is shown using Euclidean transformation. Once specific operations related to distance transformation have been applied to the image, the skeleton of the objects can be obtained.



Figure 3.10 Application of distance transformation (a) binary image as an input (b) distance transformation of the image

The calculation of city block and chessboard distances are made iteratively compared with the ED. The calculation of the city block and chessboard distance depends on the position of the object. However, the Euclidean distance does not depend on the position of the object, since it is rotation invariant. ED is preferred because it gives the

shortest distance compared to other transformation methods; hence, many algorithms have been developed to speed up the computation time of the ED transformation [38,39].

3.6 Connected Component Labelling

Labeling assigns a unique identifier to describe an object by giving different positive numbers for each different object. Connected Component Labeling (CCL) plays an important role in image processing applications such as medical image analysis, optical character recognition, object counting, and others. CCL is mostly applied to binary images to label foreground pixels features such as size, position and connected objects in the picture. Once CCL has been applied to a binary image, each pixel in the foreground has an identifier based on the connectivity (4 or 8) of the neighborhood pixels.

In 4-connectivity, the north, south, east and west pixels are considered to be adjacent to the processed pixels and these pixels are taken into consideration. Likewise, in 8-connectivity, cardinal and intercardinal pixels are taken into consideration as the processed pixels. If the processed foreground pixel has the 4-connectivity or the 8-connectivity, the same identifier is assigned to that pixel. If no identifier is found in the neighborhood, different identifier is assigned the processed pixel. After CCL is applied, all foreground clusters connected to each other have the same identifier and unconnected pixel clusters have a different identifier. Figure 3.11 shows the results of 4-connectivity and 8-connectivity algorithms. As shown in the Figure 3.11(a), 4-connectivity gives incorrect results depending on the structure of the object, but 8-connectivity gives better results. Because positive decimal numbers are used for labeling, the number of objects in the image can be found.



(a)



(b)

Figure 3.11 Implementation of the connected components algorithm of 3 ‘u’ shaped letters, (a) 4 connected, (b) 8 connected

Increasing the speed and accuracy of CCL has been studied by different researchers, so different algorithms can be found in the literature [40-42]. In real-time applications, the processing speed of the algorithm is very important. The first study about CCL is presented by Rosenfeld and Pfaltz in 1966 [43]. In the literature, this study is called classical approach which uses the two pass algorithms. At the same time, this algorithm is used as a comparison criterion for many studies. As its name suggests, CCL passes twice over all pixels in the binary image. As with many applications in image processing, each pixel is processed one after another using scan masks as shown in Figure 3.12. Scanning starts from the left-top to the end of the first row and passes through the following rows. In the first scan, preliminary labels of each foreground pixels are assigned. During that process, each processed pixel is checked; if all the

neighbor pixels of the processed pixel are background pixels, new label is assigned to that pixel. When one of the neighboring pixels has a label, the current pixel is assigned with that label. If more than one label are found in neighboring pixels, the smallest label is assigned to the processed pixel and then the provisional label and the equivalence label are added to the equivalency table (ET) that is used during the merging of the different labeled components. Parts of objects are sometimes connected at the bottom so that the upper parts of that object can be labeled with different identifiers, which often occurs 'u' shaped objects. After finishing the first scan of all the pixels, ET is sorted by the smallest label and then the smallest label will be assigned to connected objects with the different labels.

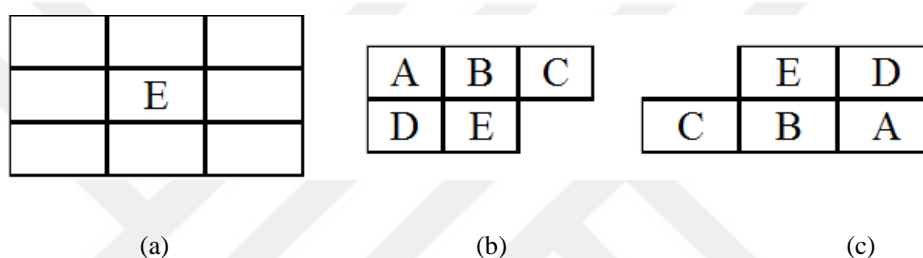


Figure 3.12 Eight connected neighborhood, (a) central pixel E and the eight neighborhoods, (b) forward scan mask, (c) backward scan mask

Haralick et al. developed a new algorithm in which all the pixels were scanned forward and backward masks until labeled pixels were not changed. Firstly, all the pixels are labelled in the same way with two pass algorithm. Label conflict has occurred because the initial process is similar to two pass algorithm. Label conflicts are solved using forward and reverse scan mask as shown in Figure 3.12(b) and 3.12(c). Since it does not use ET, the number of raster scanning may be high based on the complexity and the dimensions of the input image but it uses less memory compared to the two pass algorithm [44].

Contour tracing based CCL was implemented by Chang et al. in 2004 [45]. In this study, pixels which are inside the detected contours of the objects are assigned with the same label. This method also traces the pixels one by one but only one pass is required to label all connected components during the raster scanning, when the processed pixel is a background pixel, the processed pixel is shifted to the next pixel.

When an unlabeled foreground pixel is detected, the algorithm starts to find contour of the object and it continues until it reaches back to the starting pixel. At this time, it also assigns the same label to all contour pixels. After the contour tracing has finished, the label is increased by one and continues to search for other pixels. If the processed pixel is already labelled and the following pixel is an unlabeled foreground pixel, the labeling of the area between the contour pixels begins. In this process, all the pixels between the first encountered and the next encountered labelled pixels in the same row are assigned with the same label. For comparison with two pass and multiple scan algorithms, the label conflict does not occur in the contour tracing based CCL, hence merging is not required.

3.7 Image Filtering

Noise in the image may result from analog to digital converter, low light, quality of the sensor and so on. Quality of an image affects the result of the analysis. The objective of filtering is to reduce noise while preserving the information.

Spatial domain filter can be grouped into two categories which are linear filters and non-linear filters. Similar to CCL, masks are used to perform this operation. Unlike CCL, size of the mask may vary in dimensions, but generally 3x3 matrix size is preferred.

Linear filtering in spatial domain is performed by convolution or correlation. In correlation, center of the kernel is aligned with the processed pixel and then the operation is performed. Kernel is moved through in each pixel, computed value assigned to that location. This value equals to the summation of overlapped mask components and image values multiplication. The difference between convolution and the correlation is that kernel is rotated 180° before starting computation in convolution. Therefore, when the mask is symmetrical, the both operations give the same result [26,46]. Any point in the image, the calculation of correlation and convolution is given below

$$F(x, y) = h * f(x, y) = \sum_{i=-k}^k \sum_{j=-l}^l h(i, j) f(x+i, y+j) \quad (3.5)$$

and

$$F(x, y) = h * f(x, y) = \sum_{i=-k}^k \sum_{j=-l}^l h(i, j) f(x-i, y-j) \quad (3.6)$$

respectively. Where h denotes the kernel with dimension of $(2k+1) \times (2l+1)$ and f represents the input image and F is the filtered output image.

The square matrices of which the number of total elements are odd numbers are used mostly in image processing which is equal to $(2k+1, 2k+1)$, where k can take positive integer numbers. Filter mask exceeds the image dimension during the process of filtering outer rows and columns of the image. This problem can be solved by either reducing dimensions of the image or padding outer rows and columns of the image. There are different types of padding methods such as zero, constant, replicate, wrap, mirror and extend. In the zero padding, outer edges of the image are padded with zeros. In constant padding method, specified constant value is used for padding the array. In the replicate padding method, image's border pixel intensity values are padded. In the wrap padding method, image can be thought as a cylindrical form in which right border of the image is considered to merge with left border. It is also valid for the top and bottom of the image borders as well. For this reason, padding of the image is started from the opposite outermost line of pixels. Padding continues with one line of pixel closer to the padding edge. This also continues depending on the kernel size of the filter. Mirror padding also called symmetric padding that pads the array as if a mirror was put to the outer rows and columns of the image and pads the image using reflected intensity values. Padding with symmetric and wrap methods are presented in figure 3.13. In the extended padding method, which is the last method, padding is fulfilled by mirrored padding intensity values subtracted from the edge pixel intensity value [46].

124	102	102	124	121	138	133	133	138	124	138	142	142	156	124	138	142	142
150	140	140	150	125	128	142	142	128	116	120	115	122	146	116	120	115	122
150	140	140	150	125	128	142	142	128	128	142	140	150	125	128	142	140	150
124	102	102	124	121	138	133	133	138	138	133	102	124	121	138	133	102	124
131	146	146	131	129	114	142	142	114	114	142	146	131	129	114	142	146	131
130	137	137	130	130	129	151	151	129	129	151	137	130	130	129	151	137	130
154	162	162	154	156	130	114	114	130	130	114	162	154	156	130	114	162	154
142	142	142	142	156	124	138	138	124	124	138	142	142	156	124	138	142	142
122	115	115	122	146	116	120	120	116	116	120	115	122	146	116	120	115	122
122	115	115	122	146	116	120	120	116	128	142	140	150	125	128	142	140	150
142	142	142	142	156	124	138	138	124	138	133	102	124	121	138	133	102	124

(a)

(b)

Figure 3.13 Padding part of an image with, (a) symmetric padding method, (b) wrap padding method

3.7.1 Spatial Domain Smoothing Filters

High frequency components of the image are prone to noise compared to the low frequency components. Applying smoothing filter can reduce the noise on the image but it also adds a blur to the image. Therefore, the edges in the image become smoother. Mostly used spatial domain smoothing filter types are Mean, Gaussian low pass, and bilateral filtering [26,46,47].

Mean Filter :

Calculation of the mean filter is one of the easiest one. Mean filter is a linear filter and also called as an averaging filter because filtered pixel value is determined by calculation of the average intensity values of the neighborhood pixels. Therefore, neighborhood pixel has equal contribution to the processed pixel value. The number of pixels taken into consideration is based on the filter size. When the size of the filter is bigger, more pixels intensity values affect the processed intensity value of the pixel. Mean filtered intensity value of the pixel is demonstrated as

$$image(i, j) = \frac{1}{mn} \sum_{k \in m} \sum_{l \in n} f(k, l) \quad (3.7)$$

where m and n are sizes of the filter, $f(k,l)$ are the intensity values of the neighborhood, $image(i,j)$ is the processed pixel intensity value after averaging of the neighboring pixel intensity values.

Size of the kernel determines the reduction of noise and the smoothing scale of an image. When the size of the mask increases, noise decreases but blur on the image expands. Consequently, details on the image decreases. In Figure 3.14, increasing size of averaging filter is applied to a gray scale image. When size of the filter increases from 3x3 to 7x7, transition between the objects border become smoother.

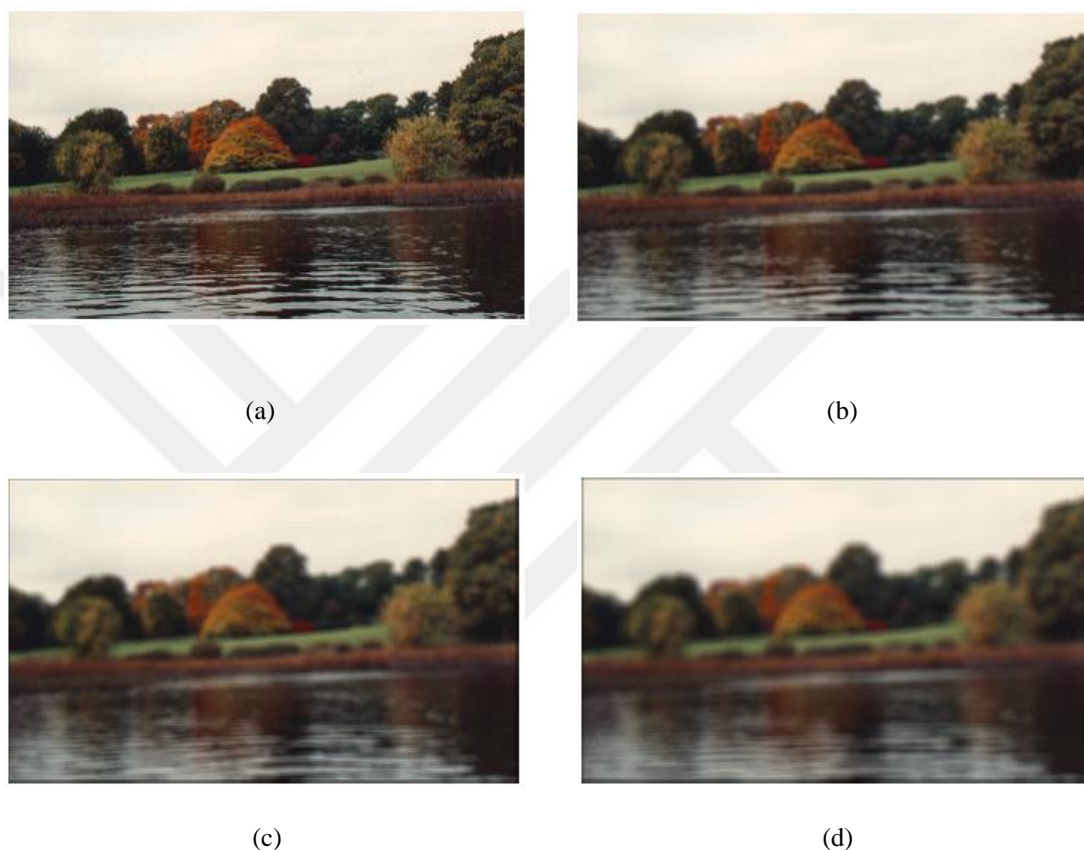


Figure 3.14 (a) Autumn image as an input RGB image and increasing filter size of the averaging mask applied images with, (b) 3x3, (c) 5x5, (d) 7x7

Median Filter :

Median filter is one of the mostly used type of nonlinear filters in noise reduction. During operation of the median filtering, center of the mask is aligned with processed pixel, and intensity values in the neighborhood is sorted in ascending order. When total number of elements in the kernel is odd number, the middle of the intensity value is assigned to the processed pixel. If filter dimensions are even number, there are two middle values. In that case, average of these intensity values is assigned to the

processed pixel. In Figure 3.15, computation of the median filter for one of the pixels using with 3x3 kernel is demonstrated.

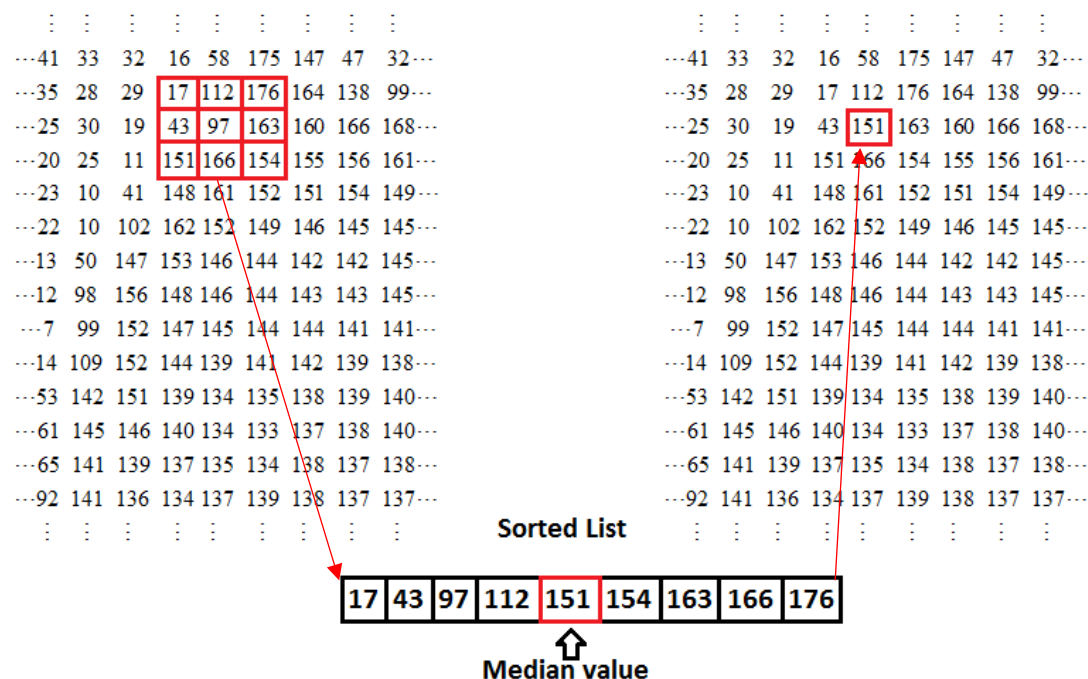


Figure 3.15 Process of the median filter with 3x3 kernel and output

While both median and mean filters are used to reduce the noise on the image, the success of filtering to reduce the noise on the image depends on the noise type. In certain noise types, such as impulse noise, salt and pepper noise, median filter yields good results because in this type of noise, intensity values of the noisy pixels have different intensity value compared to the neighborhood pixels intensity value. After these pixels in the kernel are sorted, noisy pixels are located either close to the first or last element. Therefore, these pixels are not taken into consideration, while assigning the processed pixel's intensity value. But, in the average filtering, all the pixels in the kernel has equal contribution to the processed pixel value. So, noise in the image is distributed to the pixels in the average filtering. This leads to blur in the edges after averaging filter applied to the image. Therefore, quality of the picture is decreased and information on the edges are reduced. On the contrary, median filter removes the noise on the image, while maintaining the details of the image.

Generally, 3x3 mask is used for median filtering because, as stated in the averaging section, filter size has an effect upon blur of the image. In Figure 3.16, salt and pepper added to a gray scale liftingbody image and 3x3, 7x7 median filter applied images are shown. 3x3 median filter results is effective for salt and pepper noise reduction while preserving the transitions in the image. When the size of filter is increased, the noise reduces, but the blur of image expands.

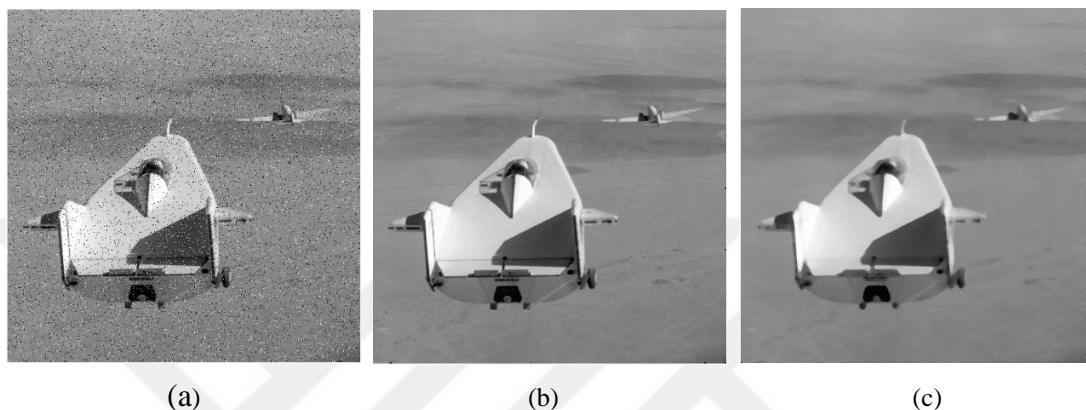


Figure 3.16 (a) Salt and pepper noise added lifting body image, (b) 3x3 median filter applied image, (c) 7x7 median filter applied image

Aside from the other mentioned filters, the other nonlinear filters are maximum filter, minimum filter, midpoint filter and so on. In the minimum filter, after neighboring intensity values are sorted from the lowest to the highest, the lowest intensity value is assigned to that pixel, so removing a salt noise is possible using with minimum filter that has high intensity values. Apart from minimum filter, maximum filter assigns maximum intensity value in the neighborhood to the processed pixel. Pepper noise comprise of lower intensity values; hence maximum filter can be used for noise reduction. Midpoint filter, which assigns the average of the minimum and the maximum intensity values in the neighborhood pixels, is mainly used for randomly distributed noise [26,46].

Gaussian Filter :

Gaussian low pass filter is a linear filter which is more convenient to remove Gaussian noise from the image. It is similar to averaging filter, but coefficients of each element

in the kernel is not equal. Coefficients of each element in the Gaussian filter mask are calculated based on Gaussian function

$$G(x, y; \sigma) = \frac{1}{2\pi\sigma^2} e^{-\frac{x^2+y^2}{2\sigma^2}} \quad (2.8)$$

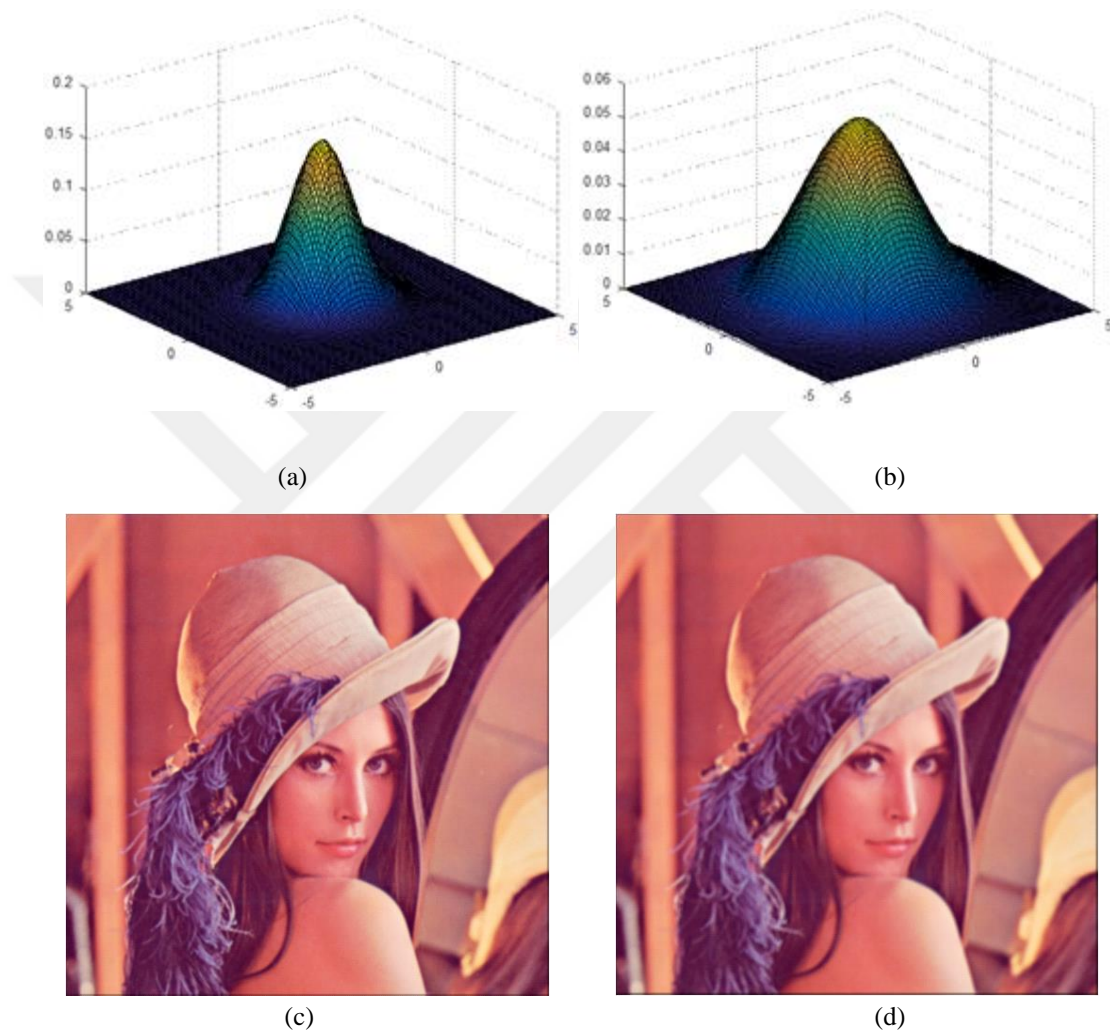


Figure 3.17 3D representation of the Gaussian kernel with 5x5 mask size and 1σ and 3σ (a), (b) respectively, (c) Gaussian filter with parameters in (a) applied image, (d) Gaussian filter with parameters in (b) applied image.

If the distance between central pixel of the mask and neighborhood pixels is increased, the weight of the pixels in the mask decreases. Therefore, pixels closer to the central pixel have higher weight and vice versa. Smoothing degree in the Gaussian filter is based on standard deviation. When it increases, Gaussian curve becomes wider,

therefore, difference between coefficients of the mask's element is decreased. Different standard value of the Gaussian filter mask and their application on the image are shown in Figure 3.17. If standard deviation of the filter increases, Gaussian curve becomes smoother and more details on the image are lost [26,48].

3.7.2 Spatial Domain Sharpening Filters

Sharpening filters are used for emphasizing details of the image. Therefore, they reduce blurs and accentuating transitions in the image. On the contrary to sharpening filters, the spatial domain smoothing filters add blur to an image. Spatial differentiation is used for performing spatial sharpening filters while averaging intensity methods are generally used in spatial smoothing filters. Similar to smoothing filter methods, mask is moved over in each pixel; however, coefficients of the kernel contain negative values. Accordingly, processed pixels' intensity value may take negative values after the operation. When using unsigned eight-bit integer numbers, storing a negative value is not possible, so negative values of the processed pixel are assigned to zero [47].

Differentiation of an image helps to demonstrate transitions on the image. The higher transition changes are indicated by the colors close to white, and the slower transition changes are represented by the colors close to black. [47]. Enhanced images can be obtained by adding specified amount of sharpening filter applied image to the original image. Spatial sharpening image defined as

$$y(i, j) = f(i, j) + c * h(i, j) \quad (3.9)$$

where, h represents the line structures and edges in the image which can be generated by applying high pass filter to the image. c determines the sharpening scale which is a constant value. f and y refer the input and the sharpened image respectively. High pass filtered and enhanced images are shown in Figure 3.18.



Figure 3.18 (a) High pass filter applied cameraman image, (b) sharpened cameraman image with $k = 1$

Laplacian Filter :

Laplacian filter is one of the spatial domain sharpening filtering in the image processing. It emphasizes the fast intensity change and also trivializes the slowly changing intensity values. Laplacian filter uses the second derivative of an image, while Sobel, Prewitt, Robinson and Kirsch filters use the first derivative to process an image. First derivative of one-dimensional function is equal to difference between subsequent intensity pixel values is defined as

$$\frac{\partial f}{\partial x} = f(x+1) - f(x) \quad (3.10)$$

Second order derivative of one-dimensional function is expressed by

$$\frac{\partial^2 f}{\partial x^2} = f(x+1) - 2f(x) + f(x-1) \quad (3.11)$$

Implementation of the Laplacian filter is easy compared to the others. Moreover, it is an isotropic filter which means that it is rotation invariant. Laplacian can be defined as

$$\nabla^2 f(x, y) = \frac{\partial^2 f(x, y)}{\partial x^2} + \frac{\partial^2 f(x, y)}{\partial y^2} \quad (3.12)$$

where discrete form of Laplacian derivative is expressed as

$$\frac{\partial^2 f(x, y)}{\partial x^2} = f(x+1, y) - 2f(x, y) + f(x-1, y) \quad (3.13)$$

and

$$\frac{\partial^2 f(x, y)}{\partial y^2} = f(x, y+1) - 2f(x, y) + f(x, y-1) \quad (3.14)$$

to x and y coordinate respectively. The Laplacian kernels are shown in the Figure 3.19.

0	-1	0
-1	4	-1
0	-1	0

0	1	0
1	-4	1
0	1	0

Figure 3.19 Laplacian kernels for implementing the equation 3.14 in image processing

If the central element of the kernel is a negative number, filtered image is subtracted from the original image and sharpened image is obtained. When the center element of the kernel is positive number, filtered image is added to an input image. The Laplacian filter can also be applied in one step to reduce the computation time. Enhanced image defines as

$$\begin{aligned} g(x, y) &= f(x, y) - \nabla^2 f(x, y) \\ &= 5f(x, y) - f(x-1, y) - f(x+1, y) - f(x, y-1) - f(x, y+1) \end{aligned} \quad (3.15)$$

Laplacian filter, which is also used for edge detection, can detect the edges in various directions. However, it is prone to noise compared to others. As seen in Figure 3.20, the Laplacian filter makes the edges more explicit and the sharpened image can be obtained from original and Laplacian filtered image.

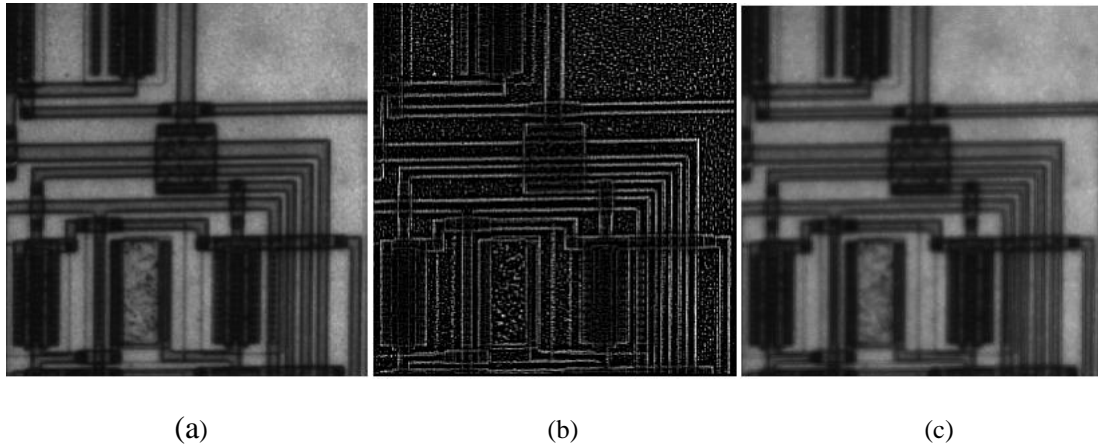


Figure 3.20 Representation of the Laplacian sharpening procedure of an image, (a) circuit gray scale image as an input, (b) Laplacian filtered image, (c) sharpened image

Generally, image sharpening methods are used to enhance the transitions in the image and detect the edges on the images, but they are prone to noise. Although, image smoothing methods are used for reducing the noise on the image, blur in the image expands [49].

CHAPTER 4

IMAGE SEGMENTATION AND CONTOUR DETECTION

Image segmentation and contour detection are frequently used methods for analyzing an image. These subjects have been excessively studied by many researchers and there is an ongoing study to find better methods. Image segmentation, which is a mid-level image processing application, builds the communication between low-level and high level image processing applications. [47]. An image is partitioned by segmentation to obtain meaningful cluster of pixels or smaller parts of areas, such as objects and humans. The extraction of objects in the image is also made possible by segmentation. Each segments of the image have similar distinctive features based on the used segmentation method. These features are intensity value, color, texture, depth and so on.

Segmentation methods can be partitioned into three groups based on the human intervention to that process. These groups are: manual, semi-automatic and fully-automatic segmentation. Manual segmentation is carried out by the human, so the segmentation is highly accurate, however the process can be time consuming and subjective. In fully-automatic methods, user intervention is not possible and the process time is short but the accuracy depends on the image. In comparison with other methods, it is susceptible to noise. Semi-automated methods use both human and computer algorithms to segment an image. They are widely used in medical image processing due to the unreliable results of fully-automatic segmentation methods and the long processing time of manual segmentation. [50-52].

The number of segments in the image determines the success of the image segmentation and affects the accuracy of further processing. Problems resulting from the number of segments in image segmentation methods are over-segmentation and under-segmentation. When the image is partitioned into too many segments, it is considered as over-segmentation. So, region of an object in the image is separated into

more than one segment, which a single segment is sufficient. In order to overcome this problem, region merging techniques are used based on the determined criteria. Another problem of the segmentation, the image is partitioned into very few segments, called as under-segmentation. Since the image obtained in the under-segmentation includes bigger parts, they can contain more than one object. This reduces the truthfulness of the segmentation results. For example, in Figure 4.1(a), input grayscale is segmented into 3 parts, and each segment is demonstrated by 3 different shades of gray, 4.1(b) input image is segmented into 15 segments, and segments are represented by 15 different colors of gray. As seen in Figure 4.1(a), one segment represents more than one object. On the other hand, in Figure 4.1(b), one object is composed of more than one segment.



(a)



(b)

Figure 4.1 Over segmentation and under segmentation image (a) Lena is segmented into 3, (b) Lena image is segmented into 15.

4.1 Thresholding

Thresholding segments the image into two partitions which are foreground and background. These partitions are obtained by the intensity values of each pixel that are used for the segmentation of the image. As mentioned in previous chapter, lower intensity values of the pixels are closer to black color and it usually represents the background. Foreground pixels, which correspond to the objects in the segmented image, are determined by the higher intensity values. But, it may be the opposite based on the application. For example, nucleus pixels correspond to lower intensity values in the gray scale image. Whether the processed pixel belongs to the foreground or background is determined based on the threshold value T . Any location which is a foreground pixel is assigned as “1”.

If the intensity value is smaller than the threshold value T , assigned value is 0, and considered as a background pixel. After all the pixels in the image is processed, binary image is obtained. Segmented image can be written as

$$g(i, j) = \begin{cases} 1 & \text{if } f(i, j) > T \\ 0 & \text{if } f(i, j) \leq T \end{cases} \quad (4.1)$$

where g represents the segmented image, which is a binary image, f represents the input grayscale image and T is the threshold value which is used for converting a grayscale image into a binary image.

The threshold value T is extremely significant on thresholding methods. When threshold value is high, most of the pixels in the image considered as a background pixels even if they belong to an object pixels. When the threshold value T is lower than the adequate value, most pixels are considered as object pixels. In that case, recognized object pixels consist of both object pixels and plenty of background pixels. These pixels do not belong to the object pixels. Therefore, selected threshold value determines the accuracy of the segmentation and affects the process afterwards. In literature, plenty of methods have been developed to find out an adequate threshold value.

Threshold value can be global or adaptive based on the selected thresholding method. In the global threshold methods, threshold value is a constant value determined by either calculation or entered by user. This value is determined firstly and then applied to the entire image. Based on the image, global thresholding can yield good results. However, in case of nonuniform illumination of the same object's pixels, global thresholding fails at some points. This situation stems from the lighter and darker regions of the same object. To avoid this case, adaptive thresholding methods can be used to increase the performance of the segmentation. In the adaptive thresholding methods, threshold value is adjusted by computing the neighborhood intensity values and changes during the process. This method is also called local thresholding.

To find an optimal threshold value, histogram of the grayscale image can be used. Histogram of the grayscale image shows the number of pixels in each gray level which are between 0 and 255 in the eight-bit grayscale image. In optimal conditions, threshold value can be selected by examining the histogram. Generally, threshold value is chosen between two peaks in the histogram.

When all the object pixels are homogeneous and the background pixels have also the same intensity value, choosing the threshold value becomes easy because a clear distinction occurs in the histogram between intensity values of the object pixels and the background pixels' intensity value.

Figure 4.2 (b) shows the histogram of the created input image in Figure 4.2(a). As seen in Figure 4.2(b), it has four different intensity values in the histogram: the shortest bar on the histogram represents the smallest object 'i', the second shortest bar in the histogram represents the second object 'L', which is bigger than the first object and smaller than the third object 'A'. The second tallest line represents the biggest object 'A' which covers more area than the second object. The longest bar represents the background pixels' intensity value. Background intensity value bar is the longest one because it contains more pixels compared to objects. The size of the input image is the summation of objects pixels' number and background pixels'.

In reality, distribution of the foreground and background intensity values are not easily separated from each other due to the noise on the image, nonuniformity of the

illumination and so on. Therefore, optimum threshold value is determined by benefiting from peaks and valleys of the histogram. In Figure 4.2 (d) is the histogram of the image in Figure 4.2 (c).

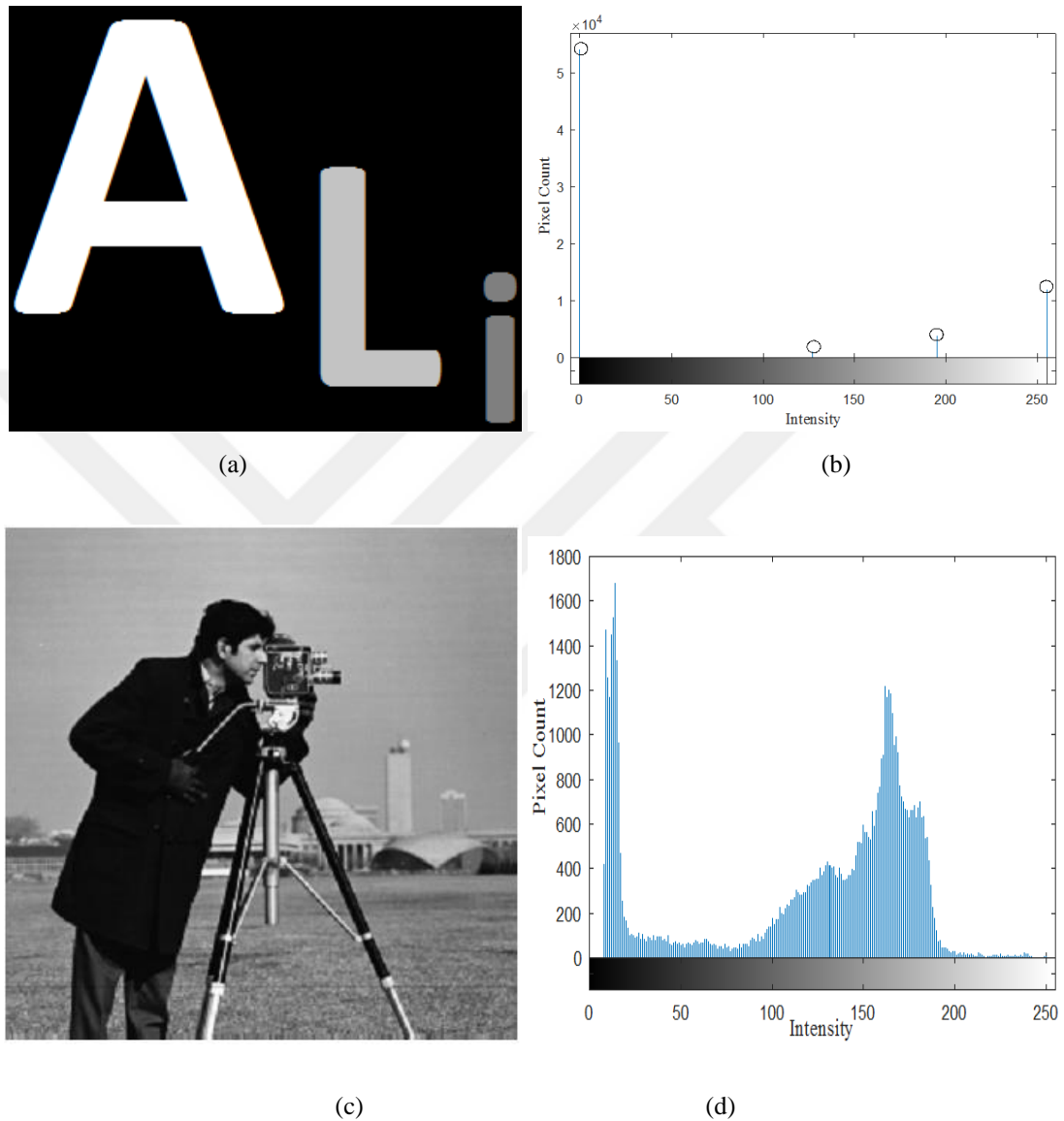


Figure 4.2 (a) Image with 3 letters with different intensity values, (b) histogram of the image (a), (c) Cameraman image, (d) histogram of the cameraman image (c).

As seen in Figure 4.2(d), it is obvious that there is no clear separation between the foreground and background intensity values. Therefore, finding an optimal threshold value is hard. Plenty of algorithms have been developed to find an optimal threshold

value. Sezgin et al. classified 40 different image thresholding methods into 6 groups according to the information to be processed, which are [53]:

- Histogram shape based techniques
- Cluster based techniques
- Entropy based techniques
- Object attribute based
- Spatial techniques
- Local techniques

As explained above, shape of the histogram can give some information about the foreground and background separation intensity values, and it is used in the histogram shape based techniques [54,55]. Due to the fact that binary image is obtained after thresholding operation and only two values are presented in the output, these are 0's and 1's. Therefore, the cluster number is equal to two in the clustering based thresholding techniques. In this group, some of the methods used fuzzy logic based clustering technique which assigns membership to the pixels using with mean intensity value of each class and intensity values of the pixels. In addition, other methods calculate the threshold value by minimizing the difference between the average intensity values of each cluster [56,57].

Entropy is used in many different areas. It is also used in the image thresholding methods. Entropy evaluates disorderedness of the system. In entropy based techniques, threshold value which gives the highest entropy of the summation of both clusters is chosen as a threshold value. In some methods of entropy based thresholding, it is intended to find the smallest possible value of the cross entropy between the input grayscale image and the thresholded image. [58,59].

In the object attribute based thresholding techniques, threshold value is chosen depending upon attribute quality or similarity measurements, such as grayscale image moments, edge matching, fuzzy similarity and so on [60,61].

In spatial thresholding methods, distribution of the gray level and neighborhood pixel dependencies are used simultaneously [62,63].

In the local thresholding techniques, threshold value is changed based on the neighborhood pixels. On the contrary to global thresholding methods, same threshold value is not applied to the entire image. To find a threshold value in this group, average intensity, median, average of the maximum and minimum intensity values and some others can be used [63,64].

4.1.1 Basic Global Thresholding

One of the easiest methods to determine a threshold value is basic global thresholding method. The background and foreground pixel clusters are sometimes easily distinguishable in some images. Peaks and valleys in the histogram can be observed. In this case, object and background pixels' separation point is straightforward and equals to one of the smallest points between peaks of two clusters. To find an appropriate threshold, firstly, initial threshold value is chosen from the range between the minimum and maximum intensity values of the input image. Generally, the mean value of all pixels in the image is chosen as an initial threshold value. Then, background and foreground pixels are determined by the formula in equation 4.1. Thresholding operation applied in all the pixels on the image, and hence foreground and background pixels are determined. After that, mean intensity values of each group are calculated and stored in μ_1 and μ_2 as background and foreground intensity values, respectively. After that, calculation of the new threshold value is obtained by

$$T_{new} = \frac{\mu_1 + \mu_2}{2} \quad (4.2)$$

Finally, the process is repeated until the difference between new threshold value and previously calculated threshold value is lower than the predefined value ΔT , which is initially defined before the process starts. Flow chart of the implementation is described in Figure 4.3.

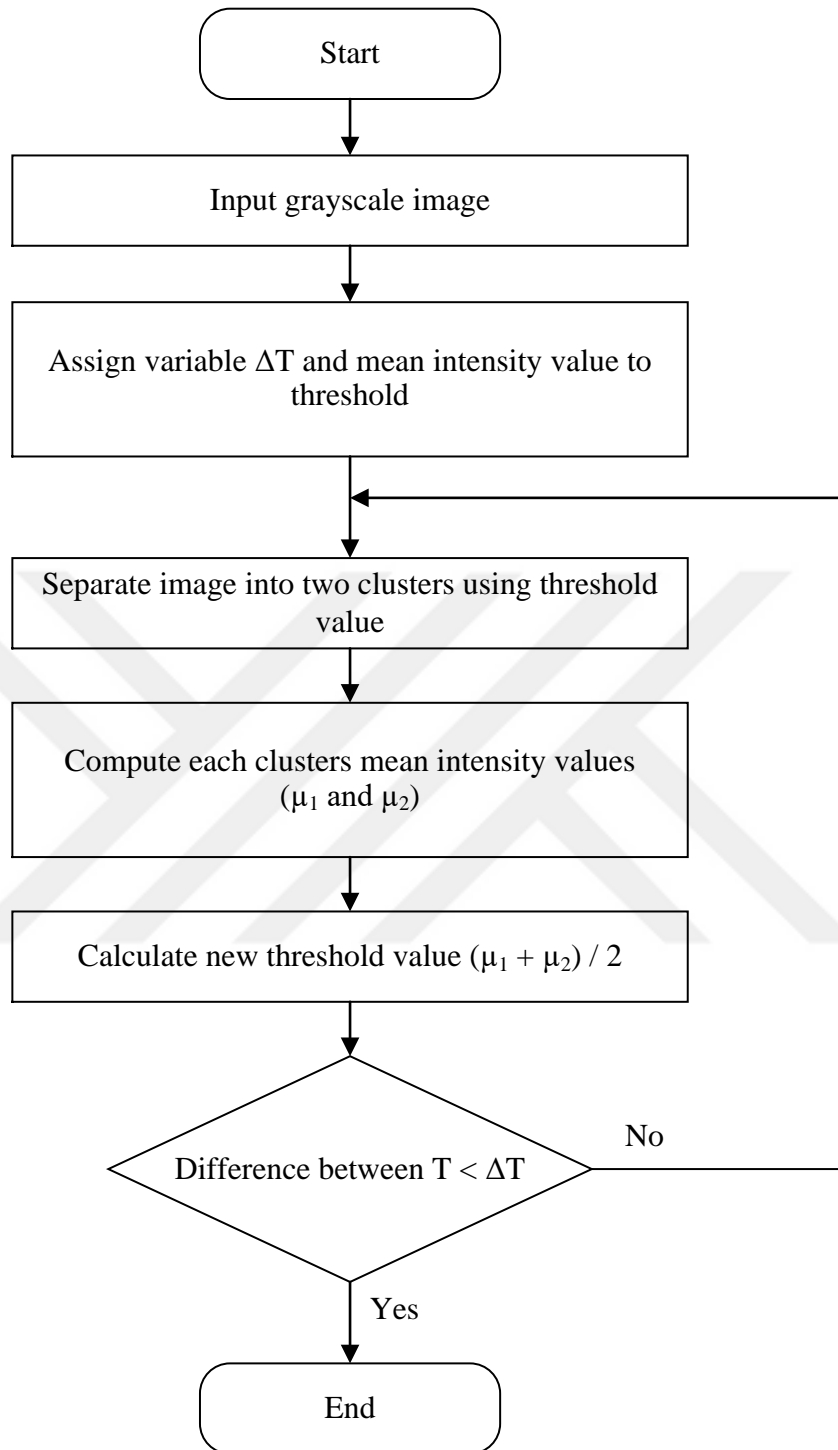


Figure 4.3 Flowchart of the basic global thresholding method

4.1.2 Otsu's Thresholding Method

The OTSU threshold method which is one of the most famous methods in global threshold methods, was introduced in 1979 [56]. OTSU's method, which is one of the unsupervised techniques, aims to minimize the weighted within-class variance of foreground and background classes with the computed threshold value. By means of minimizing within-class variance, maximization of the between-class variance is obtained. Statistical methods are used for finding the threshold value.

In calculation of the OTSU's thresholding, n_i denotes number of pixels at the i^{th} grayscale intensity value and N represents the number of all the pixels in the image which is equal to the $n_0 + n_1 + n_2 + \dots + n_{L-1}$. Probability of the i^{th} pixel is represented with p_i and it is obtained from division of n_i to the total number of pixel, N . Probability of the within-class and between-class variance are computed as

$$w_1 = P_1(k) = \sum_{i=0}^k P_i \quad (4.3)$$

and

$$w_2 = P_2(k) = \sum_{i=k+1}^{L-1} P_i \quad (4.4)$$

respectively. Class means are described by

$$\mu_1 = \sum_{i=0}^k iP(i/C_1) = \sum_{i=0}^k \frac{iP_i}{w_1} \quad (4.5)$$

and

$$\mu_2 = \sum_{i=k+1}^{L-1} iP(i/C_2) = \sum_{i=k+1}^{L-1} \frac{iP_i}{w_2} \quad (4.6)$$

respectively. Variances of each class is described as

$$\sigma_1^2 = \sum_{i=0}^k (i - \mu_1)^2 P(i / C_1) = \sum_{i=0}^k (i - \mu_1)^2 \frac{P_i}{w_1} \quad (4.7)$$

and

$$\sigma_2^2 = \sum_{i=k+1}^{L-1} (i - \mu_2)^2 P(i / C_2) = \sum_{i=k+1}^{L-1} (i - \mu_2)^2 \frac{P_i}{w_2} \quad (4.8)$$

By using means and variances of each class, within-class and between-class variances are calculated by

$$\sigma_w^2 = w_1 \sigma_1^2 + w_2 \sigma_2^2 \quad (4.9)$$

and

$$\sigma_b^2 = w_1 (1 - w_1) [\mu_1 - \mu_2]^2 \quad (4.10)$$

where σ_w^2 represents within-class variance and σ_b^2 represents between class variances. Total variance is equal to the summation of within-class variance and between-class variance. Optimum threshold value is determined by examining the within-class variance or between-class variance. For this purpose, all the intensity values in the range starting from 0 to 255 are computed to find the threshold value. Following that, the intensity value which makes the within-class variance value minimum or between-class variance value maximum is selected as a threshold value. Flowchart of the OTSU's threshold algorithm is exhibited in Figure 4.4.

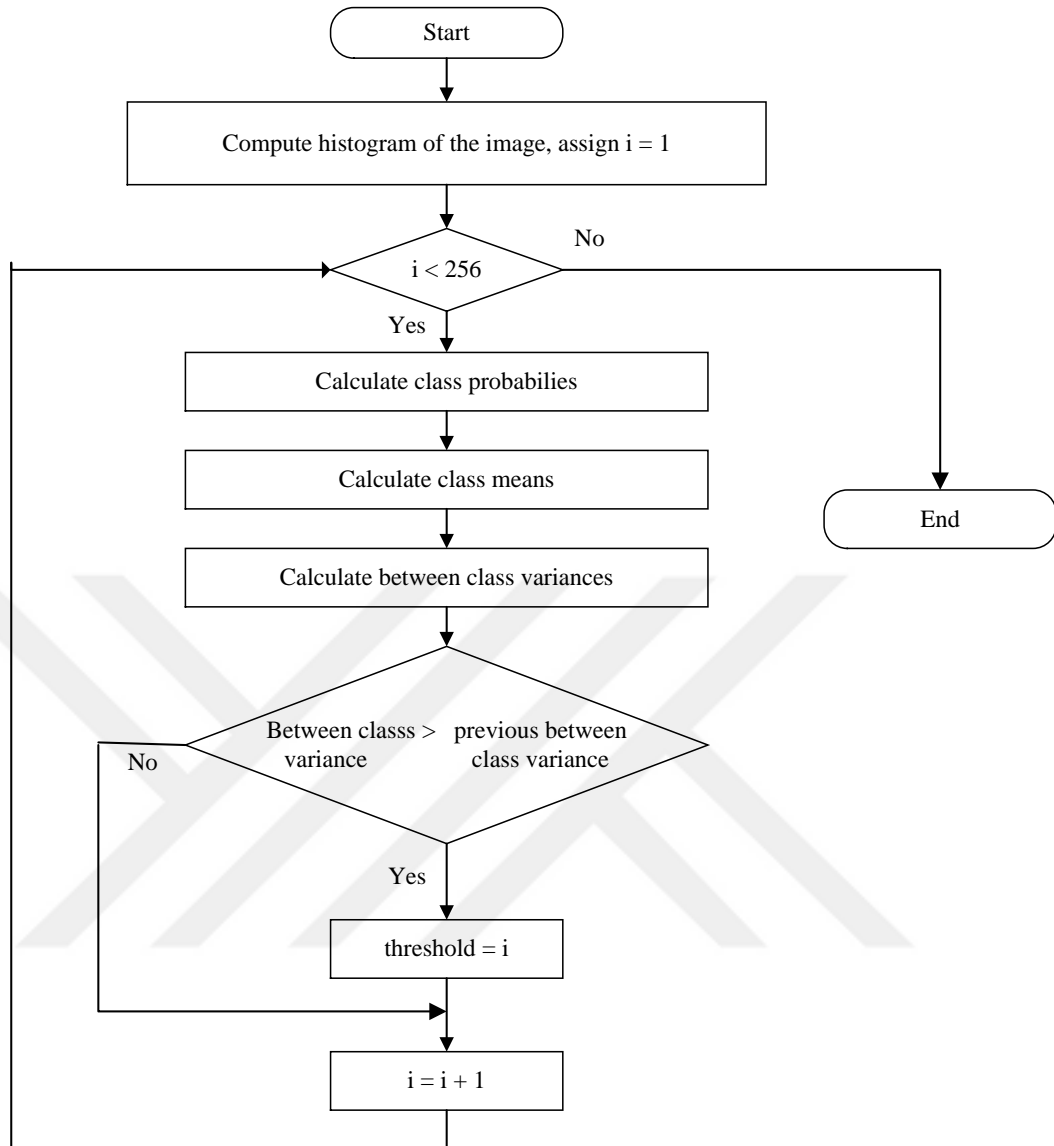


Figure 4.4 Flowchart of the Otsu's thresholding method

4.2 Edge Detection

Edges of the image contains semantic and shape information of the image. Edges are composed of pixels which have rapid intensity changes in neighborhood. To determine the location of higher intensity changes and extract these points from the input image, differentiation operators are used. According to Steve Seitz, edges are resulted from several contributing causes such as surface normal discontinuity, depth discontinuity, surface color discontinuity and illumination discontinuity [65]. As seen in the Figure 4.5, surface normal discontinuity occurs at the top of the packaging tape. Depth

discontinuity occurs in discontinuous depth field in the image. It is mostly originated from complexity, color, brightness changes of the same object and the quantity of the objects in the scene. If the scene contains a large number of objects, at least one of them is more likely to be behind the other. This causes depth discontinuity. When carnation tree is examined for depth discontinuities, leaves of the tree, which overlap each other, cause the depth discontinuity. Surface color discontinuity is easy to find. Because when the color of the area changes, it causes color discontinuity. Most of the time, objects block the incoming light or incident light coming with an angle, therefore it is not uniformly distributed. As a consequence, shades of the objects constitute edges, which is called illumination discontinuity. As seen in Figure 4.5, shadow of the reading lamp causes illumination discontinuity.

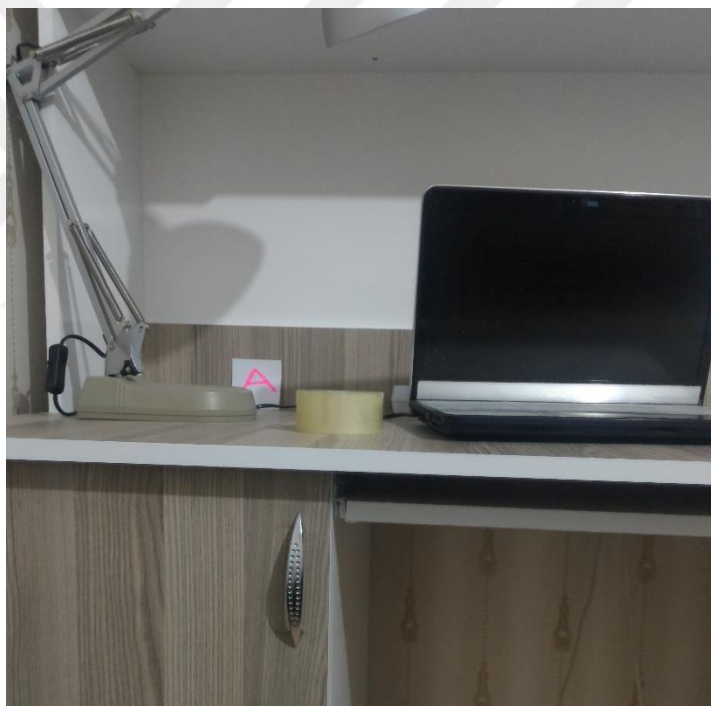


Figure 4.5 Source of edges

Objective of the edge detection is to find the higher intensity changes on the image. It can be obtained from the gradient of an input image. After gradient of the image has been obtained, the direction and magnitude of the change in intensity values can be calculated. The gradient of an image is demonstrated as

$$\nabla f = \begin{bmatrix} G_x \\ G_y \end{bmatrix} = \begin{bmatrix} \frac{\partial f}{\partial x} \\ \frac{\partial f}{\partial y} \end{bmatrix} \quad (4.11)$$

Since the image can be presented as two dimensional, the derivative is taken in both x and y directions. Magnitude of the gradient gives an information about the intensity change. Higher values in the gradient magnitude correspond to the higher intensity changes. Gradient magnitude is represented by

$$\|\nabla f\| = \sqrt{\left(\frac{\partial f}{\partial x}\right)^2 + \left(\frac{\partial f}{\partial y}\right)^2} \quad (4.12)$$

and direction of the gradient is calculated by

$$\theta = \tan^{-1} \left(\frac{\frac{\partial f}{\partial y}}{\frac{\partial f}{\partial x}} \right) \quad (4.13)$$

Derivative of an image is described in equation 4.11. In Figure 4.6 (a) only x directional derivative of the image and in Figure 4.6 (b) only y directional derivative of the image is presented. In the x directional derivate, horizontal changes in the intensity value are highlighted while in the y directional derivative, vertical changes in the intensity of the input image are demonstrated.

There is not a single method that is suitable for finding all kinds of edges in a grayscale image. For this reason, many methods have been developed to accurately determine the edges of the image. The first order derivative or second order derivative can be used to find out the intensity change in the grayscale image. Mostly used methods for the detection of the edges in the image are Roberts Cross, Prewitt, Sobel, Laplacian, Laplacian of Gaussian and Sobel. These methods use either the first order or second order derivative operators during the edge detection process [66-68].

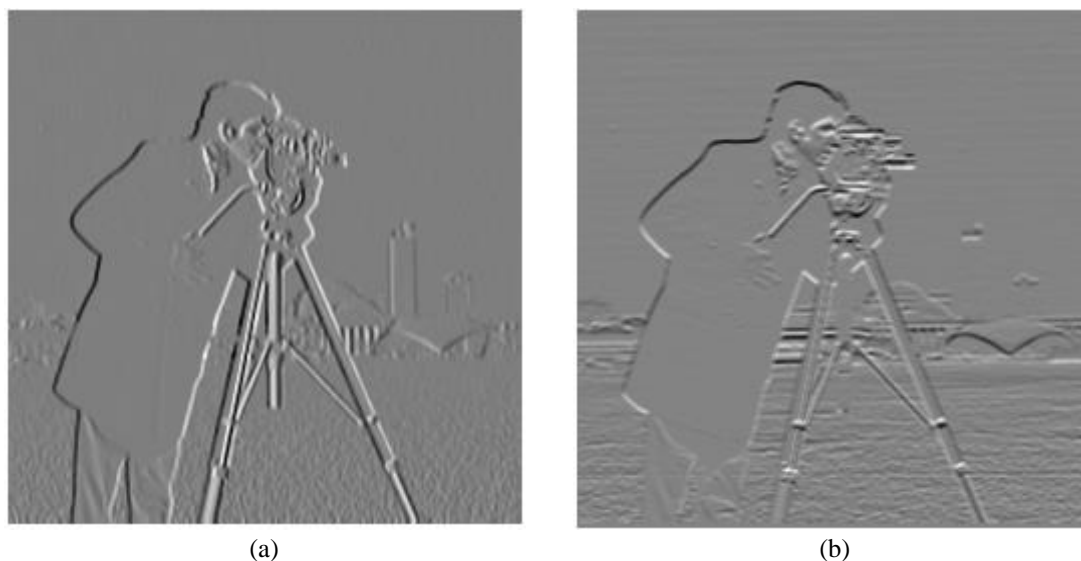


Figure 4.6 (a) X directional derivative of Cameraman image, (b) y directional derivative of cameraman image

In the first order derivative, local maximum or local minimum corresponds to the edge locations, while zero crossing locations correspond to the edges in the second order derivative operations. Thicker edges are generally produced when the first order derivative methods are used. Both the first order and second order derivative methods are prone to noise because the intensity of noisy pixels is different from the neighborhood pixels. Although the second order derivative methods are better than the first order methods to enhance rapid transitions in the image, effects of the noise become greater in the second order derivative. Transitions in the image from lighter to darker areas or darker to lighter areas are determined by looking at the sign of the second derivative. In Figure 4.7, Roberts Cross, Prewitt and Sobel operator masks are presented in both x and y directions. Sobel and Prewitt operators are very similar to each other, but in the Sobel operator the weight of the pixels, which are closer to the processed pixel, has a higher importance. In figure 4.8, application of these operators are demonstrated.

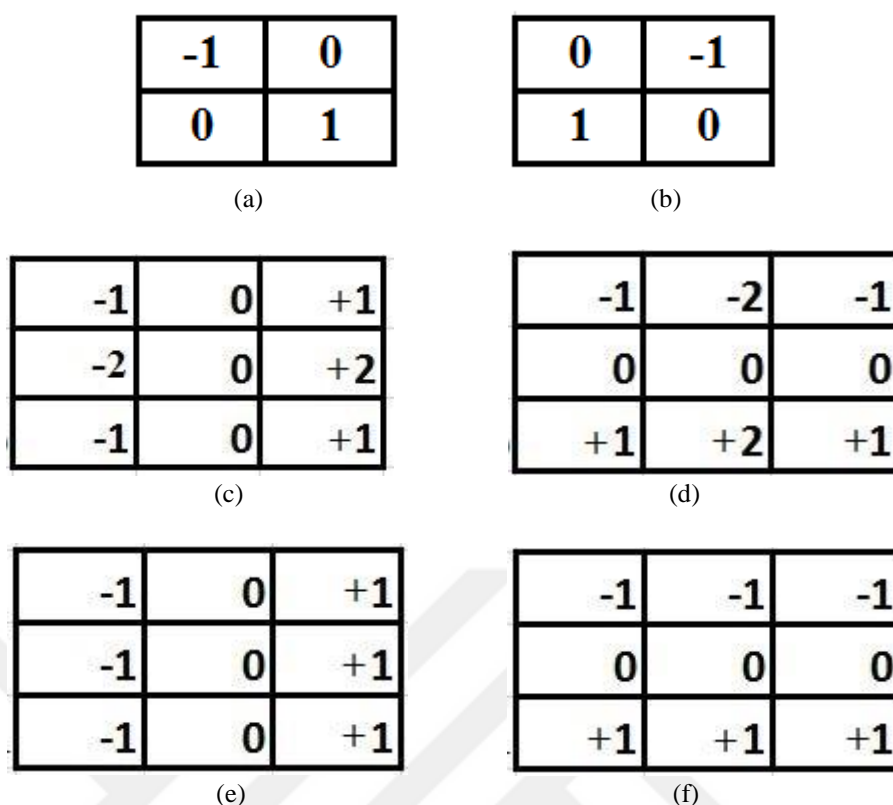


Figure 4.7 Derivative operators (a) Roberts cross x direction, (b) Roberts cross y direction, (c) Sobel x direction, (d) Sobel y direction, (e) Prewitt x direction, (f) Prewitt y direction

Simple edge detection can be carried out by applying the following steps. Firstly, the grayscale image is convolved with the horizontal and vertical operators of the chosen edge detection method. After that, gradient magnitude of every pixel on the image is calculated. Finally, the processed pixel is considered as an edge pixel when the magnitude of the processing pixels gradient is higher than the defined threshold value. Therefore, it plays an important role in determining whether the pixel is an edge pixel or not. If it is low, more pixels are considered as an edge pixel. This increases the rate of falsely detected edge pixels. When the threshold value is high, noncontinuous edges occur. Due to the high threshold value, some edge pixels are not considered as edges.

Decision of the optimal edge detector is determined by providing several conditions which are defined by Canny [69]. These conditions designate the success rate of detection, localization and single response. Success rate of the detection is determined by maximization of the correctly detected edges. Due to the noise on the image and

improper threshold value selection, edge detection rate decreases. Points, which do not belong to an edge, are considered as an edge pixel or true edge pixels are not correctly detected. If the detected edge and the actual edge distance is minimum, the detected edges are regarded as well localized. Detected edges should not be thick for a good edge detection. When each edge point is represented with a single point for each true edge point, this is called single response.

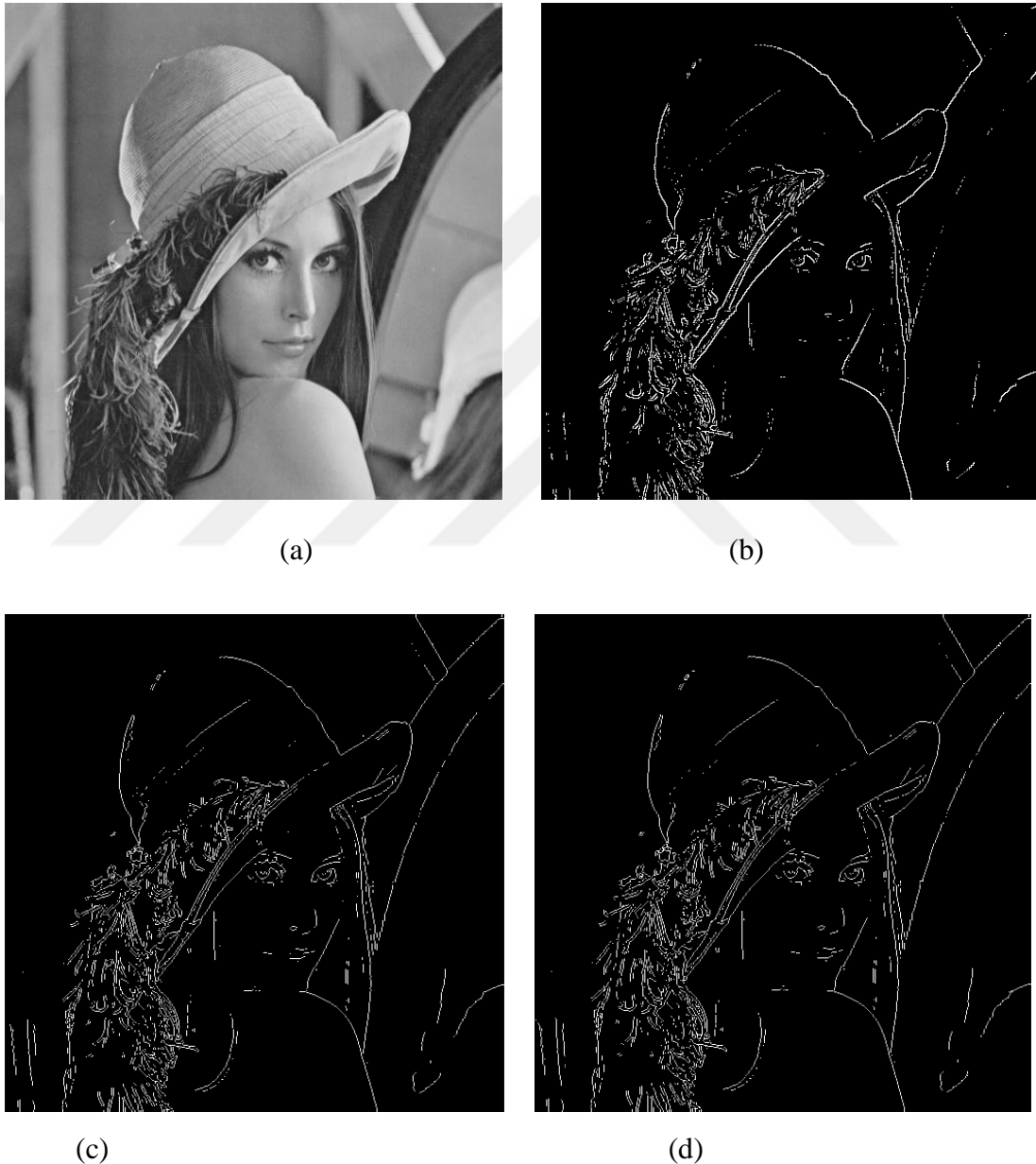


Figure 4.8 Different edge detector operators applied to an input Lenna image, (a) Lenna image, (b) Roberts cross operator applied image, (c) Sobel operator applied image, (d) Prewitt operator applied image

4.2.1 Canny Edge Detection

Canny edge detection method is one of the most famous edge detection algorithms in the image processing. This method was developed by Canny as a master thesis in 1983 and published in 1986 as an article [69,70]. Criteria of good edge detection algorithm were defined by Canny to conclude his objective of good edge detection. This can be found in the section of 4.2. At this work, procedure for increasing performance of the edge detection is presented based on the criteria. Canny's method can be accomplished by the following steps:

1. Smoothing input image
2. Gradient magnitude and angle computation
3. Non-maximum suppression
4. Thresholding

The first step of the Canny edge detection method is smoothing the input image. Because images are obtained from a camera, they contain level of noise based on the quality of the camera, lightning conditions and so on. When the quality of camera is not sufficient, or there is not enough lightning to capture a good picture, noise level on the image becomes higher. Since derivative operations are easily affected from noise in the image, it ends up with detected edge pixels which do not belong to the true edge pixels. Therefore, noise causes low detection rate which reduces the truly detected edge numbers.

To reduce the level of the noise, filtering operations can be applied to an image. Generally, Gaussian filter is applied to the input image in order to reduce the noise. Smoothing level in the Gaussian filter is depended on two parameters which are standard deviation and size of the kernel. Gaussian filter equation is explained in detail in section 3.7.1. When standard deviation of the mask increases, effect of the noise level in the input image decreases; nevertheless, the blur on the image expands. Increased standard deviation causes small amount of increase in the distance between the detected edge and the true edge, which is not compatible with good localization criteria. In some applications, the size of images is very large, so computational time for the processing increases. It is possible to decrease computational time because

Gaussian filter is one of the separable filters, so image can be processed with one dimensional Gaussian filters, by that way, required time to process reduces.

In the next step, the gradient magnitude and orientation of the gradient is computed after noise on the input image is reduced. Gradients of all pixels are calculated by convolution of the Sobel operator in both x and y directions. The magnitude of the gradient is calculated with Euclidian distance and measurements of each pixel's gradient magnitude is calculated by

$$G(i, j) = \sqrt{G_x(i, j)^2 + G_y(i, j)^2} \quad (4.14)$$

where G_x and G_y denotes, the Sobel operation applied to image in x and y directions, respectively. G represents the gradient magnitude of the image. After gradient of the image is calculated in x and y directions, calculation of the edge direction is very easy. Direction of the gradient can be computed as

$$\theta(i, j) = \tan^{-1} \left(\frac{G_y(i, j)}{G_x(i, j)} \right) \quad (4.15)$$

for each pixel where θ denotes the angle of the edge at that point. When G_x is equal to zero, an error will occur since G_x is in the denominator. At that point, the angle of direction is determined by looking at the G_y when G_x is equal to zero. When the value of G_y is zero, angle becomes 0° . When the value of G_y is a number which is different from zero, it is 90° .

The objective of the edge detection is obtaining sharp edges. Gradient magnitude of the image generally results in blurred edge lines. Therefore, non-maximum suppression method is used to obtain sharp edges. For that purpose, calculated gradient angle is rounded to the closest 45° which is computed by

$$\theta_{new} = \begin{cases} 0^\circ & \text{if } 0^\circ \leq \theta \leq 22.5^\circ \text{ or } 157.5^\circ \leq \theta \leq 180^\circ \\ 45^\circ & \text{if } 22.5^\circ \leq \theta \leq 67.5^\circ \\ 90^\circ & \text{if } 67.5^\circ \leq \theta \leq 112.5^\circ \\ 135^\circ & \text{if } 112.5^\circ \leq \theta \leq 157.5^\circ \end{cases} \quad (4.16)$$

After that, each pixel in the image is compared to the two neighbors of pixels based on the gradient direction. When the processed pixel direction is in the northeast, the pixels with its northeast and southwest of the pixels, which lie in one of the eight neighborhood, are compared. In the non-maximum suppression stage, if value of the processed pixel is not greater than the compared two neighboring pixels, it is suppressed. The compared pixels are located in the gradient direction of the processed pixel. Briefly, processed pixel value is set to zero to demonstrate that it is not an edge pixel. After applying non-maximum suppression method to a gradient magnitude, thick lines in the edges become thinner.

Falsely detected pixels still exist in the image even if non-maximum suppression is applied because of noise or color variances. The final step of the Canny edge detection method is thresholding operation. In the global thresholding, threshold value is constant and applied to all the pixels in the image. This results in that intensity values of the pixels which are higher than the predefined threshold value is assigned to one. The intensity of pixels that have lower values than the threshold value are also assigned to zero. For this reason, if the threshold value is lower, it preserves the correctly detected pixels, but it also contains incorrectly detected edge pixels. When threshold value is higher than the correct value, even though it removes the falsely detected pixels, it deletes truly detected edge pixels as well. In both cases, accuracy of the edge detection decreases depending on the threshold value.

Double thresholding algorithms are used in the Canny edge detection method. Double thresholding is applied to non-maximum suppression applied image which are T_1 and T_2 . Two binary images are obtained by applying two different threshold values [71]. In Figure 4.9, canny detection applied image is shown. If a comparison is made with the methods applied in Figure 4.8 and 4.9, it is seen that Canny edge detection method yields better edge information.



Figure 4.9 Result of the Canny edge detection image of Lenna

4.3 Contour Detection

Object contour, which can be defined as connected set of pixels, represents the boundary of object. When contour detection is made, the number of pixels to represent an object reduces. Contour detection is used in many areas such as image segmentation, shape recognition, motion tracking and optical character recognition. One of the algorithms which is used for detection of the boundaries on the image was presented by Martin et al. in 2004 [72]. Oriented energy, brightness gradient, color gradient and texture gradient features are used in this method.

Contour tracing methods are mostly applied in binary images. If the input image is an RGB image, firstly it is converted to the grayscale image, and then it should be

converted to binary image by using one of the image thresholding techniques. The object pixels in the binary image are represented by 1's. Therefore, the outermost pixels of the object are needed to find out the starting point of the contour. Initially, the pixel search starts from the top-left corner to the end of this row and it continues until an object pixel is found. If any object pixel is not found in the scan of the first row, searching continues in the following row until an object pixel is detected. When object pixel is found, it is stored into a memory and it becomes the starting point of contour. Then, contour tracing algorithm tries to find out the next pixel by looking at the eight neighborhoods of the starting point. If one of the pixel is found in the neighborhood as an object pixel, it is added to the memory and the search continues. Finally, the search stops when the initial starting point is detected or nothing is found in the neighborhood pixel. Flowchart of the contour detection algorithm is illustrated into Figure 4.10.

Contour points are stored into the memory with x and y locations of each point. Required memory to store each contour can be decreased by using Freeman code. Describing an arbitrary curve in the image with a chain code was presented by Freeman in 1961, which is also called Freeman code [34]. In this method, outer boundary pixels of the object are represented by directional numbers with either four connectivity or eight connectivity. It begins from the starting point. In this method, instead of saving both x and y coordinates of the contour pixel, only the direction of change is stored.

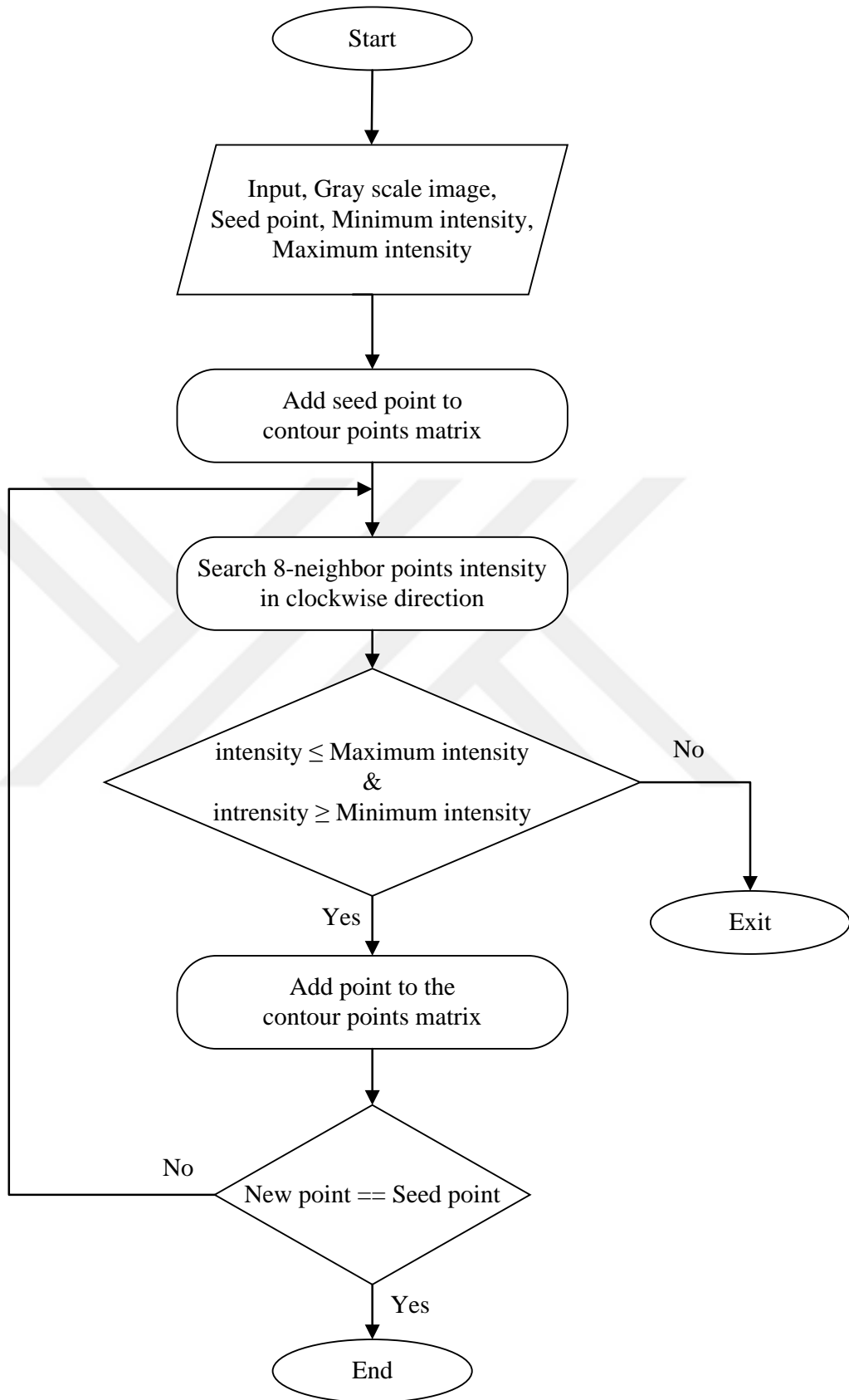


Figure 4.10 Flowchart of contour tracing algorithm

CHAPTER 5

APPLICATION OF CELL DETECTION AND CLASSIFICATION IN PATHOLOGICAL IMAGES

Invention of the glass dates back to ancient times. People were keen to investigate the usage of the glass. Besides, humans have been also interested in viewing the smaller objects that are impossible to see with eyes. Objects can be seen using larger glass, which leads to the discovery of the first magnifying device. In the late of 15th century, first magnifying device was discovered by putting multiple lenses into a tube and enables to see the objects bigger in size. The zooming capability of this device was lower than ten times but it was higher compared to the single magnifying lenses at that time. One of the ground-breaking development was made by Dutchman Antonie van Leeuwenhoek who lived in late of the 17th century. He was a cloth merchant and also a scientist. He started to make a microscope as a hobby at first. However, he succeeded to make a microscope which was capable of magnifying objects more than 250 times with a single lens, shown in Figure 5.1. Using his microscope, discovery of the bacteria was made by him. Light microscope has been widely used in the pathology to examine the pathologic samples to diagnose the disease of the sickness for a long time [73,74].

Computer Aided Diagnosis (CAD), which is used in medical science, provides statistical information and prior analysis of the medical data. Consequently, diagnosis and staging of the disease become easier and take less time. Image processing methods are used in the analysis of medical images. Image segmentation, which is one of the image processing methods, facilitates image analysis. In segmentation, input image is partitioned into smaller parts based on the properties of the pixels which are intensity, adjacency and so on. One application area of the image segmentation is medical field. Image segmentation methods are used to determine the location of the tumors, calculate the volume of tissues, diagnose the disease, decide on the treatment method, and some others.

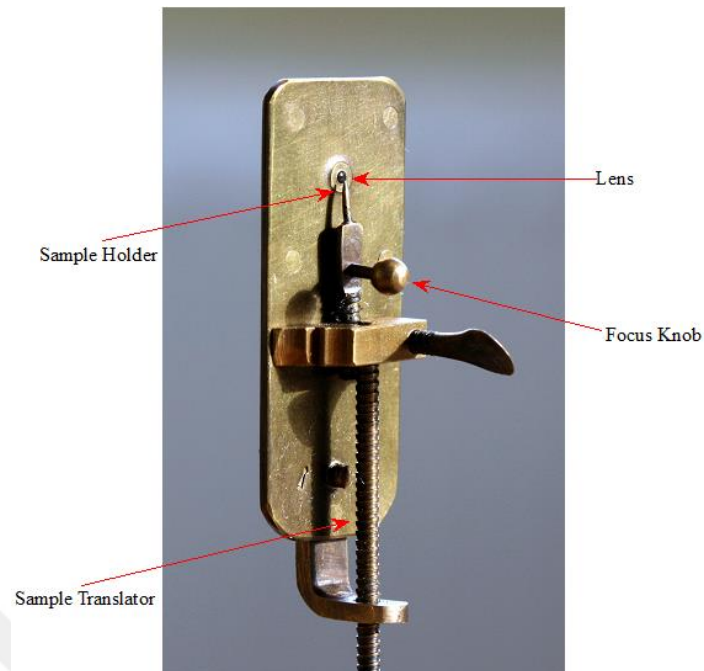


Figure 5.1 Antonie van Leeuwenhoek's microscope [75]

5.1 Application of Cell Detection and Classification in Urinary Bladder Carcinoma

Cell is the smallest structure of living organisms. Combination of cells constitutes a tissue. Organs are consisted of tissues and have certain functions. Thus, determination of cause of the disease and diagnosis can be fulfilled through analysis of the cells. In the pathology, diagnosis is made by the analysis of obtained specimen. This process is performed using a microscope. Although structure of cells can be observed under the microscope in a good way, images obtained from pathology specimens have not been capable of showing details of the cells until the invention of virtual microscopy. In recent years, studies have been performed to use CAD systems in pathology like in the other areas of medicine.

Cells are comprised of nuclei, cell membrane, cytoplasm and organelles. Depending on the tissue type and function, the size and shape of the cells vary. Dimension of the smallest cell in human body is 4-5 micron, but the biggest cell, which can be seen with a bare eye, has a diameter of 200 microns. Therefore, detection and segmentation of the cells are difficult. Many studies have been performed to increase the detection rate of

the cell nuclei, and it is still trend topic for the researchers. For example, Zhou et al. studied on nuclei detection from human tissue, automatically [76]. In the preprocessing step, stain guided mean-shift filtering was applied to overcome the problem of nonhomogeneity of the stain in the nuclei, which provides protection of the cell shape, while increasing the color homogeneity inside the nuclei. After application of the stain guided mean-shift filtering, performance of the segmentation increased. Image was converted into binary image using with Otsu's thresholding method. Next, watershed algorithm was applied to segment the image. Then, to separate overlapping cells and preventing the over segmentation, Bayes classifier was implemented. Another researchers, Sammouda et al. made detection of the cancerous nuclei from lung images [77]. Unsupervised Hopfield Neural Network algorithm was used for segmenting the lung image. Labeling of the input image to the nuclei, cytoplasm and others were performed using histograms of RGB intensity values. Filling the holes inside the nucleus was done with maximum drawable circle algorithm. To determine cancerous nucleus, the size of nucleus was used with different magnification levels.

Wienert et al. developed a contour detection algorithm for cell nuclei from virtual microscopy images [78]. In this study, dataset contains bladder tissue samples of different people. 600 x 600 pixel image region was cropped from the virtual microscopy images which were at 20x magnification level. The contour points of the nuclei were determined from these images.

5.1.1 Procedure of Cell Detection

Objective of this study is the visualization of the pathological images and determination of the grade of the bladder cancer. For this purpose, the area can be cropped from the WSI and the contours of the nuclei are determined from the selected area. Following that, the properties of each detected nucleus are calculated. Finally, grading of the bladder carcinoma, whether it is at high grade or low grade, is performed by using extracted features. The procedure to implement these operations is shown in the Figure 5.2 as a flow diagram.

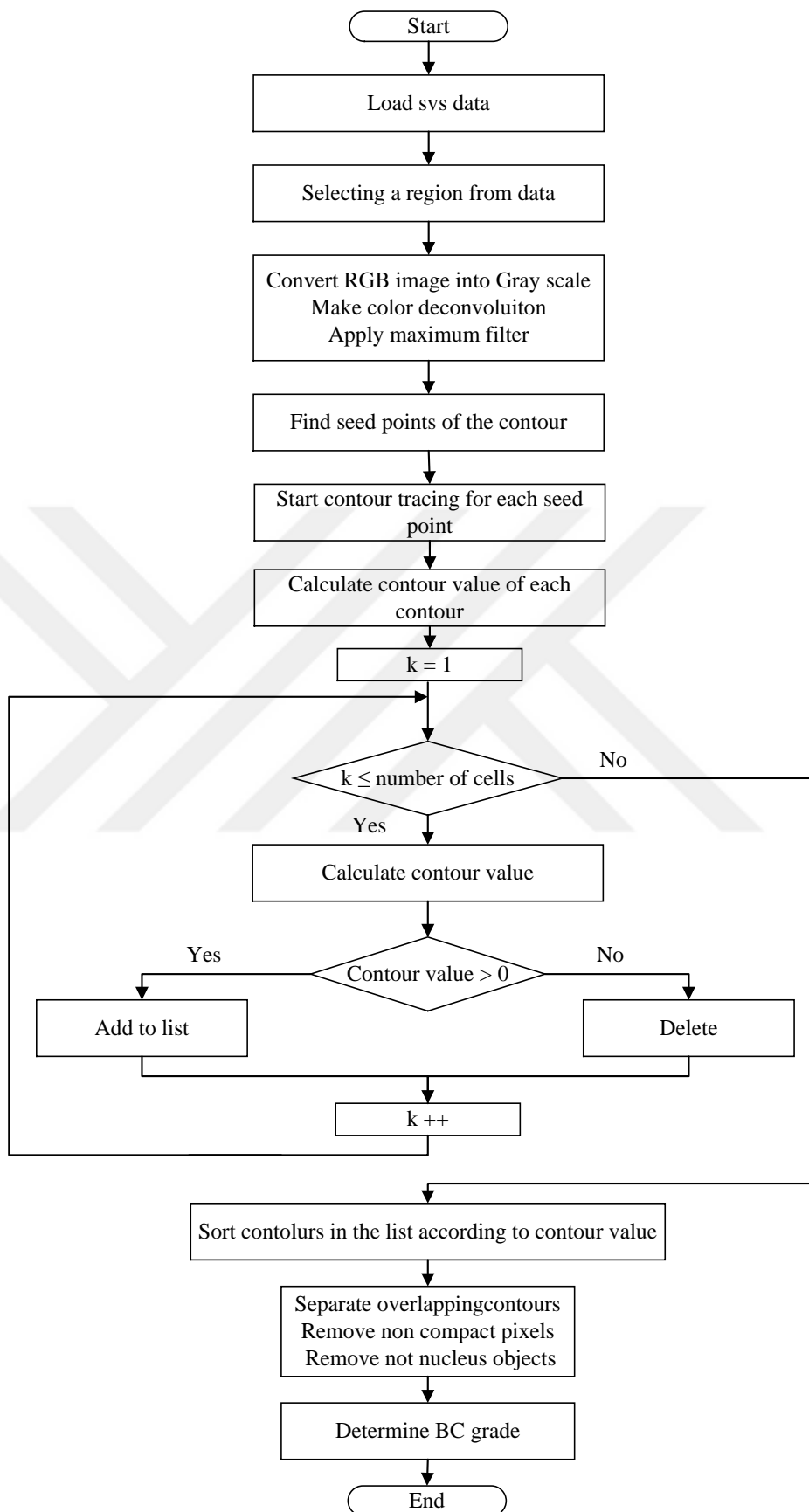


Figure 5.2 Flowchart of the bladder cancer grading application

Medical images are stored into the memory with different file formats based on the application. Therefore, managing medical data requires special processing. Pathological images are stored into the computers with “.svs” file format extension, commonly. Each “.svs” file contains more than one image, which are barcode, macro of the slide and images of the microscopic slide with different magnification levels. At a small magnification level, viewing the whole image is not a problem since the size of the image is small compared to the highest magnification level. But, as the magnification level increases, loading an entire image to carry out the process cannot be possible with most computers because of the memory requirements. Therefore, only a part of the high resolution image, which is determined by the specialist doctor or researchers, is prepared for the process.

5.1.1.1 Tracing Potential Contours

Outer border lines of the object are referred as contour. Each contour point shows the position of outline of the object. Since images are stored in memory as in a matrix form, each contour point holds the x and y coordinates. Combination of outer boundary points constitutes the contour of the nucleus. In binary images, choosing the starting point is simple because it only consists of 0 and 1 values which represent the background and the object pixels of the binary images. To find starting point of the contour detection, raster scan is started from any corner of the loaded image and continues until the first object pixel is encountered. In gray scale images, another approach is required to determine the starting points of the contour detection. A certain intensity value can be assigned and above (or below) intensity values from the determined intensity value are regarded as an object pixel. Contour tracing starts after determination of the initial point, like in the binary images. This approach may yield good results depending on the selected image and the intensity values of the pixels. However, it is prone to the failure because of the selected threshold value, noise and homogeneity of the object pixels. This leads to reduction in the accuracy of results. Moreover, assigned threshold value should be optimized based on the image. In this study, intensity value differences and local minimum and maximum points are used to determine the starting points of the contours.

In mathematics, derivative measure the difference between outputs of the function with corresponding to the Δh change in the input. In image processing, the smallest change is equal to 1 pixel. In this study, each row of the image is considered as an output of the function. Thus, calculating the differences between two adjacent pixels gives the derivative of that point. To find the starting point of the contour detection, local minimum, local maximum and local maximum gradient values are calculated and the locations of these points are stored in memory.

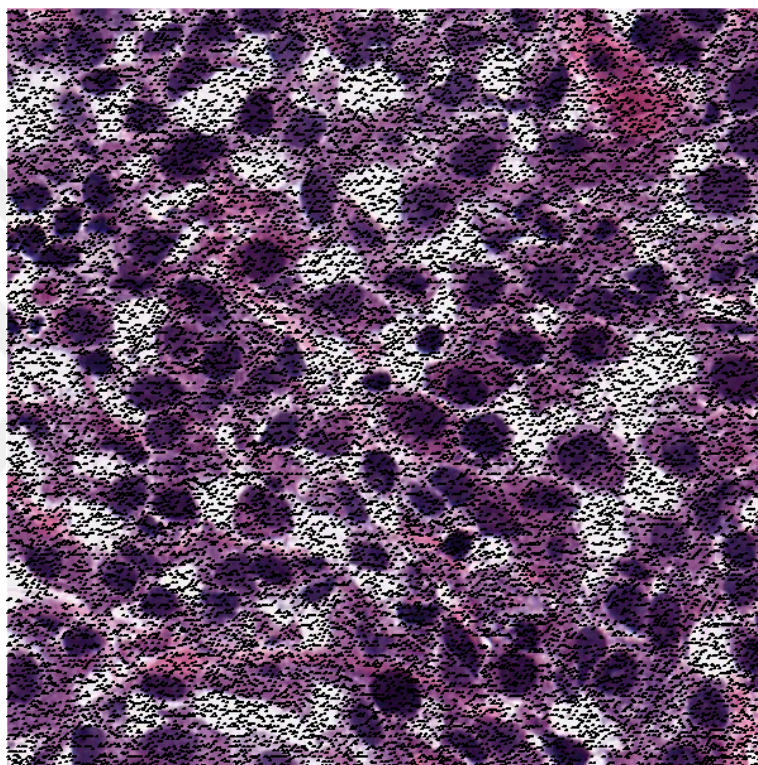


Figure 5.3 Seed points shown as black dots to input image

As seen in Figure 5.3, plenty of black dots are drawn onto the selected region of the pathological sample to show the starting points of the possible contours. Each starting point contains two intensity value information in addition to the X and Y locations of that point. The two intensity values are determined with either local maximum or local minimum points and location of the highest local gradient value. Maximum gradient point locations are determined as a starting point of the contour and the intensity value at this point constitutes one of the intensity values which are either local minimum or local maximum. Then, the second intensity value is determined by looking at

increasing or decreasing of the intensity values in the processing row. If the intensity value is increasing, it means that X location of the minimum intensity value is smaller than the maximum intensity value location. Maximum intensity value is set to 255 and minimum intensity value is assigned as intensity of the maximum gradient location. If X location of the minimum intensity value is bigger than the maximum value location, it is considered as decreasing. So, maximum intensity value is set to intensity the maximum gradient point, and minimum intensity value is assigned as 0.

Contour detection helps to extract boundary pixels of the object from the loaded image. Contour information is used to extract features of the objects. Therefore, it is used in many fields such as pattern recognition, classification and in the medical images. Seo et al. classified contour tracing method into 3 types, these are [79]:

- Pixel tracing technique
- Vertex tracing technique
- Run-Data-Based tracing technique

In the Run-Data-Based tracking technique, the object's left and right edge pairs are considered. Each row of the image is scanned left to right. Therefore, this method uses smaller memory compared to the other methods [80,81]. The crossing points of the edge pixels and background pixels are traced in the vertex-tracing technique. Therefore, it yields better information about the structure of object [82]. After determining the starting point, next contour pixel is settled by looking at the adjacent pixels and locations in the memory stored according to the determination order [83]. In this study, Moore neighborhood tracing algorithm is used for tracking the contour pixels. Instead of binary images, grayscale images are used to track the contour lines. Therefore, the pixel in the search are considered as an object pixel if intensity value of the candidate pixel is between the maximum and minimum intensity values. These values are defined for each seed point in the previous step. Tracing is made by looking at the 8-neighborhood pixel of that point. Initially, the pixel above the starting pixel is checked for the possible contour point, and searching continues to the neighborhood pixels in the clockwise direction. The starting point of the search at the subsequent pixels depends on the direction information which is obtained from the previous pixel.

To stop contour detection and to prevent it from failing, three criteria are used. After contour tracing has completed, it should return to the starting pixel, and no pixel has been considered as a contour pixel more than once, except for the starting pixel. It should not exceed predefined maximum contour length. The result of the contour detection is drawn into the loaded image with different colors and presented in to the Figure 5.4.

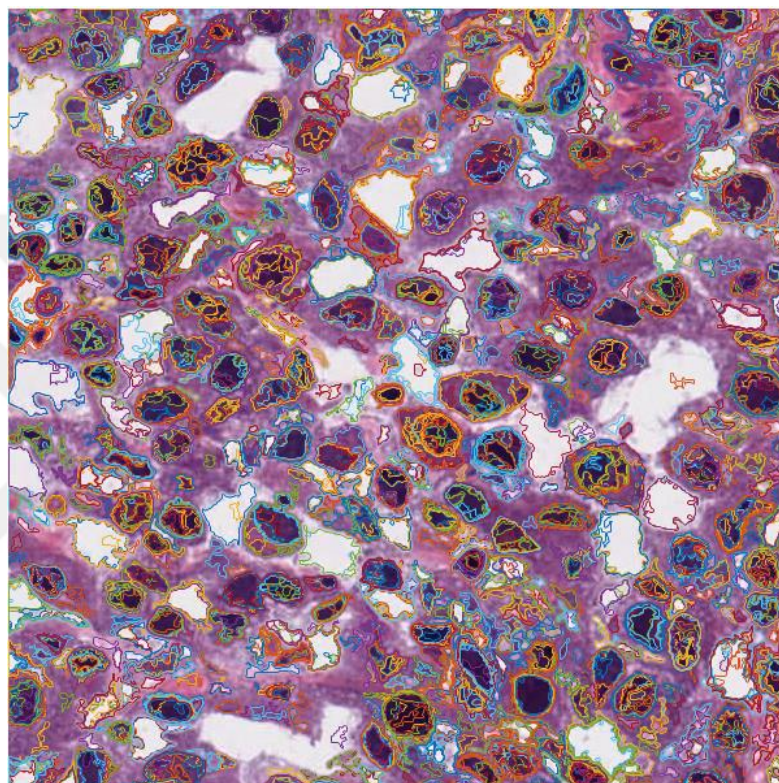


Figure 5.4 All possible valid edges drawing to the input image with different colors

5.1.1.2 Color Decomposition on Stained Tissue Images

Generally, cells in the sample are either transparent or achromatic. Histochemical stains are used for staining the cells to monitor under the microscope. Commonly used histochemical stains are H&E and DAB. Hematoxylin gives blue-purple color which represents the nuclei of the cell, eosin dyes the cytoplasm in the sample with the color of pink. Brown parts in the specimen are dyed with DAB. To separate stains, color transformation techniques are used, such as RGB to HSI, stain based transformation techniques and so on [84]. One disadvantage of using color conversion algorithms is

that the pixel is assigned to one of the stain colors based on predetermined criteria. This ends up with information loss because multiple stains are used in the histopathological staining process. Ruifrok et al. designed a color deconvolution algorithm benefitting from color absorption characteristics of the stains. [84]. Lambert-Beer law states that intensity of light passing through a solution depends on distance, concentration of the solution and amount of light absorbed. Lambert-Beer law is expressed as [85]

$$I = I_0 e^{-\varepsilon cd} \quad (5.1)$$

where ε is absorption coefficient, c refers concentration of the solution, d is the thickness of the solution in centimeter. I_0 refers to the incident light and I equals to transmitted light. Since absorbance equals to the εcd , (A) can be calculated by

$$A = -\ln\left(\frac{I}{I_0}\right) \quad (5.2)$$

In the RGB color space model, each color is represented by a different combination of these colors. Optical density (OD) helps to measure the concentration of each stain. Therefore, separation of the stain can be made by using the measured OD values for any stains. OD measurements of a stain is described by 3x1 vector

$$\vec{OD}_i = \begin{bmatrix} OD_{Red} \\ OD_{Green} \\ OD_{Blue} \end{bmatrix} \quad (5.3)$$

Since, hematoxylin, eosin and DAB are stains in the sample, OD matrix defined as

$$\begin{bmatrix} m_{r,h} & m_{g,h} & m_{b,h} \\ m_{r,e} & m_{g,e} & m_{b,e} \\ m_{r,dab} & m_{g,dab} & m_{b,dab} \end{bmatrix} \quad (5.4)$$

where each row corresponds to the stain and columns related to RGB colors. Absorbance level of each pixel is defined as

$$\vec{d} = \vec{C} \cdot \vec{M} \quad (5.5)$$

where \vec{C} is the concentration of these stains. To obtain \vec{C} , each side of the equation is multiplied by inverse of the matrix M , the result is

$$\vec{C} = M^{-1} * \vec{d} \quad (5.6)$$

The coefficients of the matrix M are determined by Ruifrok et al. [84]. In Figure 5.5, the result of the hematoxylin stain which is an extracted image from the RGB image is shown.

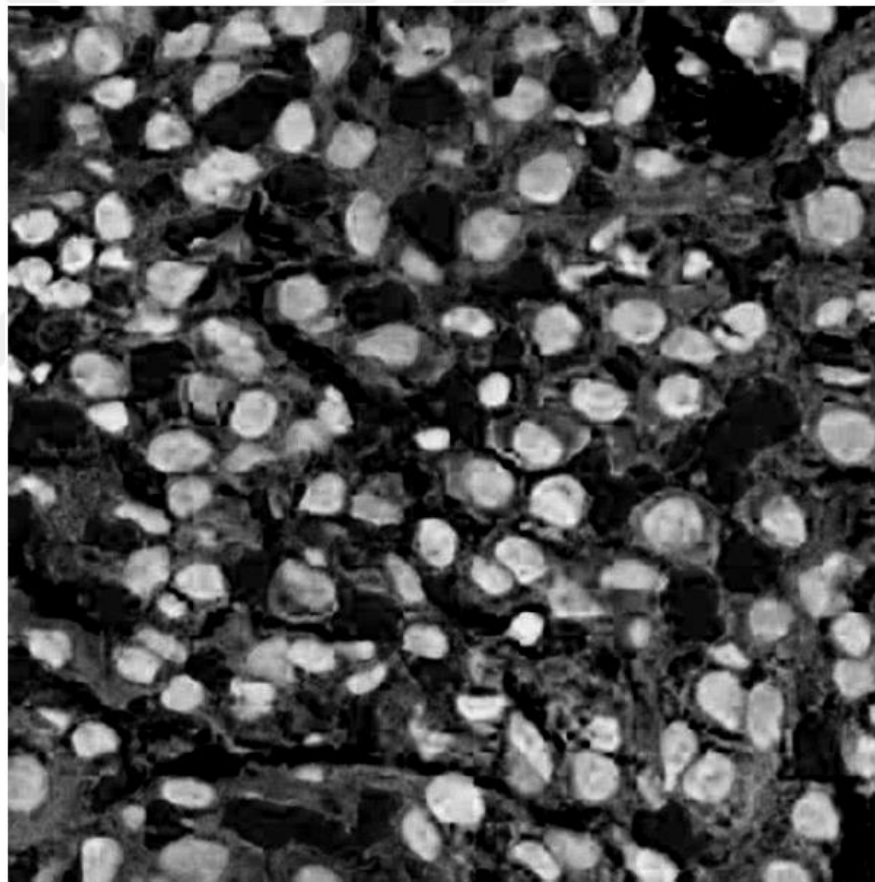


Figure 5.5 Color deconvolution applied image

5.1.1.3 Calculation of Contour Value

Contour detection determines the boundary pixel which extracts the region of object. For this reason, it can be considered as a segmentation method. Over-segmentation and under-segmentation are one of the major problems in image segmentation. Many methods have been developed to solve this problem. As can be seen in Figure 5.4, plenty of lines exist, some of which represent the cell nuclei and some of them are not even relevant to describe the contours of the cell nuclei. Calculation of contour value is performed for each successfully detected contour. The contour values are used to determine the priorities of detected contours. By this way, contour which defines the nucleus ideally remain and others are deleted. For this purpose, color deconvolution is applied to the RGB image to extract the hematoxylin stain value, and maximum filter is applied to this image. In the output image, hematoxylin stained areas are represented with higher intensity values. Later, the threshold value of this image is found using the Otsu threshold method. Mean intensity value of the contour points is calculated from color deconvolution applied image. Using color deconvolution applied image, mean intensity of the contour pixels is calculated by

$$MeanColorDeconvolution_i = \frac{\sum_{i=1}^{number\ of\ contour\ pixels} imageDeconv(i, j)}{number\ of\ contour\ pixels} \quad (5.7)$$

If the mean value of the contour pixels in the color deconvolution applied image is smaller than the threshold value of the color deconvolution applied image, this contour is deleted.

Gray scale image is obtained by dividing summation of each RGB value by 3. Sobel operators are applied to the grayscale image in both x and y direction. Gradient image represents magnitude of the gradient in each pixel. Mean contour gradient can be calculated by

$$MeanContourGradient_i = \frac{\sum_{j=1}^K GradientImage(i, j)}{K * 255} \quad (5.8)$$

Where K represents the number of the pixels in the i^{th} contour, point (i,j) represents the location of the j^{th} point's location on the gradient image. The summation is divided by 255 to normalize the mean contour gradient value. Another criterion to find out the optimum contour is calculation of the compatibility between maximum local gradient and contour points. Since higher gradient values represent the sharp transitions in the image, contour points should be located at the maximum gradient values in the image. In this operation, gradient value of the processed pixel is compared with the 8-neighborhood pixels. If the gradient magnitude of the processed pixel location is higher or equal to the maximum gradient in the neighborhood pixels, this pixel marked as 1 to show that it has the concordance with the highest gradient value, otherwise it is assigned to 0. Accordance between maximum gradient locations in the eight-neighborhood and contour points can be calculated by [78]

$$p_{ij} = \begin{cases} 1 & \text{if } \max \{|S(p_{nm})|\} = |S(p_{ij})| \quad \forall n, m \quad \begin{matrix} x_i - 1 \leq n \leq x_i + 1 \\ y_i - 1 \leq n \leq y_i + 1 \end{matrix} \\ 0, & \text{otherwise} \end{cases} \quad (5.9)$$

where p_{ij} is the matrix whose elements represent the maximum gradient points in the eight-neighborhood. Total number of maximum gradient points for each contour is equal to summation of maximum gradient points of the contour. After that, mean value of the maximum gradient points for each contour can be calculated by [78]

$$MeanMaxGradient_i = \frac{\sum_j p_{ij}^{\max}}{K} \quad (5.10)$$

where i represents the i^{th} contour. Length of the contour varies based on the nucleus size. Contours may represent the cell nucleus best but total number of maximum gradient values is low due to its length. Consequently, longer contours take precedence over the shorter contours many times. After the number of maximum gradient points in the contour is divided by the number of points in the contour, *MeanMaxGradient* value is calculated and the length of the contour does not affect the priority order. Using these calculated values which are *MeanMaxGradient* and

MeanContourGradient, precedence of each contour is calculated by multiplying these values which are defined by [78]

$$\text{ContourWeight}_i = \text{MeanContourGradient}_i * \text{MeanMaxGradient}_i \quad (5.11)$$

5.1.1.4 Removing Overlapping Contours and Non-compact Pixels

The contour which represents the object ideally is determined by contour weight. To overcome the overlapping contours, value of the contours is used for determining the priority. After calculation of each contour value, all detected contour values are sorted by descending order from starting the highest contour value. Then, each contour is labelled into the matrix started from the highest contour value. When the subsequent contour tries to label previously labelled pixel, these contours are deleted.

Nontouching contours, which represent the same nucleus, may remain after labelling the process. Moreover, small contours which are detected due to nonhomogeneity of the nucleus and other small particles still exist. This situation results in thick lines in the contour points. Elimination of these thick lines can be achieved by applying distance transformation. Initially, an empty matrix which has the same size as the processed image is created and the detected contour pixels are assigned to 1. Then, distance transformation is applied to the created matrix by using city block distance metric. Distance matrix elements which are different than zero and lower or equal to two are processed. For this purpose, matrix elements are processed twice. If the processed element does not have any distance value greater than itself in the 4-neighborhood, it is decreased by 1 in each scan. When the pixel value becomes zero after 2 scans have finished, this pixel is deleted. Non-nucleus contours can be deleted by using the mean hematoxylin stain intensity matrix values. Mean intensity value of the each detected nucleus is equal to average of hematoxylin staining intensity values. This value is compared to the threshold value of the color deconvolution applied image's threshold value. If the mean value is low, it is deleted. Compared to the Figure 5.4 and 5.6, number of contours in the loaded image is substantially decreased.

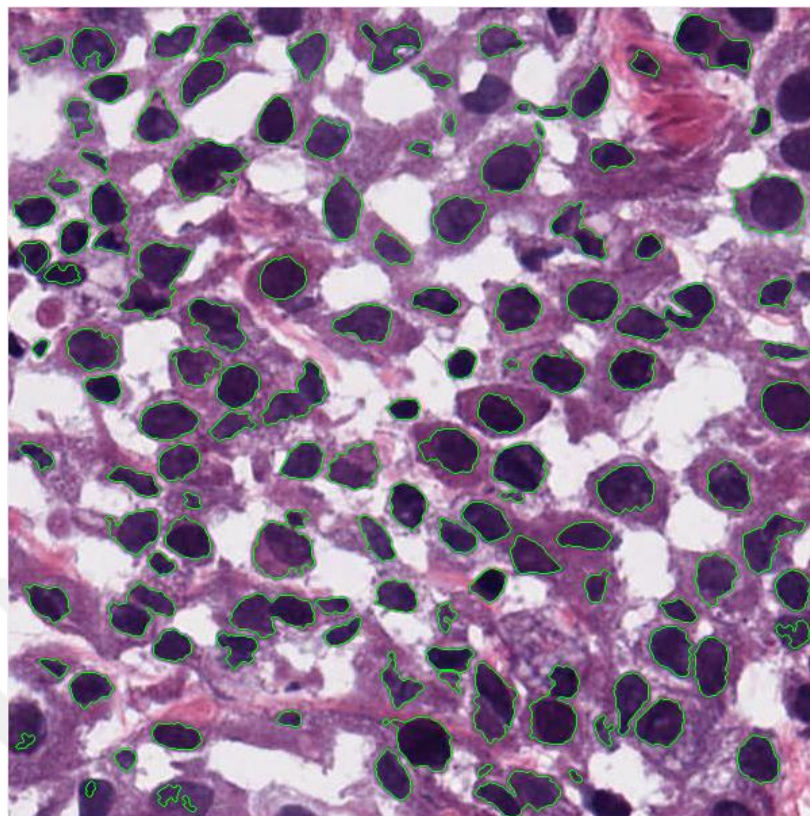


Figure 5.6 Non-overlapping segmentation and non-compact pixels removed contours

5.1.1.5 Classification

Human brain can easily identify the objects from the shown picture. Therefore, it is considered as an easy task to fulfill. However, classifying the objects in the picture with a computer is a challenging problem. Classification is used in many areas, which are remote sensing, video surveillance, object detection, medicine and so on. Therefore, classification accuracy and process time are very important and it is one of the current topics which are studied by researchers.

Objects can be described by their specific properties which show similar characteristic properties in the same type of objects. Different objects do not possess similar properties. Objects can be distinguished from each other by using individual characteristic properties of the objects, which are not in the same class. These properties are called features. Categorizing the image pixels into the different classes based on their properties is called classification.

Classification methods are grouped into two main sections, which are unsupervised classification methods and supervised classification methods. In the unsupervised classification methods, data are categorized based on the properties and user intervention is minimum compared to the supervised classification methods. In supervised classification methods, the features of each class are determined by the training data. When the classification method is tested, the input data are classified based on the extracted features of the training data.

Each pattern is demonstrated as a row vector \mathbf{x} which contains the features. Elements of the \mathbf{x} contain information of the feature. Number of elements in the \mathbf{x} shows how many number of features will be used to describe each different pattern. Minimum distance classifier is one of the supervised image classification method. In minimum distance classifier method, patterns are described by the mean vector of features. Assignment to the class can be calculated by [26]

$$d_i(x) = x^T m_i - \frac{1}{2} m_i^T m_i \quad i = 1, 2, 3, \dots, W \quad (5.12)$$

where m_i is the i^{th} pattern class feature vector and \mathbf{x} is input data feature vector which is classified. After calculation of the all classes $d_j(\mathbf{x})$ values, \mathbf{x} is assigned to the class which gives the highest value. Borderline between two classes can be defined as [26]

$$\begin{aligned} d_{ij}(x) &= d_i(x) - d_j(x) \\ &= x^T (m_i - m_j) - \frac{1}{2} (m_i - m_j)^T (m_i + m_j) = 0 \end{aligned} \quad (5.13)$$

where i and j represent classes.

After feature extraction of each nuclei, they are classified into the two classes based on their features. The first class contains the low grade cancerous nuclei and the second class represents the high grade cancerous nuclei. Low grade nuclei and high grade nuclei do not share similar characteristics in the feature of area, length and mean intensity value. For this reason, the feature vector of each class consist of these features. In the classification 5 low grade urothelial bladder carcinoma (UBC) and 5 high grade UBC area are chosen from the digital slides by pathologist for training and

d_{ij} is calculated based on these results. Then 100 high grade UBC areas were chosen from the UBC digital slides by pathologist. The result of the correctly detected high grade UBC is 83%.

UBC grading is not working 100% accurately for some cases, which is originated from the quality of prepared pathological sample, obtained image quality and nonhomogeneity of the nuclei. Based on these factors, correctly detected nuclei accuracy is decreased. To increase the performance of the classification results, different filter types are applied to increase the nuclei detection rate of the algorithm. After the contour of the nuclei was found, 19 features of each nuclei were extracted, and features which have similar characteristics within-classes and different characteristics between-classes were chosen in classification algorithm. By using minimum distance classifier with selected features, which shows different characteristics of low grade UBC and high grade UBC, decision of the patient's grade is made.

5.1.2 Graphical User Interface of the Application for Bladder Carcinoma Diagnosis

In this study, a graphical user interface is designed by using the MATLAB GUI toolbox so that the written algorithm can be used easily [86]. With the designed GUI, digital pathological images can be visualized and the operations on these images can be easily performed without any requirements. Figure 5.7 displays the Main window of the GUI.



Figure 5.7 MATLAB GUI main window

The designed GUI can be divided into 8 parts, as can be understood from Figure 5.7. These are:

- ✓ File menu editor
- ✓ Tools menu editor
- ✓ Two photo viewer axes for visualization of pathological images
- ✓ Zooming panel
- ✓ Sliding panel
- ✓ Position panel
- ✓ Area selection panel to choose desired area
- ✓ Table to show the obtained calculations

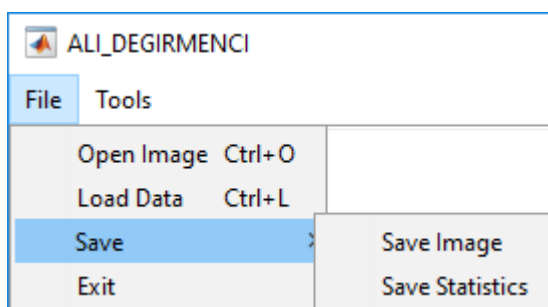


Figure 5.8 File menu

Figure 5.8 shows the expanded version of the file menu. Open Image supports 'svs' file format which is obtained from digital slide scanners, as well as most of the normal image formats such as 'jpeg', 'tiff'. By using "Load Data", it is possible to show the area where the process is performed before and each detected nucleus area properties can be shown in the table. The Save menu allows the users to save both the selected area of the image and statistical calculations of this area to the computer memory by any file name determined by the user. Lastly, "EXIT" closes the GUI window.

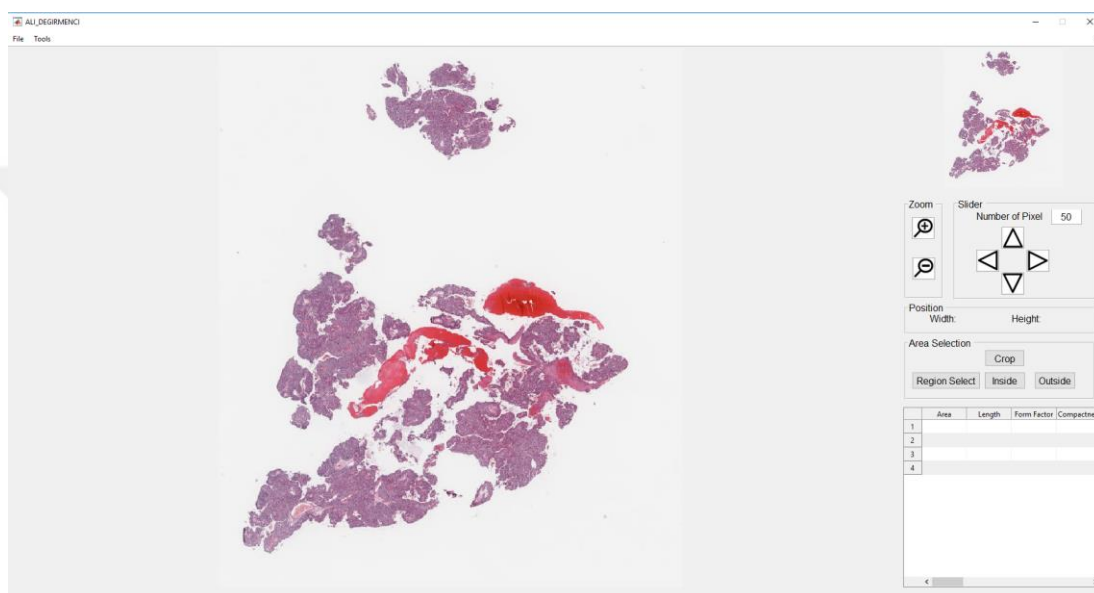


Figure 5.9 Open Image pop-up window

When "Open Image" is selected from File Menu or Ctrl + O key combination is pressed on the keyboard, the file position and the file in that position can be selected. After this process, chosen pathological file is loaded to the program. Smaller size of the thumbnail image is shown in the small axis to present general information about the sample. This is located at the upper right corner of the GUI. As shown in Figure 5.9, thumbnail image is also visualized in the bigger axis. By using this, user may be able to zoom slide and select an area from the loaded data.

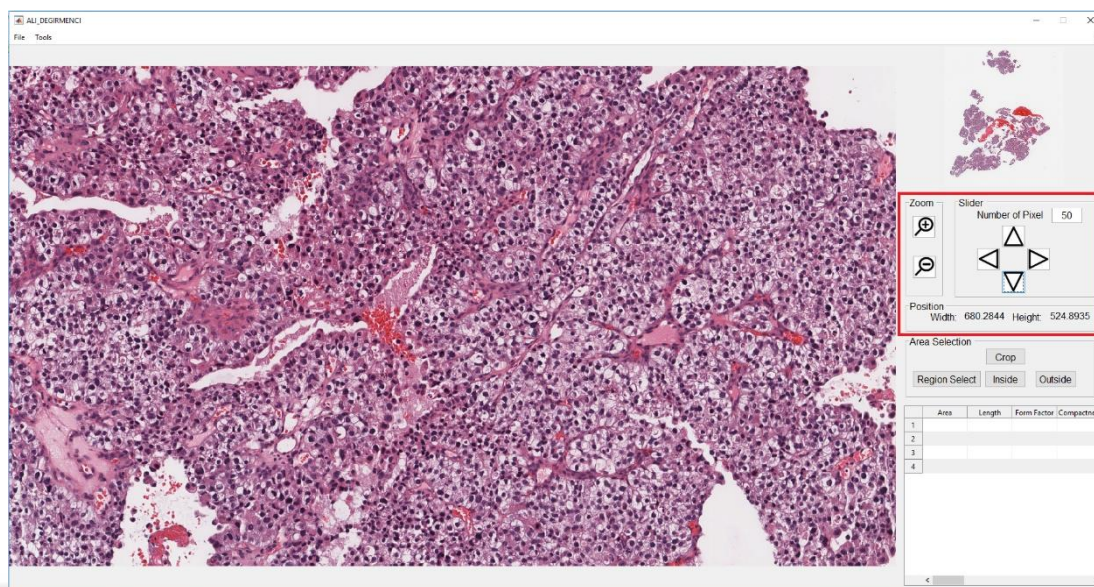


Figure 5.10 Pathological image zooming and scrolling

In Figure 5.10, red rectangle box consists of three panels which are zoom, slider and position. Zoom panel allows zooming both in and out. Slider panel enables to scroll the image in different magnification levels. In order to do this, position information on the image is determined by left clicking with mouse to the big image on the left side of the GUI and after that, position information is written dynamically to the text boxes near to the ‘Width’, ‘Height’ which are shown in the position panel. Then, determined position of the image can be enlarged by clicking the zoom plus sign button, or minimized by clicking the zoom minus sign button, which enables the access to the different zoom levels of the image. This provides transitions between different magnification levels of the WSI. Since pathological images are too big to fit on a screen, only dimension of 1600x900 pixel part is visualized in order to see the details when the magnification level is increased. As can be seen on the Figure 5.10, this corresponds to a small portion of the entire image. It is possible to scroll left, right, up and down on the image using the buttons which are shown in the directional arrow symbols to show the direction for viewing the other areas in higher magnification levels. At the same time, the user can increase or decrease the amount of scrolling with the help of editable text next to “Number of Pixel” which is set to 50 pixels by default.

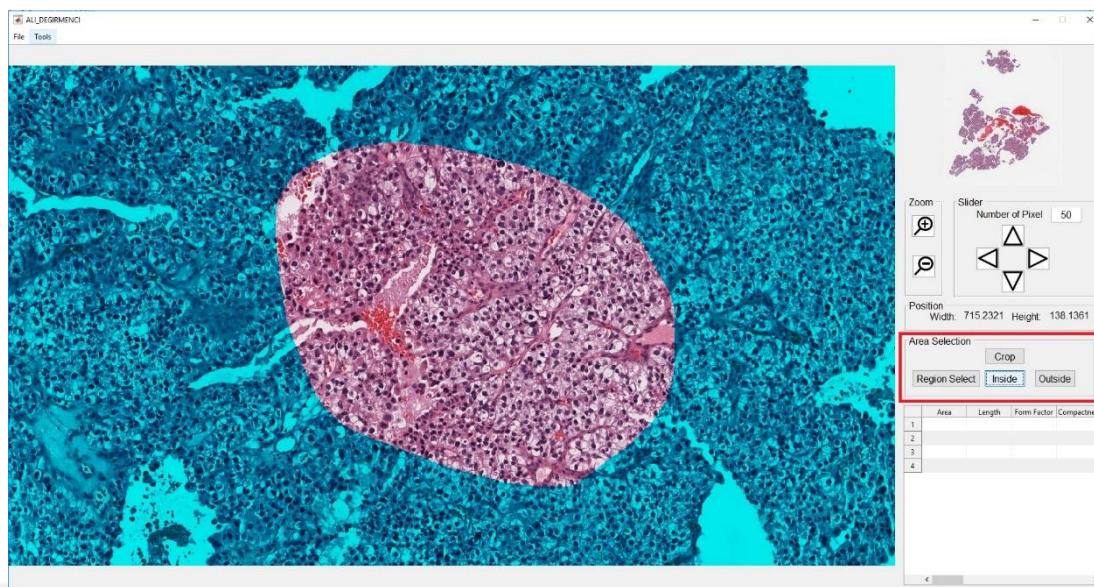


Figure 5.11 Area selection from pathological images

After the area is specified from the image to analyze, this area in the image can be extracted from the image using the “Crop” button and can be processed afterwards. In addition, doctors sometimes demand to exclude some areas from the selected area. After pressing the “Region Select” button, the area is to be extracted or the area is to be excluded. When the analysis is performed inside the selected region, it is made by 'Inside' button. When the 'Outside' button is clicked, the desired operation can be performed in the area excluding the selected area. As shown in the Figure 5.11, after the desired region is determined, the inside of the selected region is ready to be processed by using the inside button. When the Figure 5.11 is examined, the inside of the selected area remains unchanged but outside of that region is masked with the light blue color. When the “Outside” button is pressed, the interior of the selected region will be masked with a light blue transparent color, allowing the outside area to be processed.

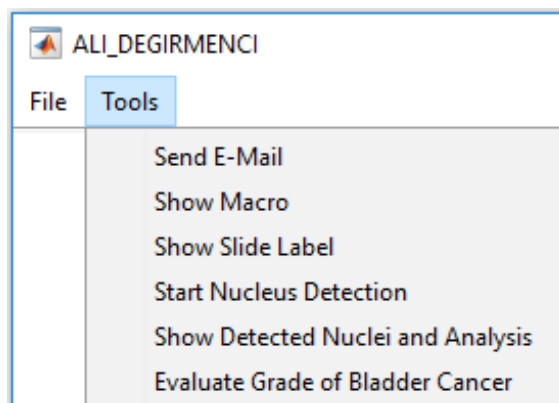


Figure 5.12 Tools menu

When “Send E-mail” is selected from the Tools menu shown in Figure 5.12, a new window is opened, which enables to send an email using with this program which is shown in Figure 5.13. Selected area from the pathological image and results of the process can be sent via e-mail using this or any file on the hard drive.

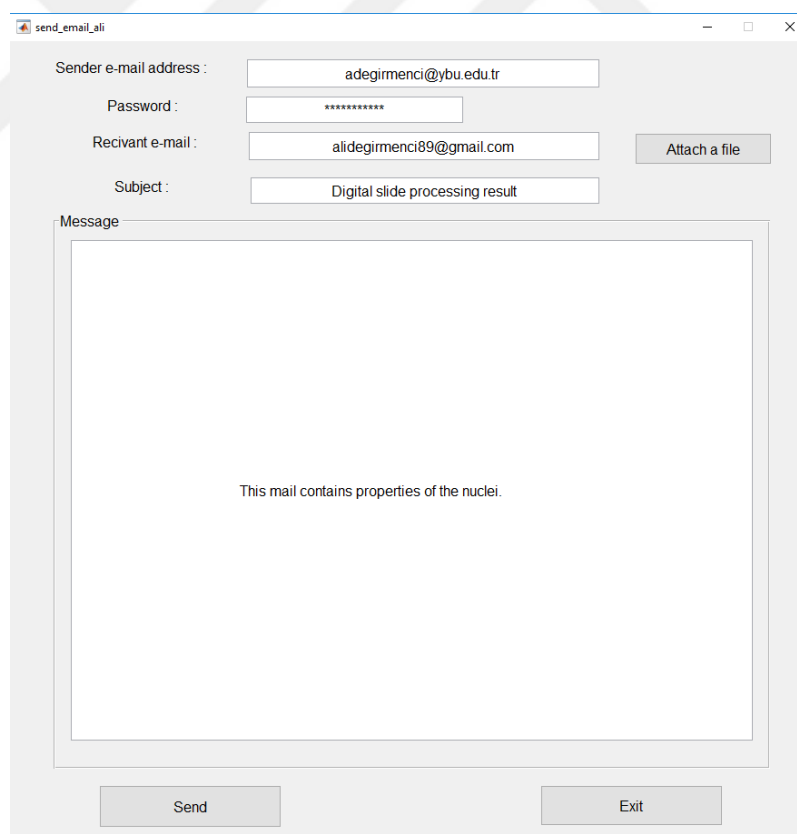


Figure 5.13 Example of sending an e-mail

When “Show Macro” is used, the macro image of prepared sample’s glass slide is displayed in the opened picture window, Figure 5.14 (a). When “Show Slide Label” is selected, it gives several information about the data. These are loaded file name, barcode, preparation time of the sample area displayed in the image window, Figure 5.14 (b).



(a)



(b)

Figure 5.14 (a) Macro photograph of the pathology sample, (b) a barcode

“Start Cell Detection” button starts the process of nucleus detection from the selected area and stores the contour pixels’ location. After the process has finished, a dialog box will open and display a message of “Nuclei detection completed”.

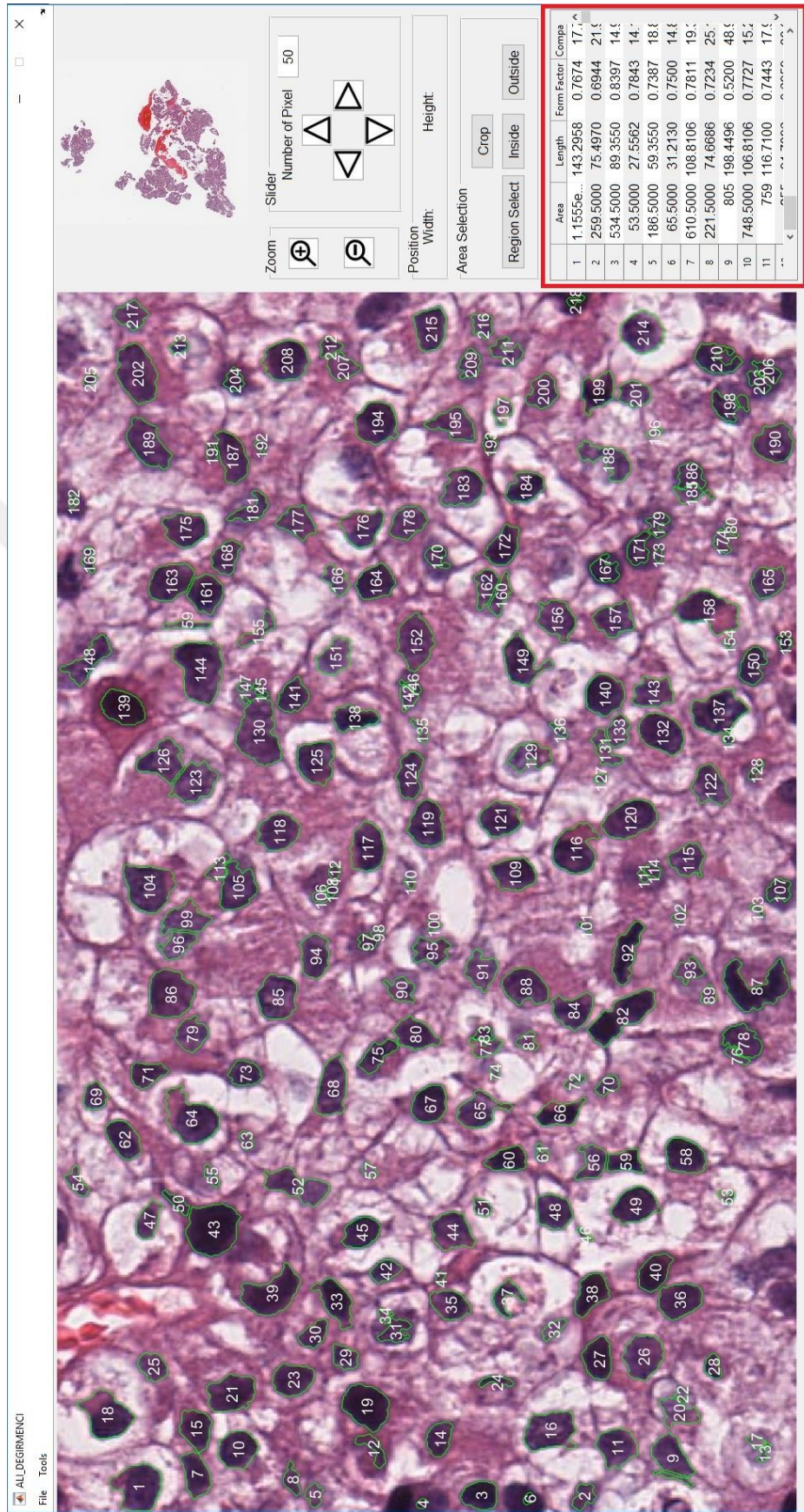


Figure 5.15 Demonstration of nuclei boundaries and calculations

Another option in the Tools menu is “Show Detected Nuclei and Analysis” button, which performs the calculation of the features of each nucleus using with contour information. Successfully recognized nucleus contour pixels are drawn in green and the calculated features of the nuclei are displayed in the table at the bottom of window. These features are area of the nucleus, length, convexity, average density, standard deviation, variance and so on.

As seen in Figure 5.15, the boundaries of the cell nuclei are drawn by the written program in green, and each cell is given a different number and these numbers are written in the center of gravity of each cell with color of white. On this point, specialist doctors can easily find out the number written on the cell nucleus by looking at the image. After that, by looking at the same number in the row of table, characteristics of the nucleus can be found out, as shown in red rectangle box in Figure 5.15.

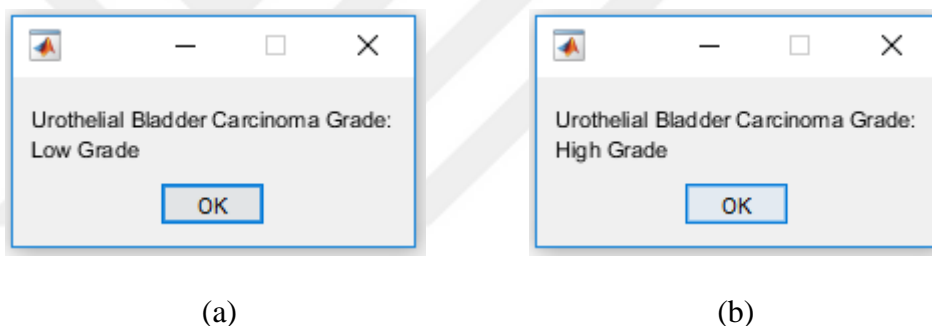


Figure 5.16 Result of cancer grading, (a) low grade (b) high grade

The last option in the tools menu is “Evaluate the grade of bladder cancer”. In this option, using the extracted features of the nuclei, mean of the all nuclei features are calculated. Following that, classification method is applied with predetermined features. As a result, one of these two dialog boxes are opened and show the grade of the BC whether it is low grade or high grade BC, as seen in Figure 5.16.

CHAPTER 6

CONCLUSIONS AND FUTURE WORKS

Medical imaging aims at obtaining the image of the region to be examined as well as assisting doctors during the procedure of the diagnosis of disease and treatment plan of the illness by providing useful information which is extracted from medical images. Since medical imaging contains image capturing, processing, analysis and extraction of the meaningful information from medical images, it is an area of multiple fields, such as electrical and electronics engineering, medicine, computer science and so on.

Since the required time for processing of medical data is reduced, medical image processing gained significant attention by researchers, which leads to noteworthy developments in the medicine in recent years. Especially, by using the existing computer technology and image processing techniques in medical images, the accuracy of results has increased. This leads to wider use of CAD systems. On the other hand, they are not subjective, so the obtained results do not change with the time and/or with different user. They also reduce the processing time. Although there are lots of advantages for using CAD systems, the final decision of the disease is diagnosed by a specialist doctor because the aim of CAD systems is only to help doctors, in some cases; provide a second opinion.

In this thesis, an algorithm is developed to determine the discrimination of the low grade and high grade bladder carcinoma from slide scanner images of the hematoxylin eosin stained urinary bladder tissue samples. Firstly, the data set was received from TCGA which contains all available UBC digital slide scanner files. Secondly, 5 high-grade and 5 low-grade image sections were determined by a pathologist and cropped from digital slide scanner images. These sections were chosen as a training data. To determine the grade of cancer, contours of the nucleus were found from training data. Then, features were extracted by using nucleus contours. To classify low-grade and high-grade BC, the features which demonstrate different characteristics in both grades are selected. Then, these features are used in the minimum distance classification method as training samples. 100 different samples were chosen to test the accuracy of

proposed classification method. The accuracy of high-grade cancer detection performance was around 83%.

In the scope of this thesis, GUI was designed to make it easier to use the BC classification algorithm with the MATLAB programming language. This application assists the pathologist during the digital slide examination and helps the diagnostic process. Using with GUI, digital slides of the pathological data can be visualized and then, zooming and sliding operations can be made in different magnification levels. Once the area to be analyzed has been selected, the cancer grading algorithm is run and it determines whether the selected region is at high or low grade. In addition to these, the properties of each detected cell nucleus can be examined.

As a future work, entire image at 40x magnification level may be analyzed. The accuracy of the BC diagnosis can be improved either applying different methods or enhancing the algorithm. Designed algorithm is only classifying the cases into the low and high grade of the BC; in addition, the type of BC can be determined. In order to increase the classification ratio of the method, different features can be extracted from the nucleus and/or other classification methods can be used. Since time is important in cancer cases, process time of the algorithm may be decreased by writing the algorithm in C or C++ programming language using graphical processing unit. By default, the MATLAB program is not installed on the computer with any operating system. So, designed GUI requires the installation of the MATLAB program. To solve this problem, NET application of this program should be made and users can access the program anytime, visualize and analyze digital slides.

REFERENCES

- [1] Jemal, A., Vineis, P., Bray, F., Torre, L., Forman, D., “*The Cancer Atlas*”, American Cancer Society; 2nd edition, April 1, 2015.
- [2] Ames, B.N., Gold, L.S., Willett, W. C., “*The Causes and Prevention of Cancer*”, Proc. Natl. Acad. Sci. USA, vol. 92, pp. 5258-5265, June 1995.
- [3] Key, T.J., Schatzkin, A., Willett, W.C., Allen, N.E., Spencer, E.A. and Travis, R.C. “*Diet, nutrition and the prevention of cancer*”, *Public Health Nutrition*, 7(1a), pp. 187–200, 2004. doi: 10.1079/PHN2003588.
- [4] American Cancer Society. *Cancer Facts & Figures 2016*. Atlanta: American Cancer Society; 2016.
- [5] American Cancer Society, “*Bladder Cancer*”, <http://www.cancer.org/acs/groups/cid/documents/webcontent/003085-pdf.pdf> [Date of access: 04.07.2016]
- [6] Dougherty, G., “*Digital Image Processing for Medical Applications*”, Cambridge University Press, New York, 2009.
- [7] Jaume, S., Ferrant, M., Macq, B., Hoyte, L., Fielding, J.R., Schreyer, A., Kikinis, R., Warfield, S.K., “*Tumor Detection in the Bladder Wall with a Measurement of Abnormal Thickness in CT Scans*”, *IEEE Transactions on Biomedical Engineering*, vol. 50, no. 3, March 2003.
- [8] Shi, Z., Yang, J., Zhang, G., Lu, H., Yang, Z., “*Characterization of Texture Features Between Carcinomatous and Normal Wall Tissue in MR Bladder Imaging*”, 2nd International Conference on Biomedical Engineering and Informatics, Tianjin, pp. 1-5, 2009.

- [9] Spyridonos, P., Ravazoula, P., Cavouras, D., Berberidis, K., Nikiforidis, G., “*Computer-based grading of haematoxylin-eosin stained tissue sections of urinary bladder carcinomas*”, *Medical Informatics and the Internet in Medicine*, vol. 26, no. 3, pp. 179-190, 2001. doi: 10.1080/14639230110065757
- [10] <https://cancergenome.nih.gov/newsevents/forthedia/backgrounder>, [Date of access: 28.08.2016]
- [11] <http://blog.nationalmicroscope.com/microscope-parts-and-their-functions/>
[Date of access: 25.11.2016]
- [12] John D. Bancroft, Marilyn Gamble Dr., *Theory and Practice of Histological Techniques*, October 2001.
- [13] Yves Sucaet, Wim Waelput, *Digital Pathology*, *Spring Briefs in Computer Science*, 2014, <http://link.springer.com/book/10.1007/978-3-319-08780-1>.
- [14] http://www.megep.meb.gov.tr/mte_program_modul/moduller_pdf/Doku%20%C3%96rneklerini%20Histolojik%20Analyze%20Haz%C4%B1rlama.pdf
[Date of access: 27.9.2016]
- [15] <http://waynesword.palomar.edu/skincan2.htm>, [Date of access: 3.12.2016]
- [16] James W.: Bacus patents. JamesBacus.com. (2014). Ref type: Electronic Citation
- [17] Aperio Technologies Inc., Patent Applications. Patentdocs. (2014). Ref type: Electronic Citation
- [18] <http://www.fileformat.info/format/tiff/egff.htm> [Date of access: 25.11.2016]
- [19] Skodras, A., Christopoulos, C., Ebrahimi, T., “*The JPEG 2000 Still Image Compression Standard*”, *IEEE Signal Processing Magazine*, vol. 18, no. 5, pp. 36-58, September 2001. doi: 10.1109/79.952804
- [20] <http://cancergenome.nih.gov/abouttcga/overview>, [Date of access: 28.08.2016]

- [21] <http://cancergenome.nih.gov/newsevents/forthemedia/quickfacts>, [Date of access: 28.08.2016]
- [22] Wilbur, D.C., Madi, K., Colvin, R.B., Duncan, L.M., Faquin, W.C., Ferry, J.A., Frosch, M.P., Houser, S.L., Kradin, R.L., Lauwers, G.Y., Louis, D.N., Mark, E.J., Mino-Kenudson, M., Misdraji, J., Nielsen, G.P., Pitman, M.B., Rosenberg, A.E., Smith, R.N., Sohani, A.R., Stone, J.R., Tambouret, R.H., Chin-Lee Wu, Young, R.H., Zembowicz, A., Klietmann, W., “ *Whole-Slide Imaging Digital Pathology as a Platform for Teleconsultation: A Pilot Study Using Paired Subspecialist Correlations* ”, Archives of Pathology & Laboratory Medicine: vol. 133, no. 12, pp. 1949-1953, December 2009. http://www.archivesofpathology.org/doi/10.1043/1543-2165-133.12.1949?url_ver=Z39.88-2003&rfr_id=ori:rid:crossref.org&rfr_dat=cr_pub%3dpubmed
- [23] Campbell WS, Foster KW, Hinrichs S H., “ *Application of whole slide image markup and annotation for pathologist knowledge capture*”, *Journal of Pathology Informatics*. 2013;4:2. doi:10.4103/2153-3539.107953.
- [24] Tomczak, K., Czerwińska, P., Wiznerowicz, M., “The Cancer Genome Atlas (TCGA): An Immeasurable Source of Knowledge”, *Contemporary Oncology*, 19(1A):A68-A77, 2015. doi:10.5114/wo.2014.47136.
- [25] https://cancergenome.nih.gov/newsevents/newsannouncements/TCGA_The_Next_Stage [Date of access: 28.08.2016]
- [26] Rafael C. Gonzalez , Richard E. Woods, *Digital Image Processing* (3rd Edition), Prentice-Hall, Inc., Upper Saddle River, NJ, 2006
- [27] Wikipedia, “ *Binary image*”, https://en.wikipedia.org/wiki/Binary_image, [Date of access: 25.06.2016].
- [28] Wikipedia, “ *Grayscale*”, <http://en.wikipedia.org/wiki/Grayscale>, [Date of access: 26.06.2016].

- [29] <http://www.cambridgeincolour.com/tutorials/camera-sensors.htm> [Date of access: 6.11.2016]
- [30] Smith, T., Guild, J., “*The C.I.E. colorimetric standards and their use*”. Transactions of the Optical Society 33 (3): 73–134, (1931–32). doi:10.1088/1475-4878/33/3/301.
- [31] Doughty, M. (2009, March 27). Graphics Color Models. Retrieved October 10, 2013, from <http://www.sketchpad.net/basics4.htm>
- [32] <http://www.greatreality.com/color/ColorHVC.htm>, [Date of access: 29.06.2016].
- [33] Ford, A., Roberts, A., “*Colour Space Conversions*”, August 11, 1998(b).
- [34] Freeman, H., “*On the Encoding of Arbitrary Geometric Configurations*”, in IRE Transactions on Electronic Computers, vol. EC-10, no. 2, pp. 260-268, June 1961. doi: 10.1109/TEC.1961.5219197
- [35] Rosenfeld, A., Pfaltz, J.L., “*Distance Functions on Digital Pictures*”, Pattern recognition, vol. 1, no. 1, pp. 33-61, July. 1968. doi:10.1016/0031-3203(68)90013-7
- [36] Fabbri, R., Costa, L daF., “*2D Euclidian Distance Transform Algorithms: A comparative Survey*”, ACM Computing Surveys, vol. 40, no. 1, February 2008.
- [37] Borgefors, G., “*Distance Transformations in Digital Images*”, Computer Vision, Graphics, and Image Processing, vol. 34, no. 3, pp. 344-371, June 1986. doi:10.1016/S0734-189X(86)80047-0
- [38] Saito, T., Toriwaki, Jun-Ichiro., “*New Algorithms for Euclidian Distance Transformation of an n-Dimensional Digitalized Picture with Applications*”, Pattern Recognition, vol. 28, no. 11, pp. 1551-1565, November 1994. doi:10.1016/0031-3203(94)90133-3

- [39] Montanvert A., Coeurjolly, D., “*Optimal Separable Algorithms to Compute the Reverse Euclidean Distance Transformation and Discrete Medial Axis in Arbitrary Dimension*”, IEEE Transactions on Pattern Analysis & Machine Intelligence, vol. 29 no. 3, pp. 437-448, March 2007.
- [40] Suzuki, K., Horiba, I., Sugie, N., “*Linear-time Connected-Component Labelling Based on Local Operations*”, Computer Vision and Image Understanding, vol. 89, no. 1, pp. 1-23, January 2003.
- [41] Sutheebanjard, P., Premchaiswadi, W., “*Efficient Scan Mask Techniques for Connected Components Labelling Algorithm*”, EURASIP Journal on Image and Video Processing, December 2011.
- [42] He, L., Chao, Y., Suzuki, K., Wu, K., “*Fast Connected-Component Labelling*”, Pattern Recognition, vol. 42, no. 9, September 2009.
- [43] Rosenfeld, A., Pfaltz, J. L., “*Sequential Operations in Digital Picture processing*”, Journal of the Association for Computing Machinery, vol. 13, no. 4, pp. 471-494, October 1966.
- [44] Haralick, R. M., “*Some Neighborhood Operations*”, Real-Time Parallel Computing Image Analysis, pp. 11-35, 1981.
- [45] Chang F., Chen, C.J., Lu, C.H., “*A Linear-Time Component Labeling Algorithm Using Contour Tracing Technique*”, Computer Vision and Image Understanding, vol. 93, no. 2, pp. 206-220, February 2004.
- [46] Szeliski, R., Computer Vision: Algorithms and Applications, September 2010.
- [47] Zhou, H., Wu, J., & Zhang, J., “*Digital Image Processing: Part I*”, ISBN-978-87-7681-541-7, 2010/a.
- [48] Deng, G., & Cahill, L. W., “*An Adaptive Gaussian Filter for Noise Reduction and Edge Detection*”, 1993 IEEE Conference Record Nuclear Science Symposium and Medical Imaging Conference, San Francisco, CA, vol.3, pp. 1615-1619, 1993. doi: 10.1109/NSSMIC.1993.373563

- [49] İlk, H.G., Jane, O., İlk, Ö., “*The Effect of Laplacian Filter in Adaptive Unsharp Masking for Infrared Image Enhancement*”, *Infrared Physics & Technology*, vol. 54, no. 5, pp. 427–438, September 2011.
- [50] Zhou, H., Wu, J., and Zhang, J., “*Digital Image Processing PartII*”, ISBN 978-87-7681-542-4, 2010/b.
- [51] Zhang, Y.J., “*A Survey on Evaluation Methods for Image Segmentation*”, *Pattern Recognition*, vol. 29, no. 8, pp. 1335-1346, August 1996.
- [52] C. Li, R. Huang, Z. Ding, J. C. Gatenby, D. N. Metaxas and J. C. Gore, “*A Level Set Method for Image Segmentation in the Presence of Intensity Inhomogeneities With Application to MRI*”, *IEEE Transactions on Image Processing*, vol. 20, no. 7, pp. 2007-2016, July 2011. doi: 10.1109/TIP.2011.2146190
- [53] Sezgin, M., & Sankur, B., “*Survey over Image Thresholding Techniques and Quantitative Performance Evaluation*”, *Journal of Electronic Imaging*, vol.13, no. 1, pp. 146-165, January 2004.
- [54] M. I. Sezan, “*A Peak Detection algorithm and Its Application to Histogram-Based Image Data Reduction*”, *Graph. Models Image Process.*, 29, pp. 47–59, 1985.
- [55] N. Ramesh, J. H. Yoo, and I. K. Sethi, “*Thresholding Based on Histogram Approximation*”, *IEE Proc. Vision Image Signal Process*, vol. 142, no.5, pp. 271–279, 1995.
- [56] Otsu, N., “*A Threshold Selection Method from Gray Level Histograms*”, *IEEE Trans. Syst. Man Cybern. SMC-9*, pp. 62–66, 1979.
- [57] Ridler. T. W., & Calvard, S., “*Picture Thresholding Using an Iterative Selection Method*”, *IEEE Trans. Syst. Man Cybern. SMC-8*, pp. 630–632, 1978.
- [58] Kapur, J. N., Sahoo, P. K., Wong, A. K. C., “*A New Method for Gray-Level Picture Thresholding Using the Entropy of the Histogram*”, *Graph. Models Image Process*, vol. 29, no. 3, pp. 273–285, March 1985.

- [59] Brink, A. D., & Pendock, N. E., “*Minimum Cross Entropy Threshold Selection*”, *Pattern Recogn*, vol. 29, no. 1, pp. 179–188, January 1996.
- [60] Tsai, W. H., “*Moment-Preserving Thresholding: A New Approach*”, *Computer Vision, Graphics, & Image Processing*, vol. 29, no. 3, pp. 377–393, 1985.
- [61] Murthy, C. A., & Pal, S. K., “*Fuzzy Thresholding: A Mathematical Framework, Bound Functions and Weighted Moving Average Technique*”, *Pattern Recognition Letters*, vol. 11, no. 3, pp. 197–206, 1990.
- [62] Kirby, R. L., & Rosenfeld, A., “*A Note on the Use of (Gray Level, Local Average Gray Level) Space as an Aid in Threshold Selection*”, *IEEE Trans. Syst. Man Cybern.* SMC-9, pp. 860–864, 1979.
- [63] Cheng, H. D., & Chen, Y. H., “*Fuzzy Partition of Two-Dimensional Histogram and Its Application to Thresholding*”, *Pattern Recognition*, vol.32, no. 5, pp. 825–843, 1999.
- [64] Nakagawa, Y., & Rosenfeld, A., “*Some Experiments on Variable Thresholding*”, *Pattern Recognition*, vol. 11, no. 3, pp. 191–204, 1979.
- [65] <http://courses.cs.washington.edu/courses/cse455/04wi/readings/edge-detection-cipolla.pdf> [Visit Date: 23.11.2016]
- [66] Jain, R., Kasturi, R., Schunck, B. G., “*Machine Vision*”, Published by McGraw-Hill, Inc., ISBN 0-07-032018-7, 1995.
- [67] Haralick, R. M. , “*Digital Step Edges from Zero Crossing of Second Directional Derivatives*”, in *IEEE Transactions on Pattern Analysis and Machine Intelligence*, vol. PAMI-6, no. 1, pp. 58-68, Jan. 1984. doi: 10.1109/TPAMI.1984.4767475
- [68] Tan, H. L. , Gelfand S. B., Delp, E. J. , “*A comparative cost function approach to edge detection*”, in *IEEE Transactions on Systems, Man, and Cybernetics*, vol. 19, no. 6, pp. 1337-1349, Nov/Dec 1989. doi: 10.1109/21.44058

- [69] Canny, J., "*A Computational Approach to Edge Detection*", in *IEEE Transactions on Pattern Analysis and Machine Intelligence*, vol. PAMI-8, no. 6, pp. 679-698, Nov. 1986. doi: 10.1109/TPAMI.1986.4767851
- [70] Canny, J., "*Finding edges and lines in image*". Master's thesis, MIT, 1983.
- [71] <http://www.cse.iitd.ernet.in/~pkalra/col783/>, [Date of access: 22.11.2016]
- [72] Martin, D. R., Fowlkes, C. C., Malik, J., "*Learning to Detect Natural Image Boundaries Using Local Brightness, Color, and Texture Cues*", *IEEE Transactions on Pattern Analysis and Machine Intelligence*, vol. 26, no. 5, pp. 530-549, May 2004. doi: 10.1109/TPAMI.2004.1273918
- [73] <http://www.leica-microsystems.com/science-lab/history/a-brief-history-of-light-microscopy-from-the-medieval-reading-stone-to-super-resolution/> [Date of access: 29.10.2016]
- [74] <http://www.history-of-the-microscope.org/history-of-the-microscope-who-invented-the-microscope.php> [Date of access: 29.10.2016]
- [75] By Jeroen Rouwkema, CC BY-SA 3.0, <https://commons.wikimedia.org/w/index.php?curid=3657142> [Date of access: 05.12.2016]
- [76] Zhou, Y., Magee, M., Treanor, D., Bulpitt, A., "*Stain Guided Mean-Shift Filtering in Automatic Detection of Human Tissue Nuclei*" *J Pathol Inform*, 2013,4:6
- [77] Sammouda, M., Sammouda, R., Niki, N., Yamaguchi, N., Moriyama, N., "*Cancerous Nuclei Detection on Digitized Pathological Lung Color Images*", *Journal of Biomedical Informatics*, vol. 35, no. 2, pp. 92-98, April 2002.
- [78] Wienert, S., Heim, D., Saeger, K., Stenzinger, A., Beil, M., Hufnagl, P., Dietel, M., Denkert, C., Klauschen, F., "*Detection and Segmentation of Cell Nuclei in Virtual Microscopy Images: A Minimum-Model Approach*", *Scientific Reports*, 2 : 503, July 2012. doi: 10.1038/srep00503

- [79] Seo, J.; Chae, S.; Shim, J.; Kim, D.; Cheong, C.; Han, T.-D., “*Fast Contour Tracing Algorithm Based on a Pixel-Following Method for Image Sensors*”, *Sensors*, 16, 353, 2016.
- [80] Shoji, K.; Miyamichi, J., Hirano, K., “*Contour Following and Reconstruction of Binary Images Stored in Run Format*”, *Syst. Comput. Jpn.*, vol.30, pp. 1–11, 1999.
- [81] Suzuki, S.; Abe, K. “Topological Structural Analysis of Digitized Binary Images by Border Following”, *Computer Vision, Graphics, and Image Processing*, vol. 30, no.1, pp. 32–46, 1985.
- [82] Miyatake, T.; Matsushima, H.; Ejiri, M. “Contour Representation of Binary Images Using Run-Type Direction Codes”, *Machine Vision and Applications*, vol. 9, no. 4, pp. 193–200, 1997.
- [83] Cheong, C., Han, T.D., “Improved simple boundary following algorithm”, *J. Korea Inf. Sci. Soc. Softw. Appl.*, vol. 33, pp. 427–439, 2006.
- [84] Ruifrok, A. C., Johnston, D. A., “*Quantification of histochemical staining by color deconvolution*”, *Analytical Quantitative Cytology Histology*, vol. 23, pp. 291–299, 2001.
- [85] https://en.wikipedia.org/wiki/Beer%E2%80%93Lambert_law, [Date of access: 5 12.2016]
- [86] Çankaya, İ., Akgün, D., Kaçar, S., “*Mühendislik Uygulamaları için MATLAB*”, Seçkin Yayıncılık, Turkey, 2016.

CURRICULUM VITAE

PERSONAL INFORMATION

Name Surname : Ali DEĞİRMENCİ
Date of Birth : 1989
Phone : +90 553 2850666
E-mail : adegirmenci@ybu.edu.tr



EDUCATION

High School : Hoca Ahmed Yesevi High School / ESKİŞEHİR
(2003-2007) (88.20/100)
Bachelor : Eskişehir Osmangazi University / ESKİŞEHİR (2008-2013)
(3.44/4.0)
Master Degree : Ankara Yıldırım Beyazıt University / (2015-continued)

WORK EXPERIENCE

Research Assist. : Ankara Yıldırım Beyazıt University / (2015-continued)

TOPICS OF INTEREST

- Signal Processing
- Biomedical Image Processing
- Image Processing
- Computer Vision